МІНІСТЕРСТВО ОСВІТИ І НАУКИ УКРАЇНИ
ІВАНО-ФРАНКІВСЬКИЙ НАЦІОНАЛЬНИЙ
ТЕХНІЧНИЙ УНІВЕРСИТЕТ НАФТИ І ГАЗУ

РОЗВІДКА ТА РОЗРОБКА НАФТОВИХ І ГАЗОВИХ РОДОВИЩ

Науково-технічний журнал

Том 24, № 1
2024

ІВАНО-ФРАНКІВСЬК
2024

MINISTRY OF EDUCATION AND SCIENCE OF UKRAINE
IVANO-FRANKIVSK NATIONAL
TECHNICAL UNIVERSITY OF OIL AND GAS

PROSPECTING AND DEVELOPMENT OF OIL AND GAS FIELDS

Scientific and Technical Journal

Vol. 24, No. 1
2024

IVANO-FRANKIVSK
2024

ISSN 1993-9973
e-ISSN 2415-332X
УДК 622;550

Засновник та видавець:
Івано-Франківський національний технічний університет нафти і газу (ІФНТУНГ)

Рік заснування: 2001

Періодичність: двічі на рік

Ідентифікатор медіа: R30-01429
(Рішення Національної ради України з питань телебачення і радіомовлення № 1154,
протокол № 24 від 26 жовтня 2023 року)

Журнал включено до категорії «Б» Переліку наукових фахових видань України
Технічні спеціальності: 133 – Галузеве машинобудування;
185 – Нафтогазова інженерія та технології
(Наказ Міністерства освіти і науки України № 1643 від 28 грудня 2019 року)
Геологічні спеціальності: 103 – Науки про землю
(Наказ Міністерства освіти і науки України № 409 від 17 березня 2020 року)

Журнал представлено в таких міжнародних наукометричних базах даних, репозитаріях та пошукових системах:
Національна бібліотека України імені В.І. Вернадського, Фахові видання України,
Crossref, Dimensions, Google Академія, German Union Catalogue of Serials (ZDB),
University of Oslo Library, Universitätsbibliothek Leipzig (UBL),
Open Ukrainian Citation Index (OUCI)

Адреса редакції:
Івано-Франківський національний технічний університет нафти і газу
76019, вул. Карпатська, 15, м. Івано-Франківськ, Україна
E-mail: info@pdogf.com.ua
https://pdogf.com.ua/uk

ISSN 1993-9973
e-ISSN 2415-332X
UDC 622;550

Founder and publisher:
Ivano-Frankivsk National Technical University of Oil and Gas (IFNTUOG)

Year of foundation: 2001

Frequency: semi-annual

Media identifier: R30-01429
(Decision of the National Council of Television and Radio Broadcasting of Ukraine No. 1154,
Minutes No. 24 of October 26, 2023)

The journal is included in category "B"
of the List of scientific professional publications of Ukraine
Technical specialties: 0716 – Motor Vehicles, Ships and Aircraft;
0724 – Mining and Extraction
(Order of the Ministry of Education and Science of Ukraine No. 1643 dated December 28, 2019)
Geological specialties: 0532 – Earth Sciences
(Order of the Ministry of Education and Science of Ukraine No. 409 dated March 17, 2020)

The journal is presented in the following international scientometric databases, repositories and scientific systems:
Vernadsky National Library of Ukraine, Professional Publications of Ukraine,
Crossref, Dimensions, Google Scholar, German Union Catalogue of Serials (ZDB),
University of Oslo Library, Universitätsbibliothek Leipzig (UBL),
Open Ukrainian Citation Index (OUCI)

Editors office address:
Ivano-Frankivsk National Technical University of Oil and Gas
76019, 15 Karpatska Str., Ivano-Frankivsk, Ukraine
E-mail: info@pdogf.com.ua
https://pdogf.com.ua/en

Редакційна колегія

Editorial Board

Зміст/Contents

Vol. 24, No. 1
2024

PROSPECTING AND DEVELOPMENT OF OIL AND GAS FIELDS

https://pdogf.com.ua/en

Received: 09.01.2024. Revised: 17.04.2024. Accepted: 31.05.2024

UDC 622.267

DOI: 10.69628/pdogf/1.2024.10

Determination of the D-factor and its effect on the stimulated volume of compact gas-saturated reservoirs

Oleh Lukin

Postgraduate Student
Ivano-Frankivsk National Technical University of Oil and Gas
76019, 15 Karpatska Str., Ivano-Frankivsk, Ukraine
https://orcid.org/0009-0005-5194-628X

Oleksandr Kondrat*

Doctor of Technical Sciences, Professor
Ivano-Frankivsk National Technical University of Oil and Gas
76019, 15 Karpatska Str., Ivano-Frankivsk, Ukraine
https://orcid.org/0000-0003-4406-3890

Abstract. Correct estimation of the possible volume of replacement of conventional reservoir structures with compacted sandstones/carbonates in existing fields and production areas is a controversial issue not only in Ukraine but also abroad, due to parametric uncertainty and the impact of formation fluid filtration in unconventional reservoirs. This leads to an overestimation of the forecasted development of compact gas-saturated reservoirs, a decrease in the replacement rate, and an increase in the rate of production decline. Therefore, the aim of the study was to assess the influence of the coefficient of additional filtration resistance, which occurs due to the high rate of upward fluid flow as one of the key uncertain parameters, on the well productivity and the resulting accumulated gas extraction. A multi-stage hydraulic fracturing was performed in a synthetic horizontal well, which was created in the Petrel software. Using typical correlations, the additional resistance coefficients (D-factor) are determined and a hydrodynamic model is constructed in the Eclipse software. Simulations with different values of the D-factor were performed to determine its effect on productivity on accumulated samples for the same type of formations. The results of the study indicate that the revaluation can reach 40%, which is significant when calculating the economic indicators of the feasibility of drilling and conducting multi-stage hydraulic fracturing. The proposed selection and methodology for low-permeability formations encountered in the fields of the Dnipro-Donetsk Basin of Ukraine can be used by gas and oil companies for a detailed analysis of uncertainties and correct planning of stabilisation of the gas production decline

Keywords: coefficient of additional resistance; fluid filtration; multi-stage hydraulic fracturing; simulation; well flow rate

Introduction

Correct determination of the forecast performance of horizontal wells that penetrate compact reservoirs is critical for development planning and optimisation. The risk of revaluation of accumulated selections causes distrust of investors and partners in joint field development schemes and increases the payback period of projects. Detailed analysis and assessment of such risks is one of the requirements when designing the development of non-traditional collectors. Any minimisation of these risks and the validity of forecast performance indicators of expensive design horizontal wells, with multi-stage hydraulic fracturing, proves the relevance of this topic. J.-Q. Zhou *et al*. (2019b) deduced the relationship between viscous inertial filtration and permeability by synthesising the results of thousands of laboratories and field filtration tests and modelling using a hydrodynamic simulator. Their research showed that

Suggested Citation: Lukin, O., & Kondrat, O. (2022). Determination of the D-factor and its effect on the stimulated volume of compact gas-saturated reservoirs. *Prospecting and Development of Oil and Gas Fields*, 24(1), 10-22. doi: 10.69628/pdogf/1.2024.10.

*Corresponding author

the permeability of a geological space can vary by several degrees of magnitude under the influence of compression, shear, decompression or fracture. Since these inertial effects are included in the viscosity and filtration components of the Forchheimer equation, their correct description or the use of certain values to compensate for this effect is critical for predicting filtration in cases where filtration and media geometry (fracture formation) evolve simultaneously. Researchers J.-Q. Zhou *et al*. (2019a) proposed a theoretical expression for the definition of permeability as a function of pressure in fracture pore space. Studies have shown that in order to adjust the theoretical dependence on the actual data, the Forchheimer equation and the coefficient of additional resistance were used, since the dependence was characterised by overestimated values on the graphs of the pressure dependence on the flow rate. A.F. Hart & O.C. Omobolanle (2023) considered the possibility of determining the coefficient of additional resistance using the example of a core sample under laboratory conditions for different temperatures – 38, 65 and 93°C. N_2 was used as the agent pumped through the core sample at various temperatures. The results of this study showed that with an increase in pumping temperature and pressure, the coefficient of additional resistance increased, and a decrease in the permeability of the proppant pack was also observed.

B.R. Jones *et al*. (2020) investigated the possibility of predicting filtration at the limit of Darcy's law using the Forchheimer equation for different values of hydrocarbon saturation. The authors have shown that the Forchheimer equation is valid for predicting the flow rates measured on the core. For all experiments, the difference between measurements and predictions was no more than 5% for any pressure interval from all tested models. However, the authors noted that additional quantitative and qualitative studies, both in the laboratory and in the field, are necessary for better predictability. D.S. Berawala & P.Ø. Andersen (2019) determined that the effect of filtering at the Darcy's law boundary is dominant in the cracks, not in the matrix. Production itself is limited by the increased gas content in the fractures as a result of additional resistance due to gas mobility, and the final recovery factor depends more on the size and shape of the fractures created during hydraulic fracturing compared to Darcy's law filtration. Scientists A. Elsanoose *et al*. (2022), attempted to derive a new correlation for determining the coefficient of additional resistance at the limit of Darcy's law using laboratory studies and conducted 358 experiments on 7 large, artificially created prototypes of a porous medium. However, at this stage of research, air and water were used as fluids, and the authors noted the feasibility of repeating experiments using other injection agents, such as CO_2 and hydrocarbon gas. The resulting logarithmic dependence is planned to be used in forecasting the main development indicators for its validation. Although there is already a scientific body of work on this topic, the issue of applying an additional resistance coefficient when assessing the predicted performance of horizontal wells with high upward flow rates using hydrodynamic simulators in the Dnipro-Donetsk Basin (DDB) fields has not been sufficiently considered, which leads to an overestimation of the predicted development indicators when designing horizontal wells. The aim of this study was to build a synthetic model of a compact gas-saturated reservoir developed by a horizontal well with multistage hydraulic fracturing and bring it to the conditions encountered in the DDB fields in order to assess the effect and perform sensitivity analysis on the resulting accumulated samples, after applying an additional coefficient of resistance that occurs due to filtering at the limit of Darcy's law.

Theoretical Overview

The topic of describing fluid filtration in non-traditional reservoirs when developed by horizontal wells in which hydraulic fracturing is carried out has always caused heated discussions. One aspect of these discussions concerns an additional resistance coefficient (D-factor), namely one of its components β, a factor that is also known by some other names. For example, the turbulence factor in research by D. Cornell & D.L. Katz (1953) or the inertia coefficient of H. Ma & D. Ruth (1993). Since the flow rate in the modified equation by P. Forchheimer (1901) is given in the second degree, most researchers focused on high values of flow rates, which usually occurs in the bottom-hole zone of gas condensate wells. Research by F. Zeng & G. Zhao (2010) showed that the use of reasonable values of additional pressure losses due to filtration at the limit of Darcy's law can reduce the resulting well productivity by up to 50%, while the conductivity of cracks after hydraulic fracturing is up to 20%. A significant decrease in well productivity after hydraulic fracturing or in fractured formations has been confirmed by other authors. K.E. Olsen *et al*. (2004) emphasised the importance of optimising the hydraulic fracturing design for wells operating in two or more phases (oil, gas, water) and evaluated the validity of the Forchheimer equation at very high well flow rates. The results showed an overestimation of the accumulated recovery after 400 days of well operation in the range of 25 to 56%, with a suboptimal operating mode and incorrect consideration of the additional resistance factor. The correct description of filtration in gas condensate reservoirs developed by high-flow wells is complicated by the increase in fluid velocity and viscosity due to phase transformations in the bottom-hole zone, as noted by P. Ghahri *et al*. (2011), namely the formation of a condensate shaft, which also affects the performance of horizontal wells, after hydraulic fracturing, when the pressure decreases below the pressure of the beginning of condensation. Also, in the work by D.D. Cramer (2004) it was found that when stimulating low-permeable reservoirs using hydraulic fracturing technology, the effect of reservoir fluid filtration at the limit of Darcy's law also affects the reduction of the resulting semi-lengths (*xf*) formed fractures.

The issue was also highlighted in discussion by D. Van Batenburg & D. Milton-Tayler (2005) on the publication of R.D. Barree & M.V. Conway (2004). This discussion essentially revolves around the limits of the

applicability of the Forchheimer equation and the adequacy of its description when filtering fluids in unconventional reservoirs. R.D. Barree & M.V. Conway (2004) summarised that new experimental data, under conditions of high upstream velocity, convincingly showed that the Forchheimer equation, just as Darcy's law. (1865) has a limited range of applications. In turn, D. Van Batenburg & D. Milton-Tayler (2005), after conducting a number of experimental studies, did not agree that the Forchheimer equation cannot be used to describe the dependence of the additional coefficient of resistance on the rate of upstream flow and presented data collected in two laboratories that the proposed Forchheimer equation is valid for most actual and physical ranges of real wells, while the values at which the deviation is observed are far beyond the real modes of well operation. D. Denney (2005) noted that β (which is considered constant for all velocities) can be a variable that depends on the speed. This makes it possible to better describe and control pressure losses, but makes it impossible to accurately predict the flow rate as a function of the pressure gradient. As can be seen after analysing the fundamental works, everything that follows in newer publications refers to the original sources in one way or another and does not directly describe their research, using only the results. In Ukrainian publications, there are almost no examples of the use of this coefficient in the design of horizontal wells. This further confirms the relevance of this study.

Materials and Methods

Modelling, design and successful application of methods for improving oil and gas production directly depends on the correctness of the description of their filtration features. H. Darcy (1865) derived the fundamental law of reservoir fluid flow dynamics in pore space:

$$-\frac{dP}{dx}=\frac{\mu v}{k}, \quad (1)$$

where P – pressure, bar; x – flow direction; μ – dynamic viscosity coefficient, Pa·s; k – permeability of the porous medium, D; v – volume flow rate of liquid, m^3/s. According to the equation (1), the volume flow rate is directly proportional to the pressure gradient. Later, experimentally, P. Forchheimer (1901) derived a deviation from the linear proportionality of Darcy's filtration law for high volume flow values. S. Ergun (1952) observed that for high flow rates, the pressure drop is greater than predicted by Darcy's law. This phenomenon has been referred to in the literature as filtering outside of Darcy's law. Forchheimer added an additional pressure loss proportional to the square of the volume flow rate. Therefore, the equation (1) has taken the following form:

$$-\frac{dP}{dx}=\frac{\mu v}{k}+\beta\rho v^2, \quad (2)$$

where β – factor used by Forchheimer for correction, Pa^{-1}; ρ – fluid density, kg/m^3. According to the equation (2), the total pressure gradient ($-dp/dx$) can be considered as the sum of the gradients required to overcome the viscosity ($\mu v/k$) and liquid – solid interactions ($\beta\rho v^2$). There is a generally accepted opinion that this effect occurs only in the bottom-hole zone at a distance of up to several meters. This is the main reason why most hydrodynamic simulators describe this effect as an additional skin factor at the well-formation level:

$$S_{total}=s+Dq, \quad (3)$$

where S_{total} – total skin; s – permanent skin factor; D – skin factor coefficient, depending on the filtration rate, D/thousand m^3. Coefficient D can be defined as:

$$D=\frac{2.715\times10^{-15}\times\beta MP_{sc}k}{\mu T_{sc}hr_w}, \quad (4)$$

where M – molecular weight, g/mol; P_{sc} – pressure under standard conditions, bar; k – permeability, mD; μ – viscosity, centipoise; T_{sc} – temperature under standard conditions, °C; h – reservoir capacity, m; rw – consolidated well radius, m. In this study, a synthetic hydrodynamic model of a single horizontal well with 5-stage hydraulic fracturing is used. The model is based on compact reservoirs in the DDB. A compositional simulator was used to take into account the phase transformations that occur along the created fractures. Typical correlations that were used in the study are summarised below.

$$\beta=\frac{45185}{\varphi^{1.5}k^{0.5}}; \quad (5)$$

$$\beta=\frac{1.82\times10^8}{k^{1.25}\varphi^{0.75}}; \quad (6)$$

$$\beta=\frac{1.58\times10^3}{k^{0.5}\varphi^{5.5}}; \quad (7)$$

$$\beta=\frac{1.88\times10^{10}}{\varphi^{-}k^{0.5}}; \quad (8)$$

$$\beta=\frac{4.8\times10^{10}}{k^{1.176}}; \quad (9)$$

$$\beta=\frac{2.018\times10^9}{k^{1.55}}; \quad (10)$$

$$\beta=\frac{2.923\times10^7}{k\varphi}\tau; \quad (11)$$

$$\beta=\frac{3.51\times10^{10}\varphi^{0.449}}{k^{1.88}}; \quad (12)$$

$$\beta=\frac{8.17\times10^9\varphi^{0.537}}{k^{1.79}}; \quad (13)$$

$$\beta=\frac{1.35\times10^7\tau^{3.35}}{k^{0.98}\varphi^{0.29}}; \quad (14)$$

$$\beta=\frac{1.01\times10^8\tau^{1.943}}{k^{1.023}}; \quad (15)$$

$$\beta=\frac{1.15\times10^7}{k\varphi}; \quad (16)$$

$$\beta=\frac{1.1\times10^9}{k^{1.11}}; \quad (17)$$

$$\beta=\frac{7.64\times10^8}{k^{-1.72}}; \quad (18)$$

$$\beta=\frac{1.429\times10^3}{k^{-1.5}\varphi^{-0.5}}, \quad (19)$$

where β – Forchheimer correction factor, Pa^{-1}; k – absolute permeability, mD; φ – porosity, fractions of a unit. It should be noted that several correlations can be applied to the same formation types, while the resulting values of additional pressure loss can differ significantly. In this case, the averaging of D-factor values is often used. Below are the average parameters of the synthetic hydrodynamic model and the results of calculating the values β and D-factor using correlations that are relevant for DDB formations according to H. Saboorian-Jooybari & P. Pourafshary (2015). The values shown in Table 1 are typical for low permeability reservoirs of the DDB. The porosity of 0.24 corresponds to a permeability of only 0.02 mD.

Table 1. Average parameters of the synthetic hydrodynamic model

k, mD	*φ*	*μ*, centipoise	*h*, m	*kW*, m	visc.
0.02	0.24	0.02	25	0.75	0.72

Source: created by the authors

The thickness of this reservoir is 25 m, and the reservoir fluid viscosity was determined from the equation of state. The resulting values in Table 2 were used in the hydrodynamic modelling on the synthetic model. The 3D hydrodynamic model was built on the basis of the synthetic well W1, one of the DDB reservoirs.

Table 2. Results of calculations of β and D-factor for various correlation dependencies

Correlation	*β*	D-factor
(6)	5.34E+10	1.61E-04
(9)	3.68E+12	1.11E-02
(12)	1.71E+13	5.15E-02
(13)	2.80E+12	8.45E-03
(16)	1.92E+09	5.79E-06
(10)	6.14E+11	1.85E-03
(8)	9.07E+12	2.74E-02
(7)	2.58E+07	7.78E-08
(18)	4.35E+11	1.31E-03
(19)	7.69E+04	2.32E-10
Average value		1.02E-02

Source: created by the authors

This model was used to estimate the effect of additional pressure losses by applying the D-factors calculated in Table 2. A 5-stage hydraulic fracturing system was modelled for this well. Parameters of the resulting fractures, their height (*h*), thickness (*Dw*), half-length (*Xf*) and the resulting permeability (K_{prop}) are shown in Table 3. Visualisation of simulated fractures for well W1 is shown in Figure 1.

Table 3. Fracture parameters

h, m	*Dw*, m	*Xf*, m	w, m	K_{prop}, md
5	0.02	100	0.002	10,000

Source: created by the authors

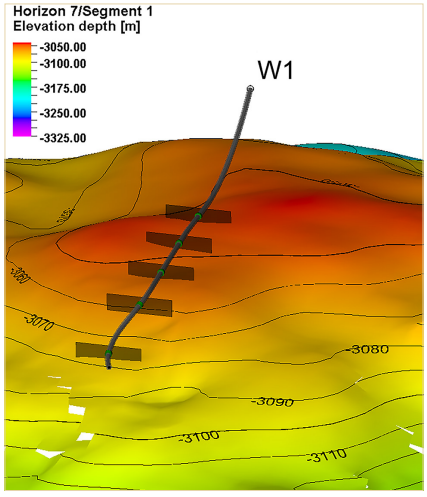

Figure 1. Visualisation of W1 well fractures

Source: created by the authors

The simulation was performed with a downhole pressure limit for well W1, at 180 bar. The initial pressure at the beginning of the simulation is 400 Bar. The reservoir developed by well W1 is composed of low-permeability reservoirs with an average permeability of 0.02 mD, while the average porosity is 0.26. The histograms of the porosity and permeability distribution throughout the reservoir are shown in Figure 2.

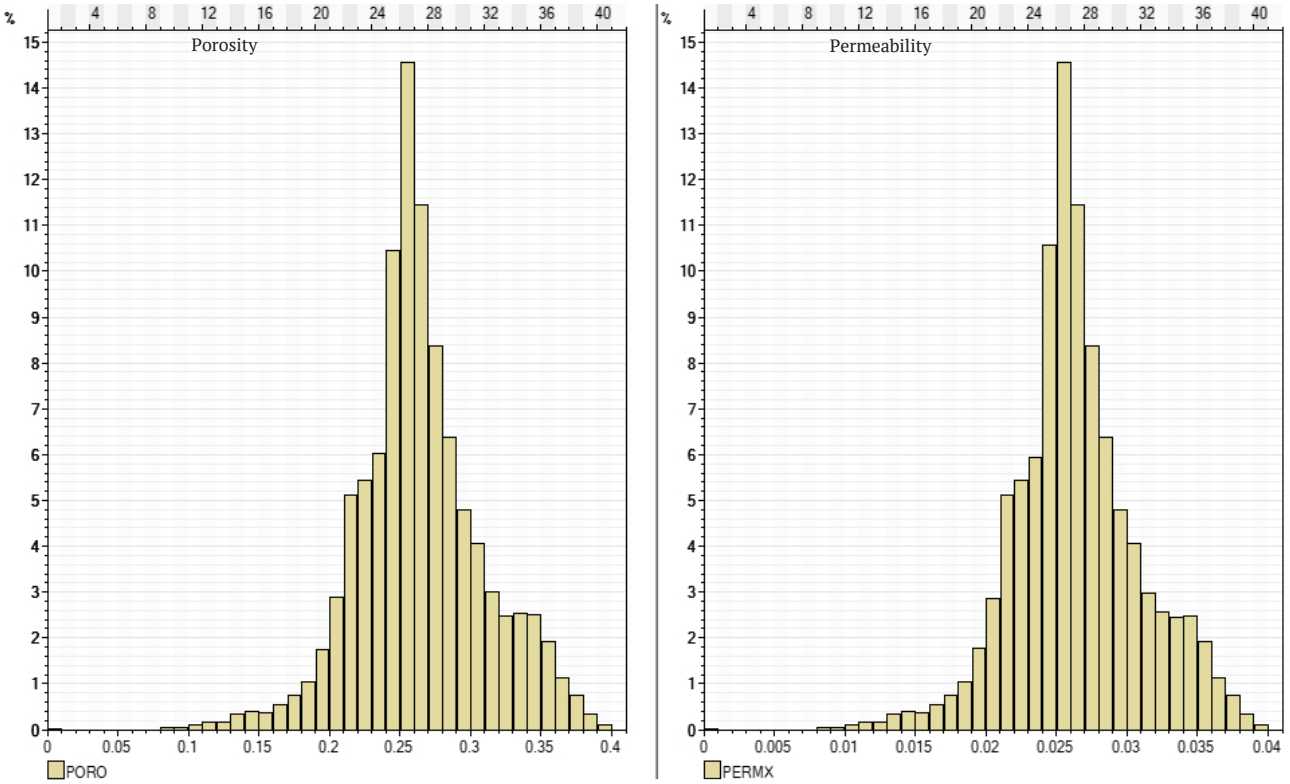

Figure 2. Histograms of porosity and permeability distribution in the formations

Source: created by the authors

The equation of state consists of 15 components, of which 3 are non-hydrocarbon. The composition is shown in Table 4. The equation of state was selected and calibrated in accordance with the behaviour of reservoir fluids under the relevant thermobaric conditions (Tpl – 133°C. Pressure – 400 bar). The results of adjusting the equation of state are shown in Figure 3.

The modified Peng Robinson equation was used as the equation of state. The resulting phase diagram and initial formation conditions are shown in Figure 4.

Table 4. Composition of the equation of state

No.	Component	%, mol
1	CO_2	2.98
2	H_2S	0.80
3	N_2	0.12
4	C_1	74.39
5	C_2	7.94
6	C_3	3.74
7	I-C_4	0.87
8	N-C_4	1.71
9	I-C_5	0.71
10	N-C_5	0.81
11	C_6	0.99
12	C_7	1.97
13	C_8	2.13
14	C_9	0.76
15	C_{10+}	0.08

Source: created by the authors

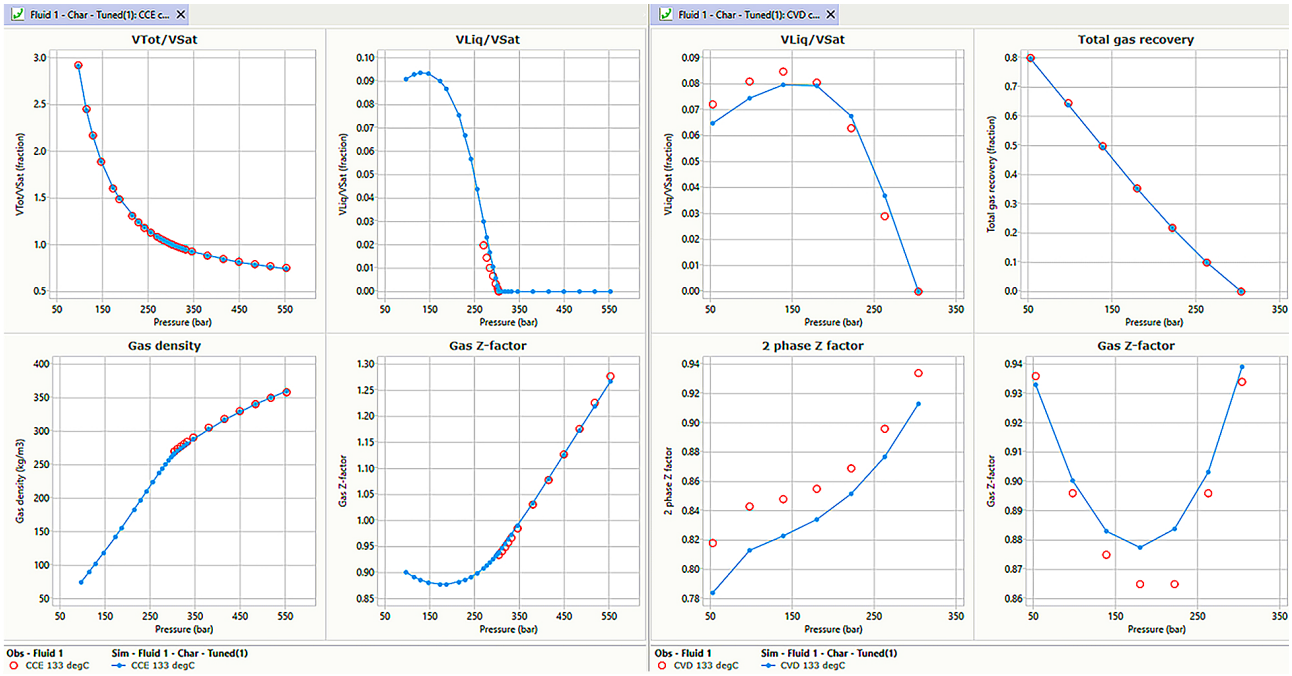

Figure 3. Results of equation of state adjustment,
constant composition expansion and constant volume depletion experiments

Source: created by the authors

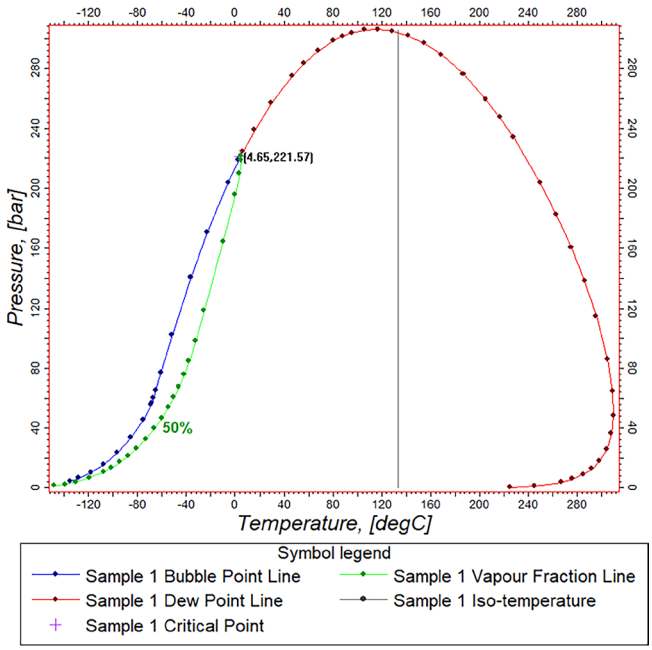

Figure 4. Phase diagram and initial formation conditions

Source: created by the authors

Relative phase permeabilities were used by analogy and were unified for the entire reservoir. Since the deposit is gas-condensate, condensate is taken as oil.

Figure 5 shows a single set of relative phase curves for the oil-water and oil-gas systems used in the model.

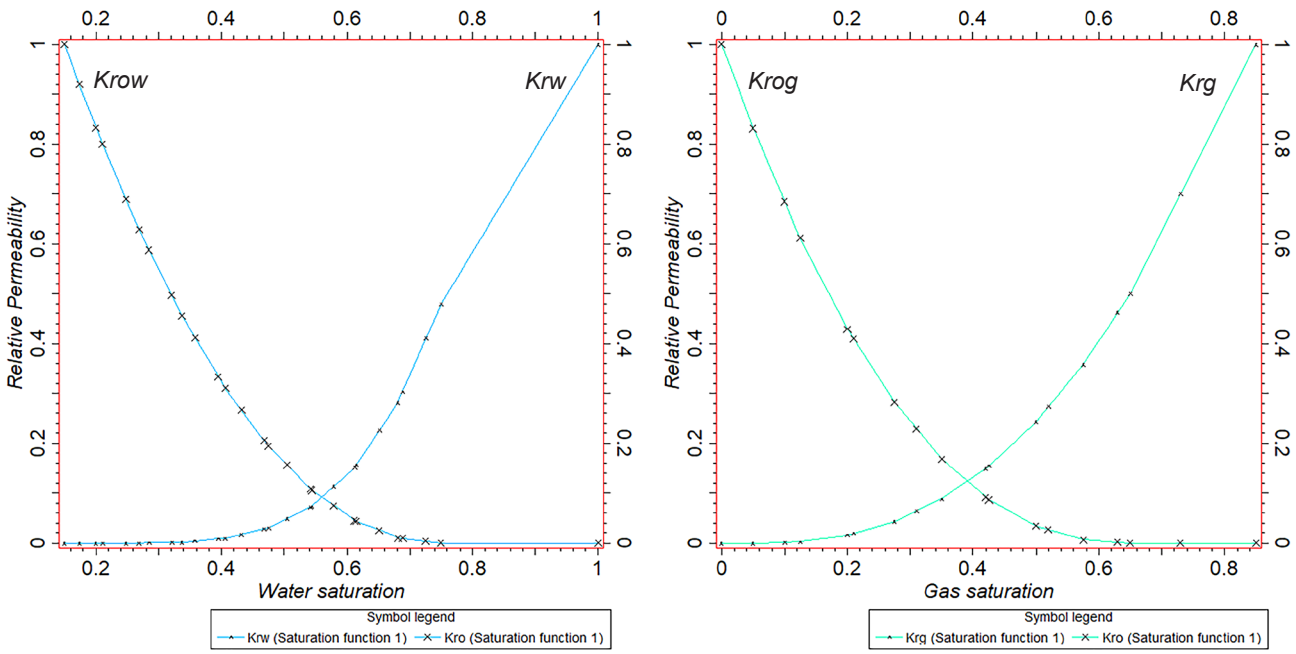

Figure 5. Relative phase permeability (oil-water, oil-gas)

Note: Krow – relative permeability to oil in presence of water; Krw – relative permeability to water; Krog – relative permeability to oil in presence of gas; Krg – relative permeability to gas

Source: created by the authors

Results and Discussion

Initial gas reserves after initialisation of the model amount to 2.7 billion m³, and initial condensate reserves – 1.05 million m³. The gas-water contact was established at a depth of –3,130 m. The initial distribution of water saturation is shown in Figure 6.

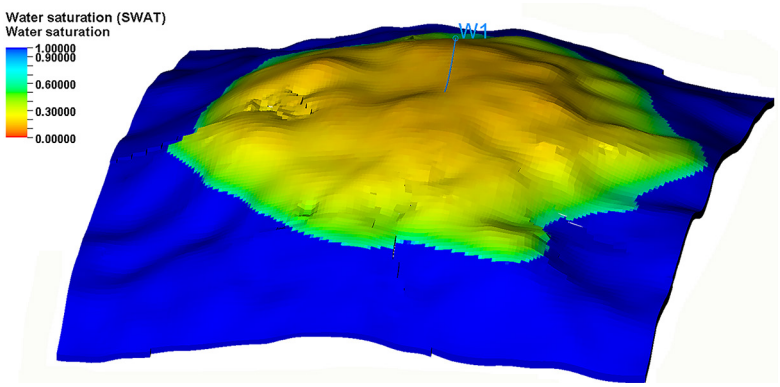

Figure 6. Initial water saturation distribution

Source: created by the authors

The simulation was run for 10 years; for comparison, the baseline scenario (red line) was first considered without taking into account additional pressure losses during reservoir fluid filtration at the Darcy's law limit (Fig. 7).

In this case, the initial flow rate of the well was 1 million m³/day, but within 2-3 months it decreased and stabilised at around 70 thousand m³/day. This is due to the relatively small stimulated volume and the rapid progression of the pressure drop to the limits of this volume. W1 almost immediately switches to 180 bar bottom-hole pressure control, as its productivity and drainage volume do not allow it to maintain a plateau for longer than 2-3 months with this fracture configuration. Projected accumulated gas production over 10 years amounted to 101 million m³, which corresponds to approximately 3% of the original gas volume. The resulting profiles of production, reservoir pressure drop and gas condensate factor (GCF) are shown in Figure 8.

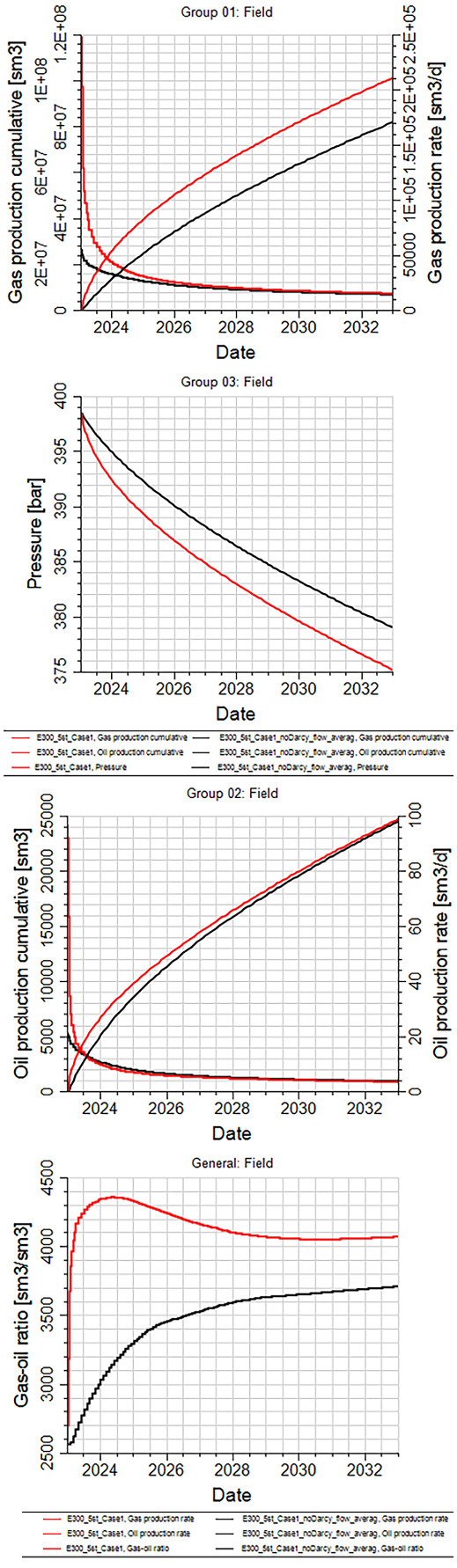

Figure 7. Comparison of the baseline and alternative scenario

Source: created by the authors

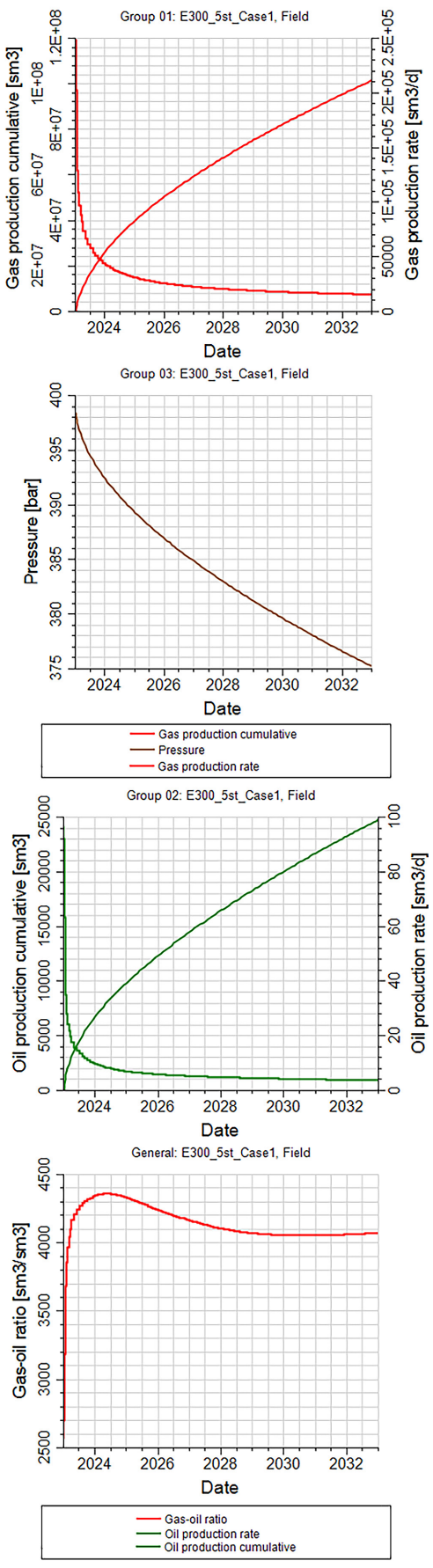

Figure 8. Production, pressure and GCF profiles for the baseline scenario

Source: created by the authors

As a rule, additional pressure losses due to filtration at the limit of Darcy's law (D-factor) are determined after processing well tests at different operating conditions using the method of A. Houpeurt (1959). However, these tests are rare for horizontal wells developing low-permeability manifolds. Therefore, due to the lack of data, typical correlations that are functions of the main reservoir filtration and capacitance properties, such as porosity, permeability, capacity or complexity of the pore channel system, have been widely used. Equations for determining β, containing τ – tortuosity of the pore channel system, which is not widely used due to the complexity of correctly determining this parameter. It should be noted that the correlations presented in this paper, some of which were used to determine the D-factor for the synthetic hydrodynamic model, showed a large discrepancy in the results. In the absence of well testing results in different operating modes, it is necessary to select a correlation from the literature, taking into account the lithology and average filtration and capacitance parameters. In the work of H. Saboorian-Jooybari & P. Pourafshary (2015), the limits of application of each correlation are given. For example, dependencies (14) and (15) are used for microscopic models in the explicit modelling of a pore channel system, which is not relevant to this study. Correlation (5) is generally applied when the presence of CO_2 or N_2 exceeds 5% in the formation fluid.

In order to account for the D-factor calculated in Table 3, an additional value was set in the simulation model in accordance with the Eclipse hydrodynamic simulator manual, using the required syntax in the simulation model. An alternative simulation was calculated using the average D-factor value from Table 3. According to the results of the alternative scenario (black line in Fig. 8), taking into account the average D-factor from Table 3, the initial gas flow rate of the W1 decreased from 1 million m^3/day up to 60 thousand m^3, at the same time, you can see that over time, the difference between the baseline and alternative scenarios decreases and almost disappears. This is due to a decrease in extraction and reservoir pressures. The greatest impact, as expected, is observed at high gas flow rates. The resulting accumulated gas production decreased from 101 million m^3 up to 83 million m^3, which is 17.8% less than the baseline scenario.

The addition of the pessimistic D-factor value from Table 3 (5.1 E-02, blue line in Fig. 9) and the optimistic value (1.6 E-04, green line in Fig. 9) and the subsequent sensitivity analysis result in a difference of 35 million m^3 in accumulated gas production, with the resulting curves of accumulated selections shown in Figure 9. This, in turn, will have a huge impact on economic indicators when designing a horizontal well in this field, for the purpose of its development. It should be noted that non-traditional collectors are usually developed by a large number of horizontal wells with hydraulic fracturing, so the influence of the D-factor can have an accumulated effect and an incorrect assessment of it can cancel the implementation of the project as a whole.

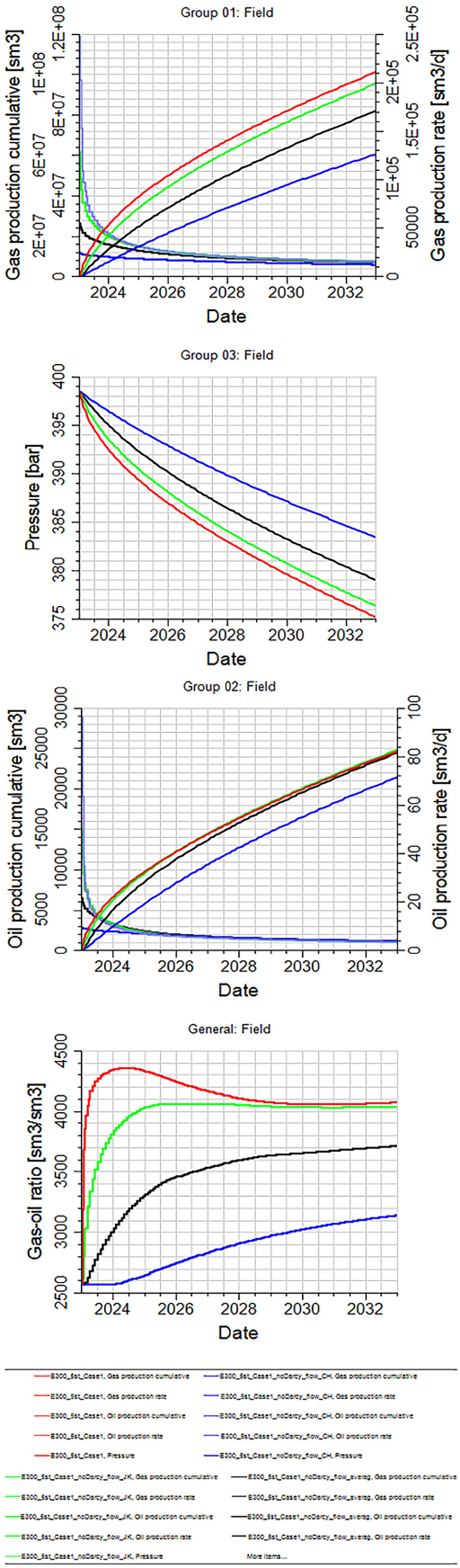

Figure 9. D-factor sensitivity analysis
Source: created by the authors

Accumulated gas withdrawals range between 60.7 million m³ (a decrease of almost 40% from the baseline scenario) and 95.7 million m³ (a 5% reduction from the baseline scenario). The results of a scenario with an average value of the D-factor are accepted as probable (P50), in order to correctly determine the optimistic (P10) and pessimistic (P90) scenarios and the range between them, which should correspond to the physical limits of the application of the D-factor, it is necessary to conduct a separate sensitivity analysis and determine the minimum and maximum values at which the change in the accumulated selections will not be noticeable. There is also an effect on the resulting stimulated volume and a significant difference between the baseline and alternative scenarios. Figure 10 and Figure 11 show the pressure distribution at the end of the forecast period of the baseline and alternative scenarios, respectively. The colour scheme clearly indicates a decrease in the area of the drained volume and a lower degree of reservoir depletion.

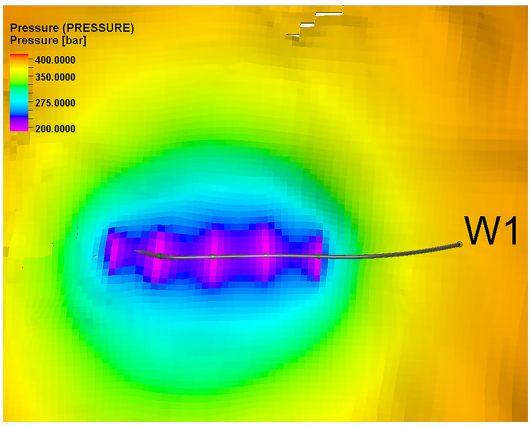

Figure 10. Pressure distribution at the end of the forecast period for the baseline scenario

Source: created by the authors

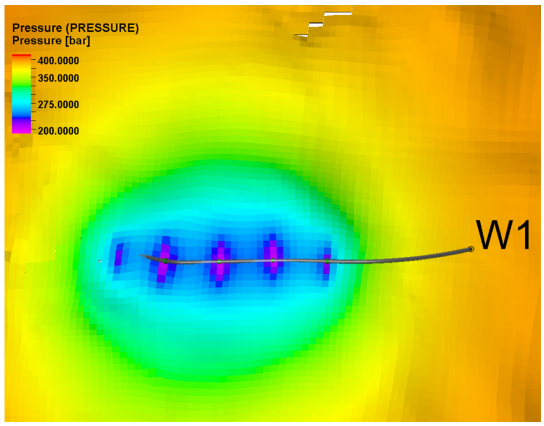

Figure 11. Pressure distribution at the end of the forecast period for the alternative scenario

Source: created by the authors

The obtained average value of the D-factor – 0.01 does not contradict the values obtained during other studies. For example, in the work of M.P. Ekeregbe (2023) the D-factor was determined by interpreting pressure recovery curves and typical curves. Values ranging from 0.013 to 0.04 were obtained, which were determined for different wells with different filtration and capacitive properties. Additional resistance coefficients were determined in this paper, compared with skin factors, and a number of flow rate dependencies were constructed. The author came to the conclusion that with an increase in the flow rate, the value of the D-factor and, in turn, the skin factor increased. The D-factor values for these dependencies varied from 0.04 to 0.07. The results of this study were supplemented with the proposed graphical method for integrating the dependence of the D-factor on the flow rate and skin factor, in order to determine the degree of fluid accumulation at the bottom of wells. The author distinguished into two separate categories the skin formed by the accumulation of fluid on the bottom-hole and the skin that depends on the speed of the upward flow. This methodology is interesting for approbation and further testing based on the results obtained in this study.

In addition to the parameters considered in this study, the work of H. Mustapha *et al*. (2015), added another, namely the effect of capillary pressure on deviation from filtration according to Darcy's law. According to their observations, capillary pressure mainly influenced the mobility of gas and water around fractures and significantly affected well productivity (up to 30%). However, in the case of the study presented in this article, the design of horizontal gas wells in low-permeability reservoirs is carried out with the maximum distance from the GCF, which minimises the appearance of water in the well production and ensures a single-phase (gas) or two-phase (gas + condensate) flow. In this case, the effect of capillary pressure on the phase distribution boundaries is minimal. However, the author noted that the influence of capillary forces can also have an impact on the level of matrix-fracture interaction, which is relevant for fractured reservoirs. The author emphasises the importance of a correct description of capillary forces using the example of the influence of the D-factor not only at the level of fractures but also in neighbouring cells. The degree of deviation from Darcy's law during filtration in fractures at different capillary pressures was also compared, and was up to 12%. However, the author noted that the uncertainties associated with the effect of capillary pressure are much larger than those associated with filtration at the Darcy's law limit and require additional analysis.

Research by S. Alakbarov & A. Behr (2020) showed a significant impact of the filtration effect on the boundaries of Darcy's law on a synthetic hydrodynamic model. However, during the simulation, the values of gas flow rates were around 750 thousand m³/day, while in this study the maximum flow rates reached only 250 thousand m³/day, and the effect of the additional coefficient of resistance was determined by the period during which the working bottom-hole pressure of the well reached the minimum values of 50 bar

(for two or more years), while in this study this occurred almost from the very beginning of the simulation, due to the significantly lower permeability between hydrodynamic models. Also in the article, S. Alakbarov & A. Behr (2020) took into account the effect of the resulting condensate shaft, when the pressure drops below the dew point pressure, when part of the pore space is occupied by condensate, and the resulting values of the gas filtration rate are lower, due to the concept of relative phase permeability.

It should be noted that this effect is also found in oil deposits with a high gas content, as demonstrated in the work by D. Li *et al*. (2020), where the D-factor was also used as one of the parameters for tuning the hydrodynamic model to historical measurements of the operating bottom-hole pressure. In other words, this parameter can be used not only to estimate the performance parameters of forecast wells, but also to adapt the operating bottom-hole pressure. In this case, the sensitivity analysis of the model to various parameters, including the D-factor, is used, the possible range of change of each parameter is determined, and the possible combined impact is estimated. A similar effect of high values of the upward flow rate can be observed in fractured reservoirs, when the matrix is characterised by minimal permeability and natural fractures satisfy high well productivity. Studies by L. Wang & W. Yu (2019) showed that even with successive injection and extraction of gas at high rates of both upstream and downstream flows, the filtration effect at the limit of Darcy's law significantly affects both well acceptability and productivity, and at some point, the dependence becomes non-linear. In such a situation, it is necessary to have a data set to calibrate the additional pressure losses arising from the fluid flow rate in the hydrodynamic model. In all of the above studies, the D-factor is one of the key parameters that affects productivity, but due to its uncertainty, it is often ignored by reservoir engineers when predicting key well performance indicators.

From the above, it is clear that ignoring the effect of reservoir fluid filtration outside the Darcy's law for both conventional and unconventional reservoirs will lead to an overestimation of production rates and accumulated production. The results presented in this paper and those of other authors once again emphasise the criticality of taking into account the additional resistance factor when predicting and drilling horizontal wells in low permeability reservoirs. However, this analysis should be accompanied by a set of additional parameters that will affect the resulting cumulative production as indicated by the authors and publications cited above. This should include such parameters as reservoir filtration and capacitance parameters, their change and heterogeneity (lateral and vertical), PVT (pressure, volume, temperature) fluid properties and condensation factor, capillary pressure, and projected well production rates.

Conclusions

Summarising the research topic, it was possible to focus on the feasibility of including such a parameter as the D-factor in the analysis when predicting the production profiles of horizontal wells developing low-permeable deposits after hydraulic fracturing. Analysing the results obtained, it is clear that ignoring additional pressure losses during reservoir fluid filtration at the limit of Darcy's law may lead to the need to reassess the forecast indicators of field development and the productivity of some wells characterised by high upstream rates. As can be seen from the sensitivity analysis on the example of W1, the revaluation can reach 40%, which is significant when calculating the economic indicators of the feasibility of drilling an expensive horizontal well or conducting a multi-stage hydraulic fracturing.

As expected, the greatest impact was observed at high gas flow rate values, i.e. with an increase in gas flow rate, the influence of the D-factor increases and vice versa, at minimum flow rate values, the influence of the D-factor is also minimal. As a result of sensitivity analysis, there is a decrease in accumulated gas production from 101 million m^3 to 83 million m^3, which is almost 18% less than the baseline scenario. For other scenarios, accumulated gas production ranged from 60.7 million m^3 (a decrease of almost 40% from the baseline scenario) and 95.7 million m^3 (5% decrease from the baseline scenario). However, the choice of correlation dependencies for calculating the D-factor should be reasonably approached and sensitivity analysis should be applied to cover the uncertainty field and generate scenarios such as P10 (optimistic), P50 (probable) and P90(pessimistic).

This work is planned to expand and investigate the influence of such parameters as PVT properties of fluids, namely condensate factor and retrograde processes occurring at the fracture level. Determine the component composition of condensate that falls out in the bottom-hole zone and blocks part of the pore space. The combined effect of D-factor and condensate shaft formation after multi-stage hydraulic fracturing is one of the further areas of this study that should be considered. It is also planned to implement the use of the D-factor in predicting the main development indicators on the example of a real DDB field and supplement this study. All these points are areas of further research.

Acknowledgements

None.

Conflict of Interest

None.

References

[1] Alakbarov, S., & Behr, A. (2020). Explicit numerical evaluation of productivity impairment in hydraulically fractured wells of gas condensate reservoirs. *SPE Petroleum Technology Conference*, 2020, article number SPE-201953-MS. doi: 10.2118/201953-MS.

[2] Barree, R.D., & Conway, M.W. (2004). Beyond beta factors: A complete model for Darcy, Forchheimer, and trans-Forchheimer flow in porous media. In *SPE annual technical conference and exhibition* (article number SPE-89325-MS). Houston: George R. Brown Convention Center. doi: 10.2118/89325-MS.

[3] Berawala, D.S., & Andersen, P.Ø. (2020). Numerical investigation of non-Darcy flow regime transitions in shale gas production. *Journal of Petroleum Science and Engineering*, 190, article number 107114. doi: 10.1016/j.petrol.2020.107114.

[4] Cornell, D., & Katz, D.L. (1953). Flow of gases through consolidated porous media. *Industrial and Engineering Chemistry*, 45(10), 2145-2152. doi: 10.1021/ie50526a021.

[5] Cramer, D.D. (2004). Analyzing well performance in hydraulically fractured gas wells: Non-ideal gases. In *SPE annual technical conference and exhibition* (article number SPE-90777-MS). Houston: George R. Brown Convention Center. doi: 10.2118/90777-MS.

[6] Darcy, H. (1856). *The public fountains of the city of Dijon*. Paris: Dalmont.

[7] Denney, D. (2005). Beyond beta factors: A model for Darcy, Forchheimer, and trans-Forchheimer flow in porous media. *Journal of Petroleum Technology*, 57(3), 43-45. doi: 10.2118/0305-0043-JPT.

[8] Ekeregbe, M.P. (2023). Determination of non-Darcy flow coefficient and completion skin from multi-rate test data with a decreasing effective skin. In *SPE Nigeria annual international conference and exhibition* (article number SPE-217119MS). Lagos: Expo Centre, Eko Hotel and Suites. doi: 10.2118/217119-MS.

[9] Elsanoose, A., Abobaker, E., Khan, F., Rahman, M.A., Aborig, A., & Butt, S.D. (2022). Characterization of a non-Darcy flow and development of new correlation of non-Darcy coefficient. *Energies*, 15(20), article number 7616. doi: 10.3390/en15207616.

[10] Ergun, S. (1952). Fluid flow through packed columns. *Chemical Engineering Progress*, 48(2), 89-94.

[11] Forchheimer, P. (1901). Water movement through soil. *Zeitschrift des Vereins Deutscher Ingenieure*, 45, 1781-1788.

[12] Ghahri, P., Jamiolahmady, M., & Sohrabi, M. (2011). Gas condensate flow around deviated and horizontal wells. In *SPE EUROPEC/EAGE annual conference and exhibition* (article number SPE-143577-MS). Vienna: Society of Petroleum Engineers. doi: 10.2118/143577-MS.

[13] Hart, A.F., & Omobolanle, O.C. (2023). Darcy-Forchheimer's model: Application in hydraulic fracturing design and optimisation. In *SPE Nigeria annual international conference and exhibition* (article number SPE-217106-MS). Lagos: Expo Centre, Eko Hotel and Suites. doi: 10.2118/217106-MS.

[14] Houpeurt, A. (1959). On the flow of gases in porous media. *Revue de L'Institut Francais du Pétrole*, 14(11), 1468-1684.

[15] Jones, B.R., van Rooy, J.L., & Dippenaar, M.A. (2020). *Non-Darcian flow in unsaturated rock masses: Implications for permeability assessments*. In *ISRM international symposium – EUROCK* (article number ISRM-EUROCK-2020-134). Trondheim: Clarion Hotel & Congress.

[16] Li, D., Corneliu-Liviu, I., Ehighebolo, I.T., Byron, H.Jr., Zhazbayeva, A., Yergaliyeva, B., & Francia, L. (2022). Modeling and simulation of non-Darcy or turbulent flow for oil wells. In *SPE annual Caspian technical conference* (SPE-212067-MS). Astana: Hilton Astana. doi: 10.2118/212067-MS.

[17] Ma, H., & Ruth, D. (1993). Physical explanations of non-Darcy effects for fluid flow in porous media. *SPE Formation Evaluation*, 12(01), 13-18. doi: 10.2118/26150-PA.

[18] Mustapha, H., de Langavant, L., & Ann Giddins, M.A. (2015). Darcy and non-Darcy flows in fractured gas reservoirs. In *SPE reservoir characterisation and simulation conference and exhibition* (article number SPE-175596). Abu Dhabi: Society of Petroleum Engineers. doi: 10.2118/175596-MS.

[19] Olsen, K.E., Haidar, S., Milton-Tayler, D., & Olsen, E. (2004). Multiphase non-Darcy pressure drop in hydraulic fracturing. In *SPE annual technical conference and exhibition* (article number SPE-90406-MS). Houston: George R. Brown Convention Center. doi: 10.2118/90406-MS.

[20] Saboorian-Jooybari, H., & Pourafshary, P. (2015). Non-Darcy flow effect in fractured tight reservoirs: How significant is it at low rates and away from wellbores. In *SPE Middle East unconventional resources conference and exhibition* (SPE-172948-MS). Muscat: Al Bustan Palace. doi: 10.2118/SPE-172948-MS.

[21] Van Batenburg, D., & Milton-Tayler, D. (2005). Discussion of SPE 89325, "Beyond beta factors: A complete model for Darcy, Forchheimer, and trans-Forchheimer flow in porous media". *Journal of Petroleum Technology*, 57(8), 72-74. doi: 10.2118/0805-0072-JPT.

[22] Wang, L., & Yu, W. (2019). Mechanistic simulation study of gas puff and huff process for Bakken tight oil fractured reservoir. *Fuel*, 239, 1179-1193. doi: 10.1016/j.fuel.2018.11.119.

[23] Zeng, F., & Zhao, G. (2010). The optimal hydraulic fracture geometry under non-Darcy flow effects. *Journal of Petroleum Science and Engineering*, 72(1-2), 143-157. doi: 10.1016/j.petrol.2010.03.012.

[24] Zhou, J.-Q., Chen, Y.-F., Tang, H., Wang, L., & Cardenas, M.B. (2019a). Disentangling the simultaneous effects of inertial losses and fracture dilation on permeability of pressurized fractured rocks. *Geophysical Research Letters*, 46, 8862-8871. doi: 10.1029/2019GL083355.

[25] Zhou, J.-Q., Chen, Y.F., Wang, L., & Cardenas, M.B. (2019b). Universal relationship between viscous and inertial permeability of geologic porous media. *Geophysical Research Letters*, 46, 1441-1448. doi: 10.1029/2018GL081413.

Визначення D-фактору та його вплив на стимульований об'єм ущільнених газонасичених колекторів

Олег Лукін

Аспірант
Івано-Франківський національний технічний університет нафти і газу
76019, вул. Карпатська, 15, м. Івано-Франківськ, Україна
https://orcid.org/0009-0005-5194-628X

Олександр Кондрат

Доктор технічних наук, професор
Івано-Франківський національний технічний університет нафти і газу
76019, вул. Карпатська, 15, м. Івано-Франківськ, Україна
https://orcid.org/0000-0003-4406-3890

Анотація. Коректна оцінка можливого об'єму заміщення фонду структур традиційних колекторів ущільненими пісковиками / карбонатами діючих родовищ і районів видобувної діяльності є дискусійним питанням не лише в Україні, а й за кордоном, що викликано параметричною невизначеністю та впливом особливостей фільтрації пластових флюїдів у нетрадиційних колекторах. Це призводить до завищення прогнозних показників розробки ущільнених газонасичених колекторів, зменшення коефіцієнту заміщення та збільшення темпів падіння видобутку. Тому метою дослідження була оцінка впливу коефіцієнта додаткового опору фільтрації, що виникає у зв'язку з великою швидкістю висхідного потоку флюїду як одного з ключових невизначених параметрів, на продуктивність свердловин та результуючі накопичені відбори газу. Проведено багатостадійний гідророзрив пласта в синтетичній горизонтальній свердловині, що була створена в програмному забезпеченні Petrel. За допомогою типових кореляцій визначено коефіцієнти додаткового опору (D-фактору) та побудовано гідродинамічну модель у програмному забезпеченні Eclipse. Проведено симуляції з різним значенням D-фактору для визначення його впливу на продуктивність на накопичені відбори для одного типу породи. Результати дослідження свідчать, що переоцінка може сягати 40 %, що є суттєвим під час підрахунку економічних показників доцільності буріння та проведення багатостадійного гідророзриву пласта. Запропонована вибірка та методологія для низькопроникних пластів, що зустрічаються на родовищах Дніпровсько-Донецької западини України, може бути використана газо- та нафтовидобувними компаніями для деталізованого аналізу невизначеностей та коректного планування стабілізації темпів падіння видобутку газу

Ключові слова: коефіцієнт додаткового опору; фільтрація флюїдів; багатостадійний гідророзрив пласта; симуляція; дебіт свердловини

Vol. 24, No. 1
2024

PROSPECTING AND DEVELOPMENT OF OIL AND GAS FIELDS

https://pdogf.com.ua/en

Received: 28.12.2023. Revised: 26.04.2024. Accepted: 31.05.2024

UDC 622.276:004.896

DOI: 10.69628/pdogf/1.2024.23

Study of the kinematic field of mixed flows

Oleksandr Panevnyk*

Doctor of Technical Sciences, Professor
Ivano-Frankivsk National Technical University of Oil and Gas
76019, 15 Karpatska Str., Ivano-Frankivsk, Ukraine
https://orcid.org/0000-0003-2765-3776

Abstract. The relevance of the study is determined by the ability of borehole jet pumps to increase the efficiency of technological processes in difficult mountainous and geological conditions. The aim was to establish the laws of transformation of the velocity profile in the production inlet chamber of a borehole jet pump based on the construction and subsequent analysis of the distribution of kinematic parameters of the total working and injected flows. Simulation of the operating process of the ejection system was performed in the ANSYS software and calculation module for four three-dimensional models of a borehole jet pump. The geometric models are constructed with an uneven density of calculation elements in places of complex geometry and a high gradient of hydrodynamic parameters. For each of the studied models, a series of velocity profiles placed at regular intervals at different distances from the pump throat section of the production inlet chamber was constructed. The constructed velocity profiles include sections with uniform and nonlinear distribution of kinematic parameters of mixed flows. It is established that the maximum values of the velocity of mixed flows are present on the axis of the jet pump and are the same for all the studied models. The axial velocity of the mixed flows decreases as the distance to the pump throat section of the production inlet chamber increases. The minimum axial velocity was obtained for a jet pump model with a maximum production inlet chamber length. For two models of a jet pump with a production inlet chamber length of 287 mm and 328 mm, stabilisation of the axial velocity values of the total working and injected flows was obtained. The immutability of kinematic parameters for these jet pump models indicates the completion of the process of equalising the velocities of mixed flows. Taking into account that if the required dimensions of the kinematic stabilisation section are exceeded, hydraulic losses in the flow part of the ejection system increase, its optimal design corresponds to a model with a jet pump production inlet chamber length of 287 mm. The practical value of the study lies in the fact that this design provides the maximum efficiency of a borehole jet pump

Keywords: borehole jet pump; ejection system; production inlet chamber; velocity profile; kinematic parameter distribution; flow stabilisation

Introduction

The rapid pace of global energy consumption has contributed to the search for alternative methods for the exploration of hydrocarbon deposits, a special group of which includes technologies for using jet pumps. The main benefits of using ejection technologies include preserving the natural permeability of productive horizons during their initial discovery, increasing the life of aging oil and gas fields, increasing well productivity during bottom-hole cleaning, implementing oil production stimulation methods, and preventing environmental pollution in hydrocarbon extraction and processing systems. The use of eddy current pumps contributes to increasing the energy efficiency of pipeline transportation of oil and petroleum products. The inclusion of jet pumps in the technological pipeline branching system helps to reduce the cost of transporting high-viscosity oils with a significant formation fluid content. The prevalence of oil and gas ejection technologies indicates their global importance and the relevance of research aimed at improving the efficiency of operation of borehole jet pumps.

V. Kotak *et al*. (2023) found that despite the simple design, the jet pump's operating process is based on the

Suggested Citation: Panevnyk, O. (2022). Study of the kinematic field of mixed flows. *Prospecting and Development of Oil and Gas Fields*, 24(1), 23-31. doi: 10.69628/pdogf/1.2024.23.

*Corresponding author

implementation of a complex mixing mechanism for coaxial potential flows separated by a boundary turbulent layer of variable structure with an uneven profile of hydrodynamic parameters. Significant complications in predicting the operating process of jet pumps are also associated with an increased tendency for cavitation phenomena to occur in their flow parts. According to J. Gan *et al*. (2022), the probability of loss of flow continuity increases with operating ejection systems with a centrally located working nozzle. Scientists Y.-D. Cho & U. Shrestha (2020) concluded in their paper that cavitation phenomena can also occur when using annular jet pumps. The solution of the system of equations that characterise the interaction of mixed flows is usually carried out by an approximate method by neglecting the value of individual components, which reduces the efficiency of modelling the operating process of a jet pump. Based on the research results of A. Kurniawan *et al*. (2023), the use of numerical simulation modelling and modern software packages makes it possible to increase the reliability of the choice of design and operating parameters of borehole gas ejection systems. In particular, in the process of modelling the interaction of gas flows, the optimal ratio of the cross-sectional areas of the production inlet chamber and the nozzle of the gas ejector is established.

Increasing the reliability of predicting the characteristics of a jet pump is provided by using neural network models, as indicated by K. Xu *et al.* (2021). In the process of optimising the flow part of the jet pump, an increase in the pressure created by it by 30.46% was obtained. By combining computational fluid dynamics (CFD) with the Kriging correlation model, K. Xu *et al.* (2020) established an optimal relationship between the flow configuration of an annular jet pump and the ratio of injection and operating flow rates. Based on the results of modelling a single-phase flow vortex in a shear layer between the operating and injected flow using a Reynolds-averaged system of Navier-Stokes equations and experimental measurements, A. Morrall *et al.* (2020) determined the influence of the nozzle diameter and flow swirl on the performance of the jet pump. The swirling of the flow due to centrifugal forces allows for an increase in the injection coefficient of the jet device. Scientists A. Rogovyi & S. Lukianets (2022) established the effect of swirling mixed flows on the energy efficiency of using jet devices. Based on the solution of the Reynolds, continuity and Rayleigh-Plesset equations in the Ansys CFX software package, it is shown that the swirling of mixed flows can double the efficiency of the jet device. The use of SNAP-type software to analyse the characteristics of a borehole jet pump makes it possible to increase the efficiency of using special application programmes, as described by E. Zafarullah *et al*. (2021). The analysis of the relationship between the productive horizon and surface equipment obtained using this software helped to increase the well flow rate by 42.9%.

A significant amount of research is devoted to optimising the design of borehole jet pumps. In the CFD process of modelling the operating process of the gas ejector, V. Kumar *et al*. (2019) found that the maximum ejection coefficient corresponds to zero distance between the working nozzle and the production inlet chamber of the jet machine. In the process of numerical modelling, Z. Wang *et al.* (2023) determined that the optimal value of the main geometric parameter of an oil jet pump provides a 10% increase in the efficiency of the borehole ejection system. The obtained result was confirmed in the course of experimental tests of an oil jet pump using orthogonal lattices developed by the Taguchi method during the planning of the experiment. By solving the Navier-Stokes equations of motion of a three-dimensional stationary flow for five models of the ejection system, Y. Yang *et al.* (2023) established the significant influence of the geometric dimensions of the diffuser on the formation of inhomogeneous eddy reverse currents in the flow part of the jet pump, which reduces its performance. The conducted studies have determined the optimal value of the production inlet chamber diameter from the point of view of ensuring maximum performance of the jet pump, which is 16-17 mm.

In the course of the analysis, it was found that when modelling the operating process of a jet pump, the influence on its characteristics of the hydrodynamic parameters of the environment, the physical properties of the mixed flows, the configuration of the elements of the ejection system, the ratio of the cross-sectional areas of the production inlet chamber and the working nozzle, their relative orientation, and the parameters of the diffuser part are usually studied. At the same time, the influence of the nature of the velocity distribution in the production inlet chamber of a jet pump on the features of its operating process is insufficiently studied. The analysis of the kinematics of mixed flows for an incompressible working medium makes it possible to optimise the borehole jet pump's operating process and increase the efficiency of oil and gas ejection technologies. The study aimed to establish regularities of transformation of the velocity profile in the production inlet chamber of a borehole jet pump. This goal involved performing the following research tasks: constructing velocity profiles of the operating and injected flows along the production inlet chamber of the jet pump; establishing the nature of changes in the maximum velocities of the mixed flows; determining the length of the velocity stabilisation section in the production inlet chamber of the jet pump.

Materials and Methods

Determining the nature of the velocity distribution of the operating and injected flows along the production inlet chamber of the jet pump involved the following stages of research: construction of a geometric model of a borehole jet pump; selection of boundary surfaces of the design volume and boundary parameters of the operation of the borehole jet pump; construction of a grid (design) model of the borehole jet pump; solving the system of equations obtained using the finite element method. The construction of mixed flow velocity profiles was carried out for four models of a jet pump with the following geometric characteristics: diameter of the working nozzle d_w = 14 mm;

production inlet chamber diameter d_i = 28 mm; basic geometric parameter of the jet pump K_{jp} = 4.0; absolute length production inlet chambers L_{i1} = 164 mm; L_{i2} = 246 mm; L_{i5} = 287 mm; L_{i4} = 328 mm; relative length of the production inlet chamber $\bar{L}_{i1} = \frac{L_{i1}}{d_i}$ = 5.86; $\bar{L}_{i2} = \frac{L_{i2}}{d_i}$ = 8.79; $\bar{L}_{i3} = \frac{L_{i3}}{d_i}$ = 10.25; $\bar{L}_{i4} = \frac{L_{i4}}{d_i}$ = 11.71; diffuser diameter d_d = 71 mm; diffuser length L_d = 280 mm.

Due to the design features of the jet pump, the typical cross-sections of the ejection system were used in the process of allocating the calculated volume (Chen *et al.*, 2020). The calculated volume was limited to the surfaces drawn at the inlet of the operating flow to the working nozzle, at the inlet of the injected flow to the receiving chamber, and at the outlet of the mixed flow from the jet pump diffuser. When choosing the restrictions imposed on the allocated design volume, the generally accepted ratio of hydrodynamic parameters is used in the form of a combination of flow rates and pressures of operating, injected and mixed flows (Deng & Dong, 2021). The boundary conditions in the process of modelling the operation of the four jet pump models were set by the corresponding flow rates of the mixed flows and pressures in the characteristic cross-sections of the borehole ejection system. Considering that for a given jet pump design, the maximum efficiency (efficiency factor) of the ejection system corresponds to the value of the injection coefficient i = 1.0, when justifying the choice of boundary conditions, the same values of the flow rates of the operating and injected flow are assumed $Q_p = Q_i$. In the studied models of the jet pump, the liquid velocity of the injected flow at the inlet to the production inlet chamber was 40 m/s, and the working flow was 100 m/s.

In the process of constructing a calculated model of a borehole jet pump, the geometric model is divided into finite elements according to the specified grid parameters. The process of building a calculation model is implemented using the built-in grid creation module in the ANSYS software product – ANSYS Meshing (Fig. 1). The constructed geometric model corresponds to zero distance between the working nozzle and the production inlet chamber of the jet pump.

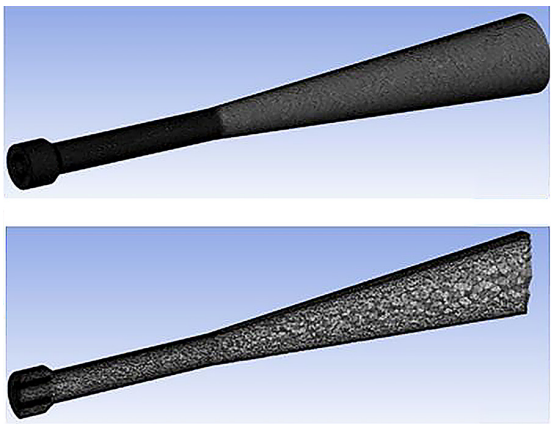

Figure 1. Calculation grid of a three-dimensional jet pump model

Note: a – internal volume of the jet pump model; b – its section
Source: created by the author

In order to reduce the duration of calculation operations while maintaining the required accuracy, an uneven density of the calculation grid was used when constructing the geometric model. The higher density of the calculated elements corresponds to the working nozzle and the receiving chamber of the internal volume of the jet pump, and the lowest density corresponds to the output section of the diffuser. For each of the studied models, a series of velocity profiles for different distances X from the inlet cross-section of the production inlet chamber in increments ΔX = 20.5 mm is constructed. Due to the different geometric dimensions of the studied models, the number of constructed profiles increases with increasing length of the production inlet chamber of the jet pump.

Modelling of the jet pump operation process was carried out in the ANSYS software and calculation module Fluent, which provides high accuracy in solving problems related to the complex interaction of mixed flows. In the process of creating the computational model, the following parameters were chosen: the type of calculator is "pressure based", which is developed and traditionally used for incompressible media; the turbulence model is k-epsilon (standard) with standard wall functions. The adopted turbulence model focuses on mechanisms that affect the turbulent kinetic energy, and allows us to take into account processes in the boundary shear layer of variable width between the operating and injected flow with a high degree of reliability.

Results

According to the classical scheme of interaction of submerged jets, the operating flow flowing out of the working nozzle gradually expands due to the addition of the injected liquid and connects to its walls at a certain distance from the inlet section of the production inlet chamber (Fig. 2). The jet boundaries are delineated by straight lines i-i, and they have an unequal slope to the pump axis in the initial and final sections.

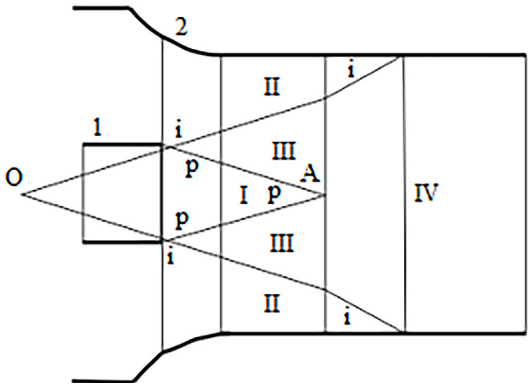

Figure 2. Flow structure in the production inlet chamber of a jet pump

Note: 1 – working nozzle; 2 – production inlet chamber
Source: created by the author

The i-i lines separating the working jet pass through its pole (point O). In the central part of the operating jet

there is a potential core I, bounded by the lines p-p, whose width decreases with a constant rate along the flow and takes on zero values at point A. The injected flow moving in the production inlet chamber (area II) has the form of an annular confuser. Areas I and II are zones of unbroken potential flow with constant values of the axial velocity along the length of the production inlet chamber. Between areas I and II, a slow-motion zone is formed (area III) – a boundary turbulent layer in which two flows mix). The most difficult area to analyse is area III, which is characterised by an incoherently variable velocity profile. Area III ends with the establishment of a fully developed current. Areas I, II, and III thus form a three-layer flow structure, the outer and central layers of which are marked by a close to uniform velocity profile, and the internal shear flow is characterised by intense eddy formation and an uneven distribution of kinematic parameters.

In area IV, the alignment of the speed profiles continues, and the mixing process of the operating and injected flows is completed. Depending on the geometric dimensions of the elements of the flow part of the jet pump and the hydrodynamic parameters of the mixed flows, point A may be located to the right of the contact section of the line i-i with the wall of the production inlet chamber. The flows of the operating and injected medium enter the production inlet chamber, where the velocity equalisation occurs, usually accompanied by an increase in pressure (Fig. 3).

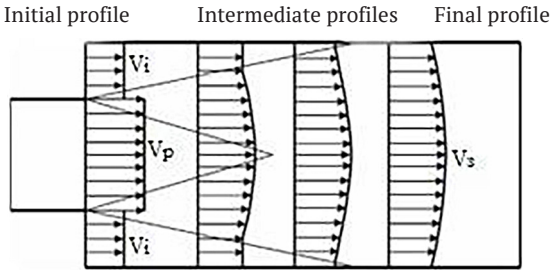

Figure 3. Dynamics of changing velocity profiles in the production inlet chamber of a jet pump

Source: created by the author

The central (operating) jet enters the production inlet chamber at a uniform speed V_p. The peripheral (injected) flow also has a uniform V_i but lower speed V_i, $<V_p$. A significant difference in velocities is the reason for the formation of a boundary turbulent layer in which energy dissipation occurs. Significant losses associated with mixing flows are the reason for the low efficiency of the jet pump. The initial velocity profile is marked by a uniform distribution of kinematic parameters of the operating and injected flow, which characterises the potential flow movement. When moving away from the inlet section of the production inlet chamber, the profile section decreases with a uniform distribution of the operating and injected flow rates. Intermediate velocity distributions are characterised by constant values of the speed of the operating and injected flows, respectively, in the central and peripheral parts of the production inlet chamber. The final velocity distribution is parabolic in nature and does not contain sections of a uniform profile. The constant velocity profile is maintained until the initial cross-section of the production inlet chamber (Fig. 4).

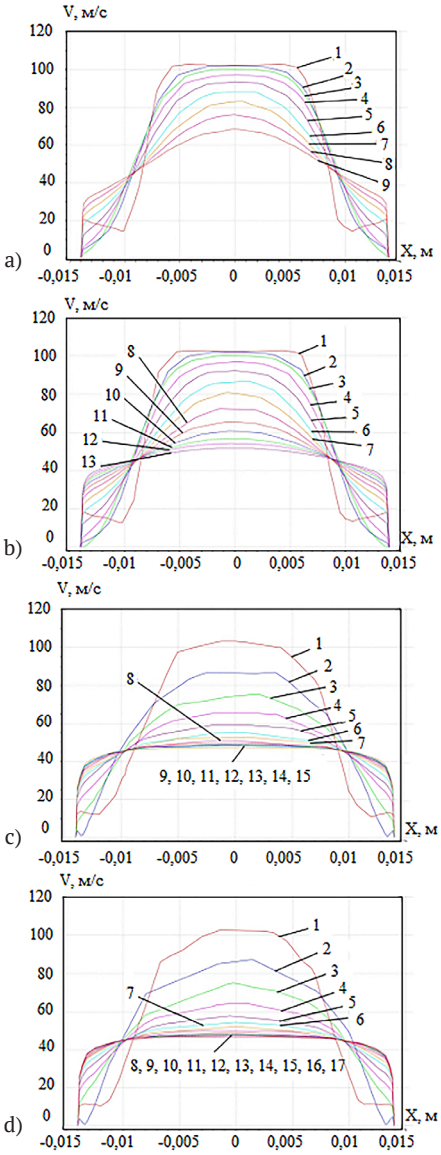

Figure 4. Velocity profiles for different distances *X* from the inlet section

Note: a) production inlet chamber length 164 mm: 1 – 0, 2 – 20.5 mm, 3 – 41 mm, 4 – 61.5 mm, 5 – 82 mm, 6 – 102.5 mm, 7 – 123 mm, 8 – 143.5 mm, 9 – 164 mm; b) production inlet chamber length 246 mm: 1 – 0, 2 – 20.5 mm, 3 – 41 mm, 4 – 61.5 mm, 5 – 82 mm, 6 – 102.5 mm, 7 – 123 mm, 8 – 143.5 mm, 9 – 164 mm, 10 – 184.5 mm, 11 – 205 mm, 12 – 225.5 mm, 13 – 246 mm; c) production inlet chamber length 287 mm: 1 – 0, 2 – 20.5 mm, 3 – 41 mm, 4 – 61.5 mm, 5 – 82 mm, 6 – 102.5 mm, 7 – 123 mm, 8 – 143.5 mm, 9 – 164 mm, 10 – 184.5 mm, 11 – 205 mm, 12 – 225.5 mm, 13 – 246 mm, 14 – 266.5, 15 – 287 mm; d) production inlet chamber length 328 mm: 1 – 0, 2 – 20.5 mm, 3 – 41 mm, 4 – 61.5 mm, 5 – 82 mm, 6 – 102.5 mm, 7 – 123 mm, 8 – 143.5 mm, 9 – 164 mm, 10 – 184.5 mm, 11 – 205 mm, 12 – 225.5 mm, 13 – 246 mm, 14 – 266.5, 15 – 287 mm, 16 – 307.5 mm, 17 – 328 mm

Source: created by the author

Alignment of the mixed flow velocity field is provided with the appropriate length of the production inlet chamber of the jet device. If the length of the production inlet chamber is insufficient, the deterioration of the pump characteristics is associated with the incomplete flow mixing process. If the required length of the mixing chamber is exceeded, hydraulic losses in the flow part of the jet pump increase and the pressure created by it decreases. Calculating the length of the mixed flow velocity field alignment section allows to determine the optimal length of the production inlet chamber of the jet pump from the point of view of ensuring minimal energy consumption. Despite the different distances to the inlet cross-section of the production inlet chamber, the calculated velocity profiles include several characteristic sections (Fig. 4). The central part of the profile is marked by a uniform or eccentric distribution of kinematic parameters, and its peripheral part has a uniform or nonlinear profile. Between the central and peripheral parts is a section of a nonlinear profile with a configuration that varies depending on the distance to the entrance to the production inlet chamber.

The width of the central section of uniform velocities decreases when the section under study is removed from the entrance to the production inlet chamber. For all the studied profiles, the maximum values of the movement velocity of mixed flows occur on the axis of the jet pump. As the distance to the inlet section of the production inlet chamber increases, the axial velocity of the mixed flows decreases. Thus, the qualitative change in the configuration of the velocity profiles of the total operating and injected flows along the production inlet chamber of the jet pump shown in Figures 2-3 is confirmed. For the studied jet pump models, the axial velocity of the mixed flows varies in the range: for a production inlet chamber with a length of 164 mm: from V_{max} = 102 m/s to V_{min} = 68 m/s; for a 246 mm production inlet chamber: from V_{max} = 102 m/s to V_{min} = 52 m/s; for a production inlet chamber with a length of 287 mm: from V_{max} = 102 m/s to V_{min} = 48 m/s; for a 328 mm production inlet chamber: from V_{max} = 102 m/s to V_{min} = 47 m/s. The maximum values of the movement velocity of mixed flows are the same for all the studied models, and the minimum value of kinematic parameters decreases with increasing length of the production inlet chamber. The change in axial velocities along the production inlet chamber for all the models under consideration is determined by an asymptotic relationship (Fig. 5).

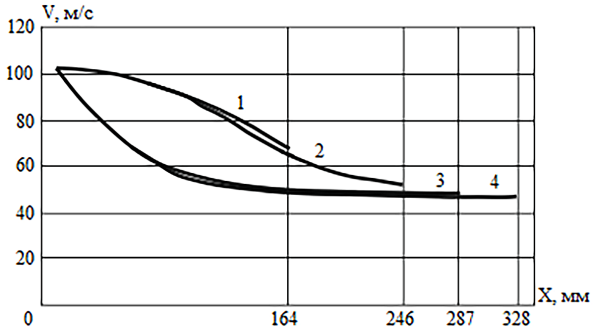

Figure 5. Change of the axial velocity along the production inlet chamber of different lengths
Note: 1 – L_{i1} = 164 mm; 2 – L_{i2} = 246 mm; 3 – L_{i3} = 287 mm; 4 – L_{i4} = 328 mm
Source: created by the author

According to the results obtained for models with a production inlet chamber length L_{i1} = 164 mm and L_{i2} = 246 mm, the axial velocity of the mixed flow decreases from the inlet to the output section. For these jet pump sizes, the speed equalisation process is not completed, which reduces the efficiency of the ejection system. For models with a production inlet chamber length of L_{i3} = 287 mm and L_{i4} = 328 mm when approaching the initial cross-section, the axial velocity takes constant values, which indicates the alignment of the velocity profile and the completion of the mixing process. Thus, in order to reduce hydraulic losses in the flow part of the jet pump, it is necessary to use a production inlet chamber with a length of L_{i3} = 287 mm (L_{i3} = 0.25).

Discussion

Based on the study of the operating process of the ejection system using the ANSYS Meshing and ANSYS Fluent software modules as part of the pressure-based calculator and the k-epsilon turbulence model, velocity profiles of the total operating and injected flows were constructed for different distances to the inlet cross-section of the jet pump production inlet chamber. The consistency of the results obtained should be analysed in comparison with the research materials of other authors. According to Y. Qian *et al*. (2021), the maximum efficiency of the jet device corresponds to the relative length of the production inlet chamber , which varies in the range from 2.5 to 4.0. This range of optimal ratios of the production inlet chamber length of the jet device was obtained in the process of numerical and experimental study of the features of transportation of various operating media with a significant content of solid inclusions. In the course of simulation modelling, a model of a jet pump was used with the diameters of the output cross-section of the working nozzle and the production inlet chamber of 8 mm and 32 mm, respectively. The nature of the interaction of mixed flows obtained in the CFD modelling process confirms the existence of an extreme dependence of the efficiency of the jet device on the length of

the production inlet chamber. The ratio of cross-sectional areas of mixed and operating flows in a jet device for hydraulic transport is twice as high as the similar parameter of the models studied by the author, as a result of which the path required for levelling the velocity profiles of mixed flows and the optimal length of the production inlet chamber are reduced.

Ye.I. Kryzhanivskyi & D.O. Panevnyk (2019) developed a three-layer mathematical model of mixing flows in the form of coaxial potential flows with a uniform velocity distribution and a variable structure with an algebraic velocity profile placed between them. Using the theory of a submerged jet moving in a concurrent flow, the flow structure at the inlet to the production inlet chamber of a jet pump is analysed, and the possibility of modelling the process of mixing coaxial flows in the form of automodel velocity profiles of potential and shear flows of variable cross-section with a three-layer structure is shown. For the regions of potential flows, a uniform velocity profile is assumed, and for the shear flow placed between them, a nonlinear profile is assumed, which retains approximate automodelicity throughout the entire initial section of the submerged jet. By integrating the accepted velocity profile taking into account the transition conditions between potential and shear flows, the theoretical velocity distribution for mixed flows in the flow part of the jet pump is determined. The mathematical model of flow mixing is supplemented with computer modelling data using the SolidWorks program. The presented research results made it possible to obtain an analytical expression for determining the velocity profile exclusively for the inlet section of the production inlet chamber and cannot be used to analyse the dynamics of changes in the kinematic field when the mixed flow propagates in the direction of the jet pump diffuser.

Researcher S. Karabaev (2021) notes that the optimal length of the production inlet chamber of a jet device should be in the range from 20 to 22. The optimal design of the jet device was obtained during bench tests of a gas-liquid oil ejector. The diameters of the working nozzle and production inlet chamber of the studied models were 3.3 mm and 5.4 mm, respectively. In the course of research, three models of jet pumps with a relative length of the production inlet chamber were used: $L_{i3} = 11.1$; 20.37; and 29.63. Industrial water was used for the operating flow, and atmospheric air was used for the injected flow. Bench tests were performed for different pressure ratios of the injected flow. The criteria for optimising the design of a gas-liquid ejector were the efficiency value and the injection coefficient value. According to the author, a significant excess of the optimal length of the production inlet chamber obtained during bench tests in comparison with the results obtained by the author is associated with the gaseous state of the injected flow. Due to the different aggregate state, the formation of a homogeneous gas-liquid emulsion requires a longer path length than the alignment of velocity profiles in a single-phase flow. The low density and viscosity of the injected flow have a significant effect on the production inlet length of the flow.

The nature of the distribution of axial velocities along the flow part of the jet pump obtained by the author is consistent with the results of studies conducted at Xi'an University of Technology (China) by T. Cao *et al*. (2023). In this paper, when analysing the operating process of an ultra-long ejection system, the inverse nature of the dependence of the operating flow rate on the distance to the inlet section of the production inlet chamber of a jet pump is confirmed. The increase in the operating flow rate at the entrance to the production inlet chamber of a jet pump is associated with the conical shape of its initial section, in contrast to the cylindrical production inlet chamber of constant diameter in the models studied by the author. The decrease in the speed of the operating flow along the production inlet chamber of the jet pump is explained by a decrease in its kinetic energy, part of which is spent on increasing the speed of the injected flow. Given that the nature of changes in the kinematic parameters of the injected flow is not presented in this paper, the conducted studies do not allow us to determine the distance to the inlet section of the production inlet chamber, which corresponds to the alignment of the velocity profile of the mixed flows.

The formation of a parabolic velocity distribution in the end sections of the production inlet chamber is confirmed by modelling the operating process of the NSFB 39/45 oil jet pump using the ANSYS software environment. A. Rogovyi *et al.* (2022). The speed of the injected and mixed flow during the construction of the computer model was assumed to be 16 m/s and 19.5 m/s, respectively. In the course of research, a cavitation mass transfer model based on the Rayleigh-Plesset equation was implemented, which made it possible to take into account the possibility of reducing the pressure in the flow part of the jet pump to the pressure of saturated vapours of well products. The article shows the velocity profiles of the mixed flows for different distances from the inlet section of the production inlet chamber, but the reverse flow of the liquid caused by cavitation led to a shift in the transit flow and a distortion of the kinematic field in the flow part of the jet pump. The significant asymmetry of the obtained velocity profiles made it impossible to determine the area of stabilisation of kinematic flow parameters and establish the optimal length of the production inlet chamber of the jet pump obtained from the results of this study.

The nature of the relationship between the ratio of the mixing path length of the flows, the axial dimensions of the production inlet chamber, and the efficiency of the ejection system is confirmed by the results of studies conducted by J. Zheng *et al*. (2022) at the China Clean Energy Research Institute. In the course of comparative studies, the hydraulic characteristics of two models of jet devices with different lengths of the production inlet chamber were determined. In one of the studied models, the length of the production inlet chamber was equal to the length of the flow mixing path, and in another model, the alignment of velocity profiles was completed at the initial section of the diffuser. According to the results of the conducted studies, if the flow mixing process is completed in the

diffuser part of the jet device, the flow rate of the mixed flow is reduced by 15.6%. The disadvantage of the results of the conducted research is the lack of an analytical expression that would combine the optimal length of the production inlet chamber of the jet pump and the pressure, cavitation and energy characteristics of the ejection system. Insufficient geometric, kinematic and hydrodynamic similarity of the working processes of ejection systems does not allow us to generalise the results obtained and effectively use them in the case of differences in the absolute and relative geometric dimensions of the elements of the flow part of the jet pump, the ratios of velocities, costs and pressures of mixed flows.

Conclusions

Hydraulic losses during the mixing of flows are associated with vortex formation in the shear boundary layer due to a significant difference in the velocity of the operating and injected flows and linear pressure losses in the production inlet chamber of the jet pump. Linear pressure losses in the production inlet chamber persist after the process of levelling the profile of kinematic parameters is completed and are characterised by high velocity values and a turbulent mode of mixed flow. Determining the length of the production inlet chamber section that corresponds to the completion of the speed equalisation process increases the energy efficiency of the jet pump operating process. The obtained velocity profiles of mixed flows at the entrance to the production inlet chamber have a three-layer structure with a predominantly uniform distribution of kinematic parameters in the central region at the inlet sections of the operating and injected flow and close to uniform distribution in the peripheral region. A section with a nonlinear distribution of kinematic parameters is located between the central and peripheral regions. The width of the central and peripheral regions decreases as the distance to the production inlet chamber of the jet pump increases. In the direction of the jet pump diffuser, the velocity profile of the mixed flows becomes parabolic.

The maximum values of the movement velocity of mixed flows occur on the axis of the jet pump. The maximum value of the operating flow rate corresponds to the inlet cross-section of the production inlet chamber of the jet pump and does not depend on its length. The limit value of the injected flow rate decreases as the length of the production inlet chamber of the jet pump increases. As the distance to the inlet section of the production inlet chamber increases, the axial velocity of the mixed flows decreases according to asymptotic dependence. The length of the production inlet chamber of the jet pump was determined, which ensures the stabilisation of the values of kinematic parameters and minimal energy loss when levelling the velocity profiles of the operating and injected flows. The determination of the axial velocity stabilisation region can be used to select the optimum length of the production inlet chamber of the jet pump, which ensures maximum efficiency of the ejection system. The task of further research is to develop a system for automated selection of the optimal length of the production inlet chamber of a jet pump in accordance with the existing operational factors.

Acknowledgements

None.

Conflict of Interest

None.

References

[1] Cao, T., Chen, X.-Y., Yu, K.-A., & Tang, L. (2023). Hydraulic modeling and optimization of jet mill bit considering the characteristics of depressurization and cuttings cleaning. *Petroleum Science*, 20(5), 3085-3099. doi: 10.1016/j.petsci.2023.04.007.

[2] Chen, X., Cao, T., Yu, K., Gao, D., Yang, J., & Wei, H. (2020). Numerical and experimental investigation on the depressurization capacity of a new type of depressure-dominated jet mill bit. *Petroleum Science*, 17, 1602-1615. doi: 10.1007/s12182-020-00472-8.

[3] Cho, Y.-D., & Shrestha, U. (2020). Cavitation performance improvement of an annular jet pump by j-groove. *The KSFM Journal of Fluid Machinery*, 23(4), 25-35. doi: 10.5293/kfma.2020.23.4.025.

[4] Deng, X., & Dong, J. (2021). Experimental and numerical investigation of two-phase flow and mass transfer in a self-excited oscillation pulse jet pump. *Experimental and Computational Multiphase Flow*, 3(2), 131-136. doi: 10.1007/s42757-020-0062-6.

[5] Gan, J., Wang, Y., Wang, D., & Zhang, K. (2022). Research on the law of head loss of jet pumps in the cavitation state. *ACS Omega*, 7, 12661-12679. doi: 10.1021/acsomega.1c06895.

[6] Karabaev, S. (2021). Investigations of the liquid-jet gas pump's mixing throat lengths for well operations and associated petroleum gas utilization. *IOP Conference Series: Earth and Environmental Science*, 666, article number 062003. doi: 10.1088/1755-1315/666/6/062003.

[7] Kotak, V., Pathrose, A., Sengupta, S., Gopalkrishnan, S., & Bhattacharya, S. (2023). Experimental investigation of jet pump performance used for high flow amplification in nuclear applications. *Nuclear Engineering and Technology*, 55(10), 3549-3559. doi: 10.1016/j.net.2023.06.017.

[8] Kryzhanivskyi, Ye.I., & Panevnyk, D.O. (2019). The study on the flows kinematics in the jet pump's mixing chamber. *Naukovyi Visnyk Natsionalnoho Hirnychoho Universytetu*, 1, 62-68. doi: 10.29202/nvngu/2019-1/7.

[9] Kumar, V., Subbarao, P.M.V., & Singhal, G. (2019). Effect of nozzle exit position (NXP) on variable area mixing ejector. *SN Applied Sciences*, 1, article number 1473. doi: 10.1007/s42452-019-1496-y.

[10] Kurniawan, A., Nuzuladzmi, R.N., & Afni, A.L.N. (2023). CFD simulation and efficiency analysis of natural gas ejector-booster system. In *National seminar on chemical engineering "Kejuangan". Development of chemical technology for processing of natural resources of Indonesia* (pp. 1-10). Yogyakarta: UPN "Veteran" Yogyakarta.
[11] Morrall, A., Quayle, S., & Campobasso, M.S. (2020). Turbulence modelling for RANS CFD analyses of multi-nozzle annular jet pump swirling flows. *International Journal of Heat and Fluid Flow*, 85, article number 108652. doi: 10.1016/j.ijheatfluidflow.2020.108652.
[12] Qian, Y., Wang, Y., Fang, Z., Chen, X., & Miedema, S.A. (2021). Numerical investigation of the flow field and mass transfer characteristics in a jet slurry pump. *Processes*, 9(11), article number 2053. doi: 10.3390/pr9112053.
[13] Rogovyi, A., & Lukianets, S. (2022). Kinematic parameters of the oil flow in a vortex chamber pump. *Bulletin of the National Technical University "KhPI". Series: Hydraulic Machines and Hydraulic Units*, 1, 59-65. doi: 10.20998/2411-3441.2022.1.09.
[14] Rogovyi, A., Kostiuk, M., & Azarov, A. (2022). Improving energy parameters of oil jet pumps. *Bulletin of the National Technical University "KhPI". Series: Hydraulic Machines and Hydraulic Units*, 1, 25-32. doi: 10.20998/2411-3441.2022.1.04.
[15] Wang, Z., Lei, Y., Wu, Z., Wu, J., Zhang, M., & Liao, R. (2023). Structure size optimization and internal flow field analysis of a new jet pump based on the taguchi method and numerical simulation. *Processes*, 11(2), article number 341. doi: 10.3390/pr11020341.
[16] Xu, K., Wang, G., Wang, L., Yun, F., Sun, W., Wang, X., & Chen, X. (2020). Parameter analysis and optimization of annular jet pump based on Kriging model. *Applied Sciences*, 10(21), article number 7860. doi: 10.3390/app10217860.
[17] Xu, K., Wang, G., Zhang, L., Wang, L., Yun, F., Sun, W., Wang, X., & Chen, X. (2021). Multi-objective optimization of jet pump based on RBF neural network model. *Journal of Marine Science and Engineering*, 9(2), article number 236. doi: 10.3390/jmse9020236.
[18] Yang, Y., Wu, S., Wang, C., Jiao, W., Ji, L., An, C., & Ge, J. (2023). Effect of effuser throat diameter on the internal flow structure and energy characteristics of the jet pump. *Energy Reports*, 9, 2075-2086. doi: 10.1016/j.egyr.2023.01.025.
[19] Zafarullah, E., Ansari, U., Habibullah, H., Ahmed, I., & Ahmed, M. (2021). Developing well performance analysis for improving the pump capacity of jet pumps using snap software. *International Journal of Current Engineering and Technology*, 11(2), 168-172. doi: 10.14741/ijcet/v.11.2.4.
[20] Zheng, J., Hou, Y., Tian, Z., Hongkui, J., & Chen, W. (2022). Simulation analysis of ejector optimization for high mass entrainment under the influence of multiple structural parameters. *Energies*, 15(19), article number 7058. doi: 10.3390/en15197058.

Дослідження кінематичного поля змішуваних потоків

Олександр Паневник

Доктор технічних наук, професор
Івано-Франківський національний технічний університет нафти і газу
76019, вул. Карпатська, 15, м. Івано-Франківськ, Україна
https://orcid.org/0000-0003-2765-3776

Анотація. Актуальність дослідження визначається здатністю свердловинних струминних насосів підвищити ефективність реалізації технологічних процесів у складних гірськогеологічних умовах. Мета полягала у встановленні закономірностей трансформації профілю швидкостей у камері змішування свердловинного струминного насоса на основі побудови та наступного аналізу розподілу кінематичних параметрів сумарного робочого та інжектованого потоків. Моделювання робочого процесу ежекційної системи здійснено в програмно-розрахунковому модулі ANSYS для чотирьох тривимірних моделей свердловинного струминного насоса. Геометричні моделі побудовані з нерівномірною у місцях складної геометрії та високого градієнта зміни гідродинамічних параметрів щільністю розміщення розрахункових елементів. Для кожної з досліджуваних моделей побудовано серію профілів швидкостей розміщених через рівні проміжки на різних відстанях від вхідного перерізу камери змішування. Побудовані профілі швидкостей включають ділянки з рівномірним та нелінійним розподілом кінематичних параметрів змішуваних потоків. Встановлено, що максимальні значення швидкості руху змішуваних потоків мають місце на осі струминного насоса та є однаковими для всіх досліджених моделей. Осьова швидкість руху змішуваних потоків зменшується при збільшенні відстані до вхідного перерізу камери змішування. Мінімальне значення осьової швидкості отримано для моделі струминного насоса з максимальною довжиною камери змішування. Для двох моделей струминного насоса з довжиною камери змішування 287 мм та 328 мм отримано стабілізацію значень осьової швидкості сумарного робочого та інжектованого потоків. Незмінність кінематичних параметрів для даних моделей струминного насоса свідчить про завершення процесу вирівнювання швидкостей змішуваних потоків. Враховуючи, що у випадку перевищення необхідних розмірів ділянки стабілізації кінематичних параметрів зростають гідравлічні втрати в проточній частині ежекційної системи, її оптимальна конструкція відповідає моделі з довжиною камери змішування струминного насоса 287 мм. Практична цінність дослідження полягає в тому, що така конструкція забезпечує максимальний коефіцієнт корисної дії свердловинного струминного насоса

Ключові слова: свердловинний струминний насос; ежекційна система; камера змішування; профіль швидкостей; розподіл кінематичних параметрів; стабілізація потоку

Vol. 24, No. 1
2024

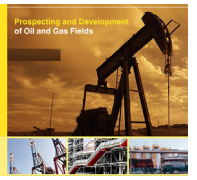

PROSPECTING AND DEVELOPMENT OF OIL AND GAS FIELDS

https://pdogf.com.ua/en

Received: 30.11.2023. Revised: 27.03.2024. Accepted: 31.05.2024

UDC 622.692.4

DOI: 10.69628/pdogf/1.2024.32

Forced oscillations of an oil pipeline at an overhead crossing during sequential pumping of various oil products

Dmytro Tymkiv*

Doctor of Technical Sciences, Professor
Ivano-Frankivsk National Technical University of Oil and Gas
76019, 15 Karpatska Str., Ivano-Frankivsk, Ukraine
https://orcid.org/0000-0003-0220-398X

Volodymyr Hrudz

Doctor of Technical Sciences, Professor
Ivano-Frankivsk National Technical University of Oil and Gas
76019, 15 Karpatska Str., Ivano-Frankivsk, Ukraine
https://orcid.org/0000-0003-1182-2512

Roman Tutko

Postgraduate Student
Ivano-Frankivsk National Technical University of Oil and Gas
76019, 15 Karpatska Str., Ivano-Frankivsk, Ukraine
https://orcid.org/0009-0003-5319-7943

Tetiana Tutko

PhD in Technical Sciences, Associate Professor
Ivano-Frankivsk National Technical University of Oil and Gas
76019, 15 Karpatska Str., Ivano-Frankivsk, Ukraine
https://orcid.org/0000-0002-9569-3035

Abstract. The method of sequential pumping of various oil products separated by a diaphragm seal is one of the most common and cost-effective. However, due to the difference in densities, significant oscillations of oil pipelines occur in their overhead part. There are practically no studies of such oscillations and their impact on the strength and stability of overhead oil pipelines, which makes this topic relevant. The aim of this article was to determine the oscillations of the oil pipeline axis and the bending moments that occur at this time, without taking into account the inertial forces of the pumped oil products for a single-span beam crossing without longitudinal deformation compensators. A mathematical model of the sequential pumping of two different oil products through a pipeline was developed. The problem was solved by decomposing the desired solution into a series of eigenfunctions of the problem of free oscillations of the overhead part of the oil pipeline using the Fourier method. As a result of calculations based on the obtained solution to the problem, it was found that in the overhead part of the oil pipeline, during the sequential pumping of various oil products, there are familiar oscillations of the oil pipeline axis relative to the abscissa axis of the deflection function of the oil pipeline axis. When the end cross-sections of the diaphragm seal enter the overhead part of the pipeline, the largest deflections occur in one of the middle sections of the part in tenths of a second. The bending moments have the highest values by modulus. The deflection curves of the oil pipeline axis and the bending moment curves for these moments of time practically coincide. It was found that the largest modulus bending moments of the pipeline during the sequential pumping of two different oil products are significantly higher than the bending moments of the same oil

Suggested Citation: Tymkiv, D., Hrudz, V., Tutko, R., & Tutko, T. (2022). Forced oscillations of an oil pipeline at an overhead crossing during sequential pumping of various oil products. *Prospecting and Development of Oil and Gas Fields*, 24(1), 32-43. doi: 10.69628/pdogf/1.2024.32.

*Corresponding author

products when they are pumped separately. The obtained results of the study will be useful in practice for designers of pipelines that will be used to pump oil products with different densities

Keywords: single-span beam crossing; pipe axis; eigenfunctions of the free oscillations problem; deflections of the pipeline axis; separating medium; bending moment

Introduction

Overhead parts of oil pipelines are among the most heavily loaded parts. In addition to the internal pressure of the pumped product, they are exposed to changes in the ambient temperature regime (daily, seasonal). The weight of the pipeline itself and the pumped oil products and the forces arising from their movement cause deflections of the pipeline axis. The topography of the area where the pipeline is laid (plain, mountainous), the length of the overhead part, and soil types require consideration of the interaction of the pipeline with the soil and its supports. In 2018-2023, a number of papers appeared that investigated some of the above problems, for example, M. Dutkiewicz *et al.* (2023) investigated the interaction of an oil pipeline with its support built in a mountainous area. With the aim of taking into account the properties of the soil base of the crossing on the strength of the transition, a mechanical and mathematical model of an overhead crossing of an oil pipeline laid in a mountainous area was developed in the study by A. Velychkovych *et al.* (2019). On its basis, simple analytical results were obtained that are suitable for practical engineering calculations. The analysis of the stress state in a damaged composite-coated pipeline was the subject of a study by T. Fan *et al.* (2022).

As noted by Y. Ding *et al.* (2021) and J. Yu *et al.* (2022), oil pipelines can be subjected to abnormal loads during construction and operation, and, according to C.N. Vanitha *et al.* (2023), to various risks. Long-term operation of pipelines leads to damage to pipeline steel at the micro level and can contribute to the emergence of macro defects, as described by K.U. Amandi *et al.* (2019). Therefore, the remaining service life of an oil pipeline is often associated with the study of the corrosion situation, as in the paper by M. Bembenek *et al.* (2022). The results of a study of the corrosion situation are used to predict the remaining service life of the pipeline and are a guide for establishing the inspection cycle and maintenance strategy, as indicated by A. Bi *et al.* (2022). Equally important are the issues of safe operation of underground parts of oil pipelines in difficult mining and geological conditions, as addressed by S. Dey & S. Tesfamariam (2022) and M. Dutkiewicz *et al.* (2022). The destruction of a single part of the pipeline can lead to a catastrophic emergency, environmental problems and significant financial losses. Therefore, for pipelines with a long history of operation, the problems of preventing the occurrence of pipeline wall defects are particularly relevant.

As can be seen from the analysis, researchers have not yet determined the forces of inertia of transported products in oil pipelines during their movement and their impact on the strength and stability of open parts of oil pipelines. This also includes the sequential pumping of different oil products through oil product pipelines. This method is cost-effective and quite common in practice. Due to the difference in the densities of the pumped products, this method causes quite significant oscillations in oil pipelines in their open parts, which is why this problem is the subject of this article. The purpose of this work was to study the oscillations of the overhead part of the oil pipeline. To achieve this goal, the following tasks needed to be solved. The first task was to build a mathematical model of the sequential pumping of two different oil products through a pipeline with a diaphragm seal between them. The second task was to find the displacements of the pipeline axis points as different oil products separated by a diaphragm seal pass through the overhead part of the pipeline. The third task was to determine the bending moments caused by the oscillations of the pipeline, which can only be found after determining these oscillations.

Materials and Methods

The deflections of the oil pipeline axis and bending moments during the sequential pumping of various oil products through an overhead pipeline crossing were determined by the analytical method. A single-span beam crossing without longitudinal deformation compensators with clamped ends was considered. The pipeline is made of 13GS steel (TU 14-3-1573-96) with an outer diameter of $D_3 = 529$ mm, wall thickness $\delta = 10$ mm, and tensile and yield strengths of this steel of $\sigma_u = 510$ MPa and $\sigma_y = 360$ MP, respectively. The pumped oil products are petrol and diesel fuel. The density of petrol and diesel fuel is $\rho_p = 750$ kg/m^3 and $\rho_d = 860$ kg/m^3, respectively. The diaphragm seal between petrol and diesel fuel is a rubber piston with a length of $\Delta x = 0.763$ m and a rubber density of $\rho_r = 575$ kg/m^3. The deflections of the pipeline axis were determined without taking into account the inertial forces of the pumped oil products.

Since the problem was solved by the analytical method, it is necessary to note how the mathematical formulation of the problem was formulated. Oil pipeline oscillations arise because oil products and a diaphragm seal with different densities pass through the overhead part of the pipeline. If a single oil product were being pumped, there would be no oscillations in any of the crossings of the pipeline. At the boundaries between the oil products and the diaphragm seal, a density jump occurs, which is the source of oscillations in each part of the pipeline. On the right-hand side of the differential equation are the force loads created by the pumped oil products and the diaphragm seal, which are multiplied by certain unit asymmetric functions (Korn & Korn, 1968), and for the diaphragm seal by the difference of the asymmetric functions.

The asymmetric functions are chosen in such a way that knowing the moment of time from the assumed initial

moment and the specific cross-section of the pipeline, it is possible to immediately tell which force factor at a given moment of time creates pressure on a given cross-section of the oil pipeline. The boundary conditions in the problem are determined by the fact that the ends of the overhead part of the pipeline are clamped. This means that the displacements of the endpoints of the axis of the overhead part and the angles of rotation of the sections of the pipeline passing through these points must be zero. At the initial moment of time, the entire part of the pipeline contains only petrol. This determined the initial task of the problem. The problem was solved by expanding the desired solution into a series of eigenfunctions of free oscillations of the part of the oil pipeline (Fridman, 2018). The deflections of the oil pipeline axis in its overhead (open) section (Fig. 1) were determined during the sequential pumping of two different oil products separated from each other by a diaphragm seal.

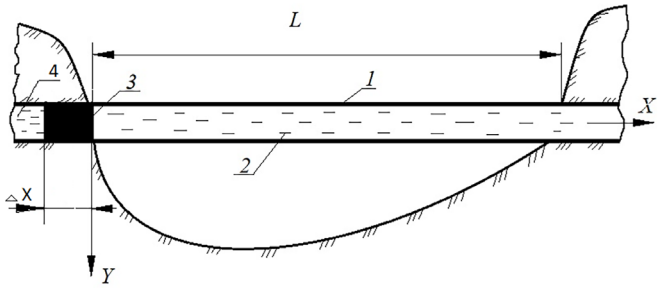

Figure 1. Schematic of an overhead crossing for sequential pumping of two different oil products
Note: 1 – oil pipeline; 2 – pumped petrol; 3 – diaphragm seal; 4 – diesel fuel
Source: created by the authors

Figure 1 shows the moment when the diaphragm seal (its right part) is at the beginning of the abscissa axis X ($x = 0$). The pumped products move at a constant velocity υ. The axial length of the diaphragm seal is Δx. The ends of the open part of the oil pipeline should be assumed to be clamped. In this problem, the displacements of the points of the oil pipeline axis in the direction perpendicular to the initial (horizontal) position of the oil pipeline axis were considered, taking into account the weights of oil products and the diaphragm seal and without taking into account their inertial forces during movement. In this case, the differential equation describing the movement of the points of the pipeline axis has the following form:

$$\frac{\partial^2 u}{\partial t^2} + a^2 \frac{\partial^4 u}{\partial x^4} = \frac{1}{\rho A}\{q_1 S_+(x - \upsilon t) + q_2[S_-(\upsilon t - x) - \\ -S_+(\upsilon(t - \Delta t) - x)] + q_3 S_+(\upsilon(t - \Delta t) - x)\}. \quad (1)$$

In this case, the initial and boundary conditions will be as follows:

$$u_{/t=0} = \frac{q_1}{2EI}\left(\frac{x^4}{12} - \frac{Lx^3}{6} + \frac{L^2x^2}{12}\right), \frac{\partial u}{\partial t}/_{t=0} = 0; \quad (2)$$

$$u_{/x=0} = 0, \frac{\partial u}{\partial x}/_{x=0} = 0, u_{/x=L} = 0, \frac{\partial u}{\partial x}/_{x=L} = 0, \quad (3)$$

where u is the displacement of the points of the oil pipeline axis in the direction perpendicular to its initial position; $a^2 = EI/(A\rho)$; ρ, A, I, E are the density of the oil pipeline material, its cross-sectional area, axial moment of inertia of the cross-section of the oil pipeline pipes and the elastic modulus of the material; x, t are the coordinate of the oil pipeline axis and time from the beginning of the movement of pumped products in the overhead crossing; q_i, ($i = 1, 2, 3$) are weights per unit length of the distributed load of petrol, diaphragm seal and diesel fuel; υ is the speed of movement of oil products in the overhead crossing; $\Delta t = \Delta x/\upsilon$; L is the length of the overhead crossing; $S_+(x)$ are the asymmetric unit functions (Fridman, 2018).

$$S_-(x) = \begin{cases} 1, & \text{if } x \geq 0, \\ 0, & \text{if } x < 0, \end{cases} \quad S_+(x) = \begin{cases} 1, & \text{if } x > 0, \\ 0, & \text{if } x \leq 0. \end{cases}$$

The created mathematical model was used to find the displacements of the oil pipeline axis points and bending moments of the pipeline overhead crossing part. The Fourier method was used to solve the problem.

Results

The value on the right-hand side of equation (1) in curly brackets is denoted by $q(x, t)$, i.e:

$$q(x, t) = q_1 S_+(x - \upsilon t) + q_2[S_-(\upsilon t - x) - \\ - S_+(\upsilon(t - \Delta t) - x)] + q_3 S_+(\upsilon(t - \Delta t) - x). \quad (4)$$

The formulated problem should be solved by decomposing the desired solution into a series of eigenfunctions of the problem of free oscillations of an overhead crossing (Fridman, 2018). To do this, it is necessary to represent $q(x, t)$ as a series:

$$q(x, t) = X_1(x)S_1(t) + X_2(x)S_2(t) + \ldots + X_i(x)S_i(t) + \ldots. \quad (5)$$

In the form of a series, it is necessary to find a solution for deflections (displacements) of the centres of gravity of the pipeline pipe cross-sections (Fourier method):

$$u(x, t) = X_1(x)T_1(t) + X_2(x)T_2(t) + \ldots + X_i(x)T_i(t) + \ldots, \quad (6)$$

where $X_1(x)$, $X_2(x)$, etc. are eigenfunctions in the case of free oscillations of the overhead part of the pipeline; $S_1(t)$,

$S_2(t)$, ..., $T_1(t)$, $T_2(t)$, etc. are unknown functions. Using the Fourier method, it can be shown that the eigenfunctions of this problem are as follows:

$$X_k(x) = K_4(\lambda_k)K_3\left(\frac{\lambda_k}{L}x\right) - K_3(\lambda_k)K_4\left(\frac{\lambda_k}{L}x\right), \qquad (7)$$

where $K_3\left(\frac{\lambda_k}{L}x\right), K_4\left(\frac{\lambda_k}{L}x\right)$ – are Krylov's functions (Filippov, 1965): $K_3\left(\frac{\lambda_k}{L}x\right) = \frac{1}{2}\left(ch\left(\frac{\lambda_k}{L}x\right) - cos\left(\frac{\lambda_k}{L}x\right)\right)$; $K_4\left(\frac{\lambda_k}{L}x\right) = \frac{1}{2}\left(sh\left(\frac{\lambda_k}{L}x\right) - sin\left(\frac{\lambda_k}{L}x\right)\right)$; λ_k – are the roots of the transcendental equation $ch\ cos\ \lambda = 1$. To determine the time function $S_i(t)$, it is necessary to multiply both parts of equation (5) by the eigenfunction (7) and integrate the result over the entire length of the overhead part of the oil pipeline. Due to the orthogonality of the eigenfunctions, only one term remains on the right-hand side, corresponding to the number k, so that:

$$S_k(t) = \frac{1}{\int_0^L X_k^2(x)dx}\int_0^L \{q_1 S_+(x-vt) + q_2[S_-(vt-x) - \\ -S_+(v(t-\Delta t)-x)] + q_3 S_+(v(t-\Delta t)-x)\} \\ [K_4(\lambda_k)K_3\left(\frac{\lambda_k}{L}x\right) - K_3(\lambda_k)K_4\left(\frac{\lambda_k}{L}x\right)]\,dx. \qquad (8)$$

Next, it is necessary to integrate the numerator and denominator of equation (8). The value of the integral in the denominator is known (Filippov, 1965):

$$\int_0^L X_k^2(x)dx = \frac{L}{4}[K_4(\lambda_k)K_1(\lambda_k) - K_3(\lambda_k)K_2(\lambda_k)]^2. \qquad (9)$$

The integrals of the numerator must be found. Once they are found, the following is obtained:

$$S_k(t) = \frac{4}{\lambda_k[K_4(\lambda_k)K_1(\lambda_k) - K_3(\lambda_k)K_2(\lambda_k)]^2}\left\langle q_1\{[K_4^2(\lambda_k) - K_3(\lambda_k)K_1(\lambda_k)] - \left[K_4(\lambda_k)K_4\left(\frac{\lambda_k}{L}vt\right) - K_3(\lambda_k)K_1\left(\frac{\lambda_k}{L}vt\right)\right]\right\} + \\ +q_2\left\{K_4(\lambda_k)\left[K_4\left(\frac{\lambda_k}{L}vt\right) - K_4\left(\frac{\lambda_k}{L}v(t-\Delta t)\right)\right] - K_3(\lambda_k)\times\left[K_1\left(\frac{\lambda_k}{L}vt\right) - K_1\left(\frac{\lambda_k}{L}v(t-\Delta t)\right)\right]\right\} + \\ +q_3\left[K_4\left(\frac{\lambda_k}{L}v(t-\Delta t)\right) - K_3(\lambda_k)K_3\left(\frac{\lambda_k}{L}v(t-\Delta t)\right)\right]\right\rangle. \qquad (10)$$

In order to shorten the writing for further presentation in (10), the following notation should be introduced:

$$\frac{4}{\lambda_k[K_4(\lambda_k)K_1(\lambda_k) - K_3(\lambda_k)K_2(\lambda_k)]^2} = C_1;$$
$$K_4^2(\lambda_k) - K_3(\lambda_k)K_1(\lambda_k) = C_2.$$

Given that each term of series (5) causes a motion described by the corresponding term of series (6), equation (1) can be written in the following form:

$$X_k\ddot{T}_k + a^2X_k^{IV}T_k = \frac{X_kS_k}{\rho A}. \qquad (11)$$

Dividing both parts of equation (11) by $X_k\,T_k$, the following is obtained:

$$-a^2\frac{X_k^{IV}}{X_k} = \frac{\ddot{T}_k}{T_k} - \frac{S_k}{\rho AT_k}. \qquad (12)$$

The left-hand side of equation (12) is equal to $-p_k^2$ (p_k – natural oscillation frequency, $p_k = \frac{\lambda_k^2}{L^2}\sqrt{\frac{EI}{A\rho}}$ (Filippov, 1965). Therefore, the differential equation for the function T_k is as follows:

$$\ddot{T}_k + p_k^2T_k = \frac{S_k}{\rho A}. \qquad (13)$$

The general solution of equation (13) is represented by the analytical expression:

$$T_k(x) = \frac{1}{\rho Ap_k}\int_0^t S_k(\tau)\,sin\,p_k\,(t-\tau)\,d\tau. \qquad (14)$$

When substituting the analytical expression (10) into (14), it is necessary to perform integration and, using (6), find a solution to problems (1-3). It is necessary to take into account the fact that the number of eigenfunctions is infinitely large. It should also be taken into account that at the initial time ($t = 0$), the pumped petrol fills the entire overhead part of the pipeline and causes a deflection of its axis, which must be determined by revealing the static uncertainty of the overhead part of the pipeline using the method of forces (Gere & Goodno, 2012). In this regard, the solution to problem (1-3) has the following final form:

$$u(x,t) = \frac{q_1}{2EI}\left(\frac{x^4}{12} - \frac{Lx^3}{6} + \frac{L^2x^2}{12}\right) + \frac{C_1}{\rho A}\sum_{k=1}^{\infty}[K_4(\lambda_k)\times K_3\left(\frac{\lambda_k}{L}x\right) - K_3(\lambda_k)K_4\left(\frac{\lambda_k}{L}x\right)]\left\langle q_1\left\{\frac{C_2}{p_k^2}(1-cos\,p_k\,t) - \right.\right. \\ -K_4(\lambda_k)\left[\frac{sh\left(\frac{\lambda_k}{L}vt\right)}{2\left(\left(\frac{\lambda_k}{L}v\right)^2+p_k^2\right)} - \frac{\left(\frac{\lambda_k}{L}v\right)^3 sin\,p_kt}{p_k\left(\left(\frac{\lambda_k}{L}v\right)^4-p_k^4\right)} + \frac{sin\left(\frac{\lambda_k}{L}vt\right)}{2\left(\left(\frac{\lambda_k}{L}v\right)^2-p_k^2\right)}\right] + K_3(\lambda_k)\left[\frac{ch\left(\frac{\lambda_k}{L}vt\right)}{2\left(\left(\frac{\lambda_k}{L}v\right)^2+p_k^2\right)} - \frac{cos\left(\frac{\lambda_k}{L}vt\right)}{2\left(\left(\frac{\lambda_k}{L}v\right)^2-p_k^2\right)} + \frac{p_k^2\,cos\,p_kt}{\left(\left(\frac{\lambda_k}{L}v\right)^4-p_k^4\right)}\right]\Bigg\} + \\ +q_2\{K_4(\lambda_k)\times\left[\frac{sh\left(\frac{\lambda_k}{L}vt\right)}{2\left(\left(\frac{\lambda_k}{L}v\right)^2+p_k^2\right)} + \frac{sin\left(\frac{\lambda_k}{L}vt\right)}{2\left(\left(\frac{\lambda_k}{L}v\right)^2-p_k^2\right)} - \frac{\left(\frac{\lambda_k}{L}v\right)^3 sin\,p_kt}{p_k\left(\left(\frac{\lambda_k}{L}v\right)^4-p_k^4\right)}\right] - K_4(\lambda_k)\left[\frac{sh\left(\frac{\lambda_k}{L}v(t-\Delta t)\right)}{2\left(\left(\frac{\lambda_k}{L}v\right)^2+p_k^2\right)} + \frac{sin\left(\frac{\lambda_k}{L}v(t-\Delta t)\right)}{2\left(\left(\frac{\lambda_k}{L}v\right)^2-p_k^2\right)} - \frac{\left(\frac{\lambda_k}{L}v\right)^3 sin\,p_k(t-\Delta t)}{p_k\left(\left(\frac{\lambda_k}{L}v\right)^4-p_k^4\right)}\right] - \\ -K_3(\lambda_k)\left[\frac{ch\left(\frac{\lambda_k}{L}vt\right)}{2\left(\left(\frac{\lambda_k}{L}v\right)^2+p_k^2\right)} - \frac{cos\left(\frac{\lambda_k}{L}vt\right)}{2\left(\left(\frac{\lambda_k}{L}v\right)^2-p_k^2\right)} + \frac{p_k^2\,cos\,p_kt}{\left(\left(\frac{\lambda_k}{L}v\right)^4-p_k^4\right)}\right] + K_3(\lambda_k)\times\left[\frac{ch\left(\frac{\lambda_k}{L}v(t-\Delta t)\right)}{2\left(\left(\frac{\lambda_k}{L}v\right)^2+p_k^2\right)} - \frac{cos\left(\frac{\lambda_k}{L}v(t-\Delta t)\right)}{2\left(\left(\frac{\lambda_k}{L}v\right)^2-p_k^2\right)} + \frac{p_k^2\,cos(p_k(t-\Delta t))}{\left(\frac{\lambda_k}{L}v\right)^4-p_k^4}\right]\Bigg\} + \\ \left.\left.+q_3\left\{K_4(\lambda_k)\left[\frac{sh\left(\frac{\lambda_k}{L}v(t-\Delta t)\right)}{2\left(\left(\frac{\lambda_k}{L}v\right)^2+p_k^2\right)} + \frac{sin\left(\frac{\lambda_k}{L}v(t-\Delta t)\right)}{2\left(\left(\frac{\lambda_k}{L}v\right)^2-p_k^2\right)} - \frac{\left(\frac{\lambda_k}{L}v\right)^3 sin\,p_k(t-\Delta t)}{p_k\left(\left(\frac{\lambda_k}{L}v\right)^4-p_k^4\right)}\right] - K_3(\lambda_k)\times\left[\frac{ch\left(\frac{\lambda_k}{L}v(t-\Delta t)\right)}{2\left(\left(\frac{\lambda_k}{L}v\right)^2+p_k^2\right)} + \frac{cos\left(\frac{\lambda_k}{L}v(t-\Delta t)\right)}{2\left(\left(\frac{\lambda_k}{L}v\right)^2-p_k^2\right)} - \frac{\left(\frac{\lambda_k}{L}v\right)^2 cos\,p_k(t-\Delta t)}{\left(\frac{\lambda_k}{L}v\right)^4-p_k^4}\right]\right\}\right\rangle. \qquad (15)$$

Using the formula (15), the deflections $u(x, t)$ of the oil pipeline axis can be determined every 2 m along the overhead part for different time points in the interval from 0 to 15 s, as well as the bending moments $M = -EI\frac{\partial^2 u}{\partial x^2}$. The calculations were performed for the following initial data: $q_1 = 1{,}497$ N/m; $q_2 = 1{,}148$ N/m; $q_3 = 1{,}717$ N/m; $\upsilon = 2$ m/s; $E = 2.05\times10^{11}$ Pa; $I = 0.000549$ м^4; $\rho = 7{,}850$ kg/m^3; $\Delta t = 0.3815$ s; $A = 0.016305$ m^2; $L = 30$ m. The results are shown in Figures 2-4.

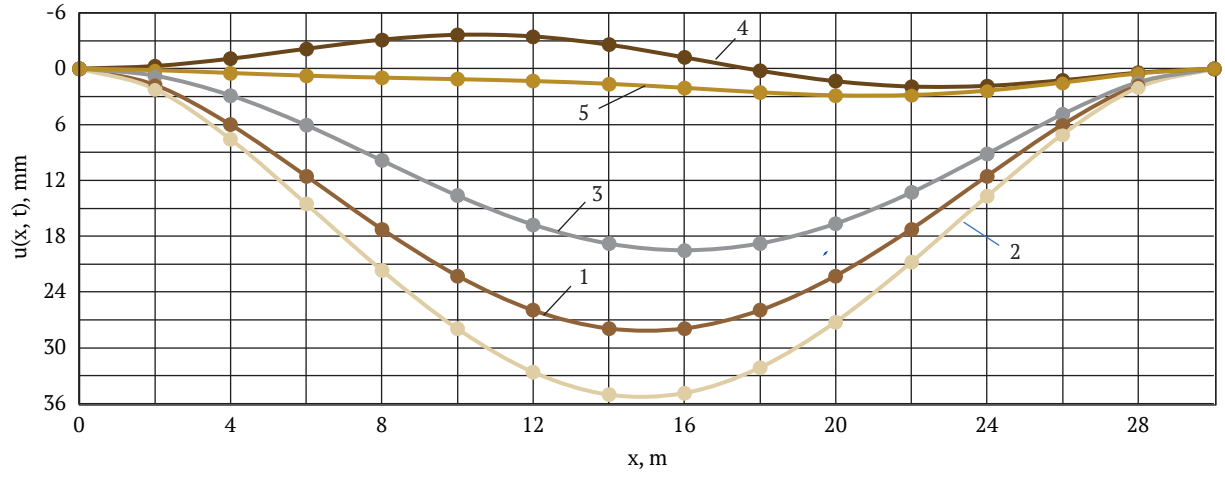

a)

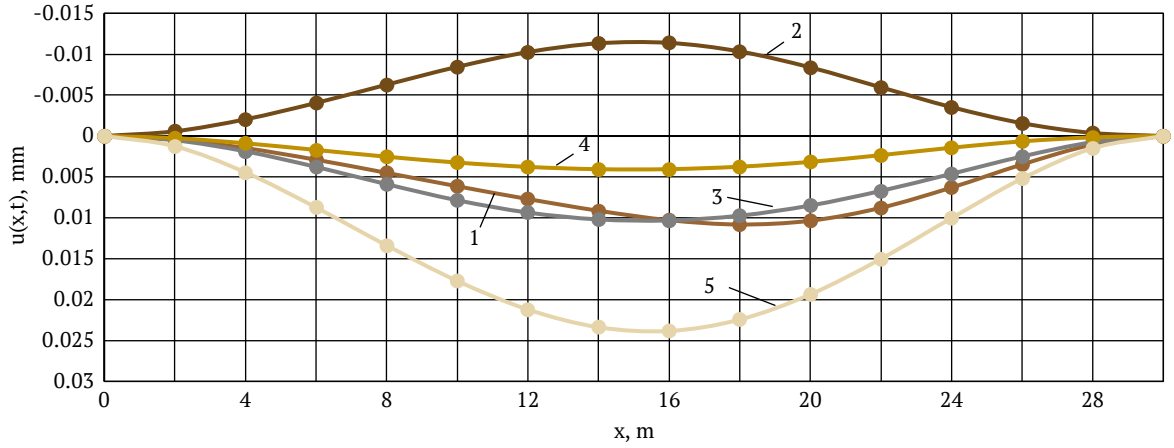

b)

Figure 2. Displacement of the oil pipeline axis points during sequential pumping of petrol and diesel fuel for different time points

Note: a) 1 = 0 s, 2 = 1 s, 3 = 4 s, 4 = 7 s, 5 = 9 s; b) 1 = 8 s, 2 = 10 s, 3 = 12 s, 4 = 14 s, 5 = 15 s
Source: created by the authors

The movements of the oil pipeline axis point every two metres for different time points from $t = 0$ s to $t = 9$ s are shown in Figure 2a. As can be seen from the graphs, when different oil products are pumped sequentially, there are familiar oscillations of the pipeline axis relative to the X-axis caused by the sequential pumping of different oil products. The largest of the displacements shown corresponds to time $t = 1$ s and u_{max}. As time t increases, the deviation of the points from the X-axis decreases. Larger deviations from the X-axis correspond to positive values of $u(x, t)$, and smaller deviations to negative values. At larger time values (from $t = 8$ s to $t = 15$ s) (Fig. 2b), the oscillation process of the oil pipeline axis continues, but with a smaller deviation from the X-axis. Figure 3 shows the bending moment graphs for the same time points as for the displacements in Figure 2. It can be noted that smaller time values correspond to larger modulus values of bending moments. In Figure 3a, for example, curve 2, corresponding to time $t = 1$ s, has the largest modulus bending moment M = −140 kN·m. The largest modulus value of the bending moment at $t > 8$ s is curve 10 (Fig. 3b), which corresponds to time $t = 15$ s and is equal to M = −95.3 kN·m.

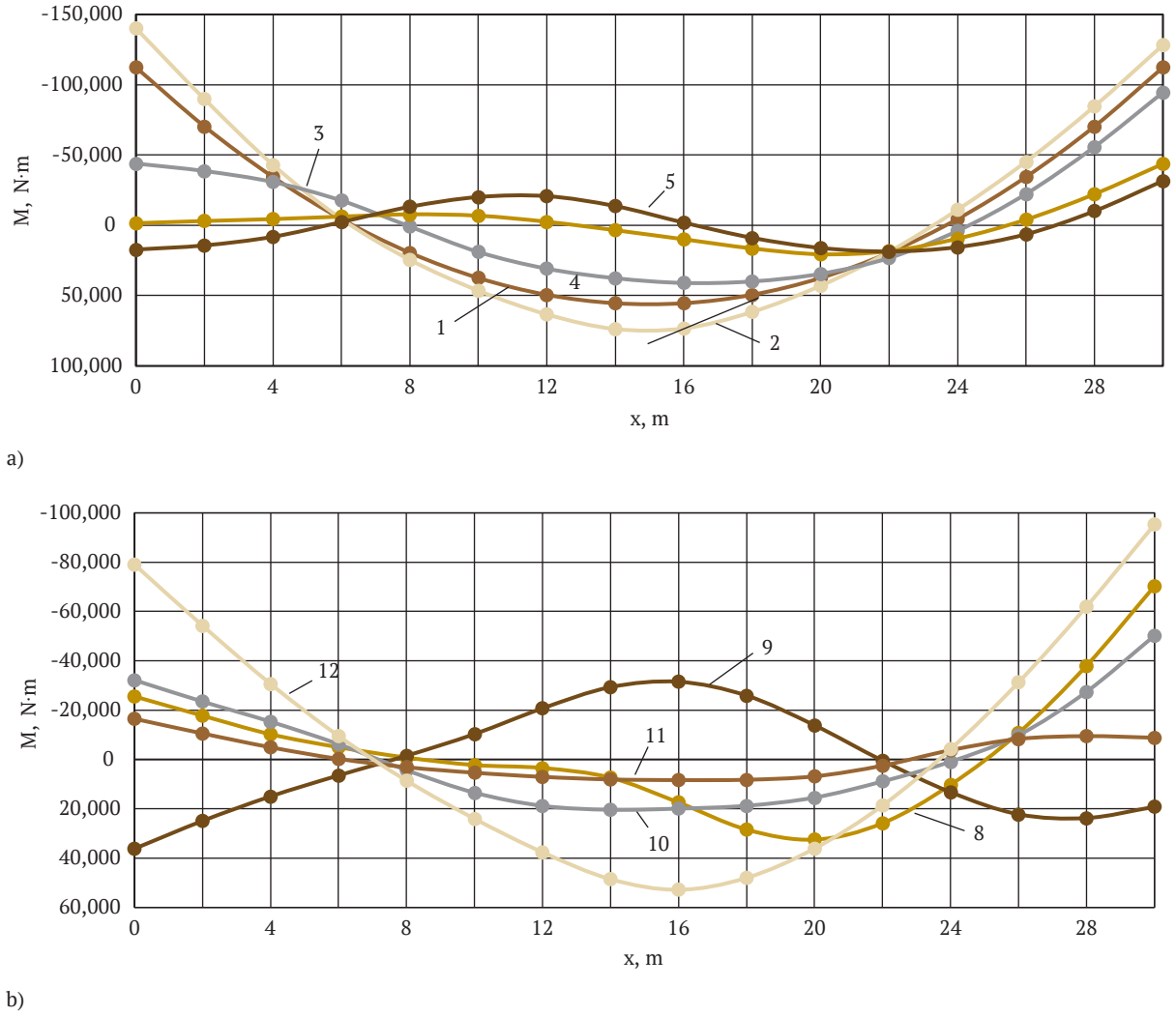

Figure 3. Bending moments of the oil pipeline during sequential pumping of petrol and diesel fuel for different moments of time

Note: a) 1 = 0 s, 2 = 1 s, 3 = 4 s, 4 = 6 s, 5 = 7 s; b) 8 = 8 s, 9 = 10 s, 10 = 12 s, 11 = 14 s, 12 = 15 s
Source: created by the authors

Since small values of time correspond to larger displacements of the points of the oil pipeline axis from the abscissa axis X, the displacements and bending moments at small values of time were calculated. The results are shown in Figure 4. The displacements of the axis of the 30 m long overhead oil pipeline crossing in Figure 4a correspond to the time points $t = 0.3$ s, 0.35 s and 0.45 s. At $t = 0.45$ s, the displacement reaches a maximum equal to u_{max} and the same maximum is obtained at $t = 0.15$ s (this curve is not plotted in Figure 4a, it almost coincides with the displacement curve for $t = 0.45$ s). Bending moments for small values of time are shown in Figure 4b. At $t = 0.15$ s and $t = 0.45$ s, the bending moment curves, similarly to the displacements, almost coincide. The largest modulus value of the bending moments at $t = 0.45$ s is M = −144.7 kN·m, and for $t = 0.45$ s M = −143.6 kN·m, and they correspond to the final cross-section $x = 30$ m of the part of the oil pipeline. It is necessary to compare the largest bending moment modulus for the sequential pumping of petrol and diesel fuel with the largest bending moment modulus of petrol and diesel fuel for their separate pumping. When petrol and diesel are pumped separately, the formula for their bending modulus is:

$$M = EI\frac{\partial^2 u}{\partial x^2} = \frac{q_i}{2}\left(x^2 - Lx + \frac{L^2}{6}\right), i = 1;\ 3;$$
$$q_1 = 1{,}497\,\text{N/m}, q_3 = 1{,}717\,\text{N/m}. \quad (16)$$

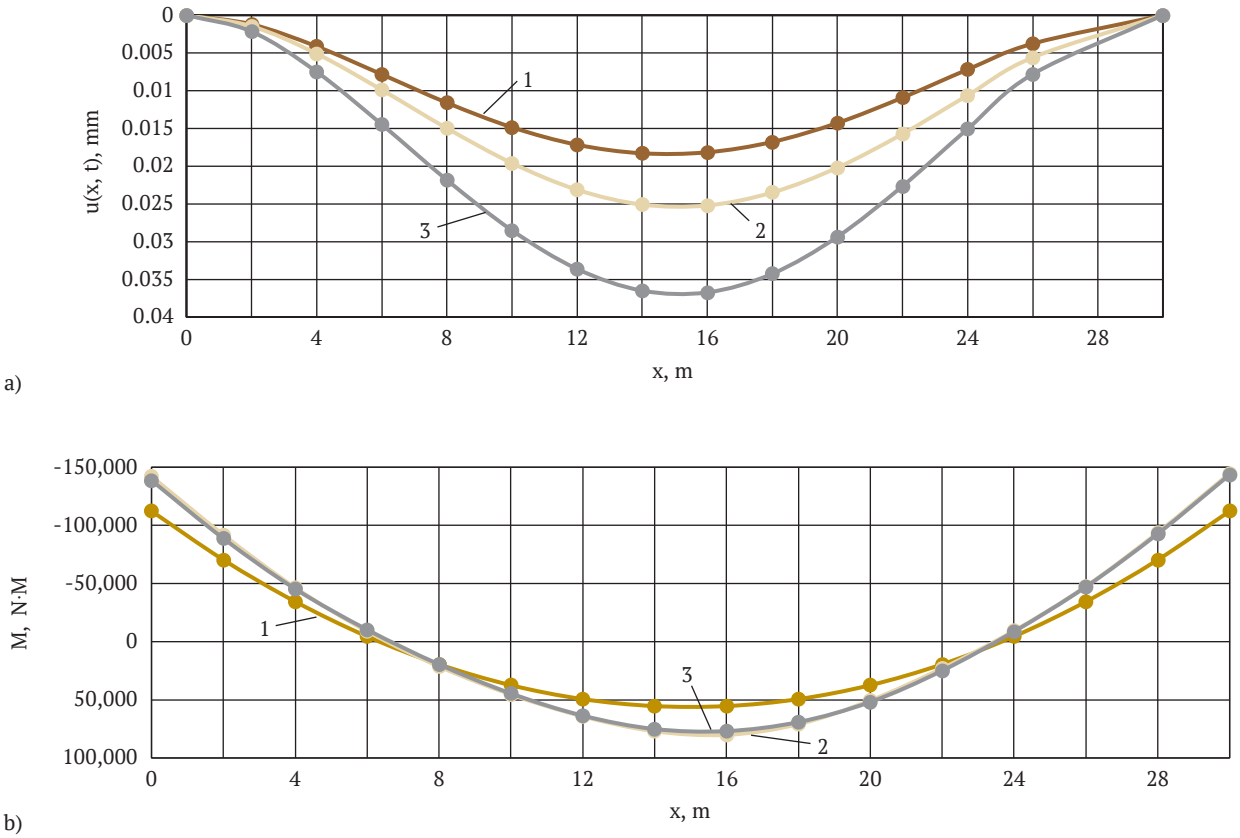

Figure 4. Displacement of the oil pipeline axis points (a) and its bending moments (b) during the sequential pumping of petrol and diesel fuel for small time values

Note: a) 1 = 0.3 s, 2 = 0.35 s, 3 = 0.45; b) 1 = 0 s, 2 = 0.15 s, 3 = 0.45 s
Source: created by the authors

Substituting q_1 and q_3 into the above formula, the bending moments of the pipeline for petrol pumping are obtained as $M_p = 112.3$ kN·m and for diesel fuel pumping as $M_d = 128.8$ kN·m. The largest bending moment during the sequential pumping of petrol and diesel fuel is 1.29 and 1.12 times higher than the bending moments during their separate pumping, respectively. When the end cross-sections of the diaphragm seal (rubber piston) enter the overhead part of the oil pipeline, which occurs at times $t = 0$ s and $t = 0.38$ s, at times $t = 0.15$ s and $t = 0.45$ s, the maximum (37 mm) deflections of the oil pipeline axis in one of its middle cross-sections in the part occur, and the end part of the pipeline section $x = 30$ m has the largest bending moments by modulus. This confirms the fact that all changes in the deflection of the pipeline axis and its bending moment in the part are caused by density oscillations between the diaphragm seal and the pumped oil products. The difference in density between the diaphragm seal and the pumped oil products leads to an increase in the deflection arc of the pipe axis at the beam crossing. This, in turn, causes a loss of pipeline stability at this crossing due to the lower axial compressive force of the pipes caused by changes in ambient temperature.

Discussion

The absence of publications found by the authors that would directly investigate the issue of sequential pumping of various oil products on the overhead part of the pipeline demonstrates the importance of current and further research in this area. However, an in-depth study of certain aspects of the topic can shed light on the technological challenges in this process, so the following studies reviewed in this chapter are worthy of attention. M.J. Brennan *et al.* (2018) investigated wave propagation due to oscillations caused by a natural gas leak from a damaged pipeline. The developed simulation model of wave propagation includes two parts: a model of amplitude damping and a model of wave propagation. It is shown that this model can be used to determine the location of a gas leak. A number of studies have focused on the behaviour of pipelines on soft ground, such as the study by J. Tang *et al.* (2023), and on permafrost, such as the study by K. Wang *et al.* (2023). The change in pipe deformations and stresses over time has been established, but these models do not take into account the oscillations of the pipes during the transportation of hydrocarbons, which reduces the informational value of the models. To improve the operating conditions of pipelines,

P.O. Ayegba *et al.* (2021) used various design and technological measures but do not take into account the occurrence of pipe oscillations. As noted by Y. Zhang *et al.* (2023), the safe operation of pipelines is currently the main challenge for the pipeline industry. The results of the conducted studies show that the assessment of the vulnerability of oil and gas pipelines is at a preliminary stage and does not take into account their oscillations.

The main causes of pipeline accidents are weld defects, as described by F. Wang *et al.* (2023), and corrosion damage, which is considered by T. Arumugam *et al.* (2023). These phenomena are stimulated by pipeline oscillations during operation, which lead to the occurrence of load cycles and acceleration of corrosion processes and fatigue destruction of steels. Therefore, when designing pipelines, in particular, overhead pipeline crossings, it is necessary to take into account their oscillations to ensure high performance. The peculiarities of stress and displacement distribution in pipeline systems have been studied in many works, including those by X. Wang *et al.* (2022) and X. Li *et al.* (2022), and general approaches to such problems can be divided into three global areas. The first direction is based on analytical methods, such as the studies by M. Witek (2021) and W. Zhang *et al.* (2022). Studies in the second area, namely A. Tsatsis *et al.* (2022) and X. Liu *et al.* (2022), are based on the finite element method and use engineering software packages. The third direction – P. Ni *et al.* (2023) – used laboratory and field measurements or modelling experiments. The study presented in this article develops the first, analytical direction of research. It is worth mentioning the study of the influence of vibration parameters during pipe welding on the state of pipeline systems, as in the study by Y. Bao *et al.* (2023a), as well as the detection of defects in them caused by these oscillations, as discussed by P. Kumar & P.K. Mohapatra (2022). Mathematically, oscillatory processes are described by hyperbolic equations or their systems, whose solutions in the class of integer functions often have the property of index boundedness in the direction of oscillations (Bandura & Skaskiv, 2018) or in a set of variables (Bandura & Skaskiv, 2019).

In the publication I. Chudyk *et al.* (2020) the relationships between the parameters of unsteady longitudinal and torsional oscillations of a drilling tool can be found and a mathematical model to study their properties is developed. As a result of solving this problem, it became possible to select the optimal modes of dynamic loading of a drilling tool in order to increase its energy efficiency. This indicates the possibility of studying the oscillatory processes that accompany various oscillatory processes. In the author's problem, the alternating oscillations during the sequential pumping of two different oil products lead to an increase in bending moments, which must be taken into account when designing oil pipelines. Forced oscillations can accompany certain technological processes and are harmful to them. Their study makes it possible to obtain results that can be used to reduce the magnitude of these oscillations. This conclusion is confirmed by the work of V. Moysyshyn *et al.* (2021), in which experimental studies of the drilling process on a drilling rig made it possible to provide practical recommendations for reducing the harmful effects of drilling tool vibrations and reducing the energy intensity of the drilling process. But there are also technological processes that require specially created vibrations. In the study by Y. Bao *et al.* (2023b) certain vibrations are set and the transient characteristics of two-phase gas-liquid flow in inclined pipes are found. It was found that inclined vibration has the most significant effect on gas-liquid flow, followed by horizontal and vertical vibration. The effect of vibration on the secondary flow increases with increasing vibration amplitude. This study should be applied to offshore oil and gas equipment.

The research of D. Guan *et al.* (2019) is devoted to the experimental study of the interaction between flow fields, scour and forced vibrational pipelines in a calm water environment. In reality, a pipeline lying on the seabed is subjected to scour around it under the influence of current fields. On the other hand, the same scour occurs under the influence of quite specific vibrations of the pipeline itself, if there are no flow fields around the pipeline. This means that there is a definite connection between the scour of the channel in which the pipeline is located and the vibration of the pipeline itself. Damping oscillations at energy facilities such as pumping stations is important, as oscillations from pumping stations are added to the oscillations of oil pipelines caused by the process of pumping oil products. More and more refurbished oil pipes are being used in oil and gas transmission pipelines in China. In the publication by S. Zhang *et al.* (2023), the case of cracks in a repaired oil pipe after eight months of operation is investigated. As a result of a series of experiments, the authors concluded that during the repair work, an external weld was made at the end of the external thread of the pipe, which resulted in the formation of a martensitic metal structure, and cold cracks appeared in the zone of thermal influence, which were detected after a rather long operation as part of the pipeline. The authors do not indicate the conditions of its operation. If the pipeline was pumping oil, this process would be accompanied by pipeline oscillations. These vibrations, in turn, would stimulate the process of cracking.

Summarising all of the above in relation to the cited literature, the following should be noted: there are technological processes that generate oscillations (vibrations) of pipes in oil pipelines and other pipelines. These oscillations are harmful, and their reduction would improve the technological process and ensure the trouble-free operation of pipelines. In this case, they should be taken into account when calculating the strength and stability of pipelines. Less common are the technological processes in which certain vibrations are required to produce them. In this case, vibrations are not harmful. The authors of the study did not find any publications on the sequential pumping of two different oil products through pipelines, which shows the need to study this issue.

Conclusions

A mathematical model of the sequential pumping of two different oil products with a diaphragm seal between them through an overhead pipeline crossing has been developed to determine both the deflection function of the pipe axis at the crossing and their bending moments relative to the horizontal coordinate axis *X*. The model takes into account static forces (weights of oil products and the diaphragm seal) and the initial condition of the problem, which corresponds to the stationary state of oil products in the pipeline. The weight of pipes at the crossing, inertial forces of oil products, the diaphragm seal and oil pipeline pipes are not taken into account. As a result of the implementation of the mathematical model, it was found that from the moment one of the end cross-sections of the diaphragm seal enters the overhead crossing of the oil pipeline, which at the initial moment of time was on the border with the overhead crossing, the alternating oscillations of the oil pipeline axis begin. At the same time, smaller values of deviations from the abscissa axis *X* correspond to negative values of the axis deflection function, and larger values correspond to its positive values. The obtained function of deflections of the oil pipeline axis at the overhead crossing was used to find the function of bending moments, which, like deflections, continuously change both in modulus and sign. The entry of each of the end cross-sections of the diaphragm seal during the sequential pumping of two different oil products into the overhead part of the pipeline causes maximum positive displacements of its axis points and the largest modulus values of bending moments, which occur literally in a tenth of a second after the entry of the end section of the diaphragm seal into the overhead crossing of the pipeline. At the same time, for a 30 m long overhead crossing, the vertical displacement reaches a maximum of 37 mm from the moment of entry of the diaphragm seal, which is 0.45 s.

The maximum bending moment modulus on the overhead part of the pipeline, when two different oil products are pumped sequentially, is significantly higher than the maximum bending moment of the pipeline on the same part when each of the two oil products is pumped separately. In particular, when petrol and diesel fuel are pumped sequentially, the largest bending moment is 1.29 and 1.12 times higher than the bending moments when they are pumped separately, respectively. After both end sections of the diaphragm seal enter the overhead crossing of the oil pipeline, with an increase in the time of movement of the pumped oil products in the crossing, the displacement of the points of the oil pipeline axis in it and the bending moments of the pipes decrease. All of the above phenomena, which occur when two different oil products are pumped sequentially with a diaphragm seal between them, are caused by density jumps between the diaphragm seal and each of the pumped oil products. This study did not take into account the weight of the part of the pipeline itself on the deflection of its axis and the value of bending moments on the part. Taking this factor into account will be the goal of further research.

Acknowledgements

The authors express their gratitude to Liubomyr Ropiak, Doctor of Technical Sciences, Professor of the Department of Computerised Engineering, Ivano-Frankivsk National Technical University of Oil and Gas, for his advice during the writing of the article. The authors are also grateful to the editor and reviewers for their comments that helped to improve the content of this article.

Conflict of Interest

None.

References

[1] Amandi, K.U., Diemuodeke, E.O., Briggs, T.A., & Pham, D. (2019). Model for remaining strength estimation of a corroded pipeline with interacting defects for oil and gas operations. *Cogent Engineering*, 6(1), article number 1663682. doi: 10.1080/23311916.2019.1663682.

[2] Arumugam, T., Vijaya Kumar, S.D., Karuppanan, S., & Ovinis, M. (2023). The influence of axial compressive stress and internal pressure on a pipeline network: A review. *Applied Sciences*, 13(6), article number 3799. doi: 10.3390/app13063799.

[3] Ayegba, P.O., Edomwonyi-Otu, L.C., Abubakar, A., & Yusuf, N. (2021). Drag reduction for single-phase water flow in and around 180° bends. *Journal of Non-Newtonian Fluid Mechanics*, 295, article number 104596. doi: 10.1016/j.jnnfm.2021.104596.

[4] Bandura, A., & Skaskiv, O. (2018). Boundedness of the L-index in a direction of entire solutions of second order partial differential equation. *Acta et Commentationes Universitatis Tartuensis de Mathematica*, 22(2), 223-234. doi: 10.12697/ACUTM.2018.22.18.

[5] Bandura, A., & Skaskiv, O. (2019). Analog of Hayman's theorem and its application to some system of linear partial differential equations. *Journal of Mathematical Physics, Analysis and Geometry*, 15(2), 170-191. doi: 10.15407/mag15.02.170.

[6] Bao, Y., Ma, T., Zhang, Y., & Wang, L. (2023b). Influence of vibration on transient flow characteristics of gas-liquid two-phase flow in inclined pipes. *Chemical Engineering Research and Design*, 196, 71-88. doi: 10.1016/j.cherd.2023.06.010.

[7] Bao, Y., Xue, R., Zhou, J., Liu, H., & Xu, Y. (2023a). The influence of oscillation parameters on the formation of overhead welding seams in the narrow-gap GMAW process. *Applied Sciences*, 13(9), article number 5519. doi: 10.3390/app13095519.

[8] Bembenek, M., Mandziy, T., Ivasenko, I., Berehulyak, O., Vorobel, R., Slobodyan, Z., & Ropyak, L. (2022). Multiclass level-set segmentation of rust and coating damages in images of metal structures. *Sensors*, 22(19), article number 7600. doi: 10.3390/s22197600.

[9] Bi, A., Huang, S., Zhang, Y., & Gao, Y. (2022). Reliability analysis of oil and gas pipelines based on step-down-stress testing in corrosive environments. *Mathematical Problems in Engineering*, 2022, article number 4055779. doi: 10.1155/2022/4055779.

[10] Brennan, M.J., Karimi, M., Muggleton, J.M., Almeida, F.C.L., Kroll de Lima, F., Ayala, P.C., Obata, D., Paschoalini, A.T., & Kessissoglou, N. (2018). On the effects of soil properties on leak noise propagation in plastic water distribution pipes. *Journal of Sound and Vibration*, 427, 120-133. doi: 10.1016/j.jsv.2018.03.027.

[11] Chudyk, I., Raiter, P., Grydzhuk, Ya., & Yurych, L. (2020). Mathematical model of oscillations of a drill tool with a drill bit of cutting-scraping type. *Naukovyi Visnyk Natsionalnoho Hirnychoho Universytetu*, 2020(1), 52-57. doi: 10.33271/nvngu/2020-1/052.

[12] Dey, S., & Tesfamariam, S. (2022). Structural performance of buried pipeline undergoing fault rupture in sand using Taguchi design of experiments. *Soil Dynamics and Earthquake Engineering*, 155, article number 107174. doi: 10.1016/j.soildyn.2022.107174.

[13] Ding, Y., Yang, H., Xu, P., Zhang, M., & Hou, Z. (2021). Coupling interaction of surrounding soil-buried pipeline and additional stress in subsidence soil. *Geofluids*, 2021, article number 7941989. doi: 10.1155/2021/7941989.

[14] Dutkiewicz, M., Shatskyi, I., Martsynkiv, O., & Kuzmenko, E. (2022). Mechanism of casing string curvature due to displacement of surface strata. *Energies*, 15(14), article number 5031. doi: 10.3390/en15145031.

[15] Dutkiewicz, M., Velychkovych, A., Andrusyak, A., Petryk, J., & Kychma, A. (2023). Analytical model of interaction of an oil pipeline with a support of an overpass built in a mountainous area. *Energies*, 16(11), article number 4464. doi: 10.3390/en 161144464.

[16] Fan, T., Liu, Z., Li, M., Zhao, Y., Zuo, Z., & Guo, R. (2022). Development of cost-effective repair system for locally damaged long-distance oil pipelines. *Construction and Building Materials*, 333, article number 127342. doi: 10.1016/j.conbuildmat.2022.127342.

[17] Filippov, A. (1965). *Oscillations of mechanical systems*. Kyiv: Naukova Dumka.

[18] Fridman, V. (2018). *Theory of elastic oscillations. Equations and methods*. Singapore: Springer Nature Pte Ltd. doi: 10.1007/978-981-10-4786-2.

[19] Gere, J., & Goodno, B. (2012). *Mechanics of materials*. Stamford: Cengage Learning.

[20] Guan, D., Hsich, S.-C., Chiew, Y.-M., & Low, Y.M. (2019). Experimental study of scour around a forced vibrating pipeline in quiescent water. *Coastal Engineering*, 143, 1-11. doi: 10.1016/j.coastaleng.2018.10.010.

[21] Korn, G.A., & Korn, T.M. (1968). *Mathematical handbook for scientists and engineers*. New York: McGraw-Hill Book Company.

[22] Kumar, P., & Mohapatra, P.K. (2022). Partial blockage detection in pipelines by modified reconstructive method of characteristics technique. *Journal of Hydraulic Engineering*, 148(4), article number 4022003. doi: 10.1061/(ASCE)HY.1943-7900.0001971.

[23] Li, X., Wu, Q., Jin, H., & Kan, W. (2022). A new stress monitoring method for mechanical state of buried steel pipelines under geological hazards. *Advances in Materials Science and Engineering*, 2022, article number 4498458. doi: 10.1155/2022/4498458.

[24] Liu, X., Sun, Z., Zhu, J., Fang, Y., He, Y., & Pan, Y. (2022). Study on stress-strain characteristics of pipeline-soil interaction under ground collapse condition. *Geofluids*, 2022, article number 5778761. doi: 10.1155/2022/5778761.

[25] Moysyshyn, V., Lyskanych, M., Borysevych, L., Vytyaz, O., & Voznyi, I. (2021). Experimental estimation of design and drilling regime option influence on drilling tool dynamics. *Metallophysics and Advanced Technologies*, 43(5), 689-712. doi: 10.15407/mfint.43.05.0689.

[26] Ni, P., Mangalathu, S., & Liu, K. (2020). Enhanced fragility analysis of buried pipelines through Lasso regression. *Acta Geotechnica*, 15, 471-487. doi: 10.1007/s11440-018-0719-5.

[27] Tang, J., Xu, J., Zhou, D., Huang, D., Zeng, K., Li, Y., & Chen, Z. (2023). Ground surface deformation caused by pipe jacking construction in a soft soil area: An experiment-based study. *Buildings*, 13(7), article number 1628. doi: 10.3390/buildings13071628.

[28] Tsatsis, A., Gelagoti, F., & Gazetas, G. (2018). Performance of a buried pipeline along the dip of a slope experiencing accidental sliding. *Geotechnique*, 68(11), 968-988. doi: 10.1680/jgeot.17.P.029.

[29] Vanitha, C.N., Easwaramoorthy, S.V., Krishna, S.A., & Cho, J. (2023). Efficient qualitative risk assessment of pipelines using relative risk score based on machine learning. *Scientific Reports*, 13, article number 14918. doi: 10.1038/s41598-023-38950-9.

[30] Velychkovych, A., Andrusyak, A., Pryhorowska, T., & Ropyak, L. (2019). Analytical model of oil pipeline overground transitions, laid in mountain areas. *Oil and Gas Science and Technology*, 74, article number 65. doi: 10.2516/ogst/2019039.

[31] Wang, F., Wu, G., Chen, D., Li, G., Qian, Y., Xi, F., & Wang, L. (2023). Mechanical response of a buried pipeline to permafrost thawing based on sequential coupling method. *Atmosphere*, 14(4), article number 620. doi: 10.3390/atmos14040620.

[32] Wang, K., Zhang, M., Guo, Q., Ma, W., Zhang, Y., & Wu, W. (2023). Failure risk prediction model for girth welds in high-strength steel pipeline based on historical data and artificial neural network. *Processes*, 11(8), article number 2273. doi: 10.3390/pr11082273.

[33] Wang, X., Li, H., Li, B., Sheng, J., Zhao, J., Ding, Y., & Lu, D. (2022). Simulation analysis of external damage and repair of the gas transmission pipeline. *Advances in Materials Science and Engineering*, 2022, article number 3978649. doi: 10.1155/2022/3978649.

[34] Witek, M. (2021). Structural integrity of steel pipeline with clusters of corrosion defects. *Materials*, 14(4), article number 852. doi: 10.3390/ma14040852.

[35] Yu, J., Chen, C., & Li, C. (2022). Safety analysis and emergency response of suspended oil and gas pipelines triggered by natural disasters. *Sustainability*, 14, article number 17045. doi: 10.3390/su142417045.

[36] Zhang, S., Xie, F., Wu, X., Yan, X., Luo, J., Ma, X., & Su, G. (2023). Failure analysis of cracked P110 repaired tubing used for gas transmission. *Materials*, 16(22), article number 7151. doi: 10.3390/ma16227151.

[37] Zhang, W., Zhang, J., Li, X., Chen, F., Guo, J., Li, W., & Cai, J. (2022). Energy pipeline strength evaluation and reliability technology based on fuzzy deep learning network algorithm. *Energy Reports*, 8, 5129-5136. doi: 10.1016/j.egyr.2022.03.203.

[38] Zhang, Y., Hou, S., Lin, L., Lou, Y., & Zhou, Y. (2023). Experimental study on the mechanical behavior of buried steel pipeline subjected to the local subsidence. *International Journal of Pressure Vessels and Piping*, 206, article number 105037. doi: 10.1016/j.ijpvp.2023.105037.

Вимушені коливання нафтопроводу на надземному переході під час послідовного перекачування різних нафтопродуктів

Дмитро Тимків

Доктор технічних наук, професор
Івано-Франківський національний технічний університет нафти і газу
76019, вул. Карпатська, 15, м. Івано-Франківськ, Україна
https://orcid.org/0000-0003-0220-398X

Володимир Грудз

Доктор технічних наук, професор
Івано-Франківський національний технічний університет нафти і газу
76019, вул. Карпатська, 15, м. Івано-Франківськ, Україна
https://orcid.org/0000-0003-1182-2512

Роман Тутко

Аспірант
Івано-Франківський національний технічний університет нафти і газу
76019, вул. Карпатська, 15, м. Івано-Франківськ, Україна
https://orcid.org/0009-0003-5319-7943

Тетяна Тутко

Кандидат технічних наук, доцент
Івано-Франківський національний технічний університет нафти і газу
76019, вул. Карпатська, 15, м. Івано-Франківськ, Україна
https://orcid.org/0000-0002-9569-3035

Анотація. Метод послідовного перекачування різних нафтопродуктів, розділених між собою роздільником середовищ, є одним із найбільш поширених та економічно вигідних, проте, виникають значні коливання нафтопроводів на їх надземних ділянках через різницю густин. Дослідження таких коливань і їх впливу на міцність та стійкість надземних ділянок нафтопроводів практично відсутні, що робить цю тему актуальною. Метою даної статті було визначення коливань осі нафтопроводу та згинальних моментів, які водночас виникають, без врахування сил інерції перекачуваних нафтопродуктів для однопрогінного балкового переходу без компенсаторів повздовжніх деформацій. Побудовано математичну модель послідовного перекачування трубопроводом двох різних нафтопродуктів. Задача розв'язувалася методом розкладання шуканого розв'язку в ряд по власних функціях задачі вільних коливань надземної ділянки нафтопроводу зі застосуванням методу Фур'є. У результаті виконання обчислень за отриманим розв'язком задачі було встановлено, що в надземній ділянці нафтопроводу під час послідовного перекачування різних нафтопродуктів виникають знакозмінні коливання осі нафтопроводу відносно осі абсцис функції прогину осі нафтопроводу. Під час входження кінцевих перерізів роздільника в надземну ділянку нафтопроводу через десяті долі секунди в одному із середніх перерізів ділянки виникають найбільші прогини. Згинальні моменти мають найбільші значення за модулем. Криві прогину осі нафтопроводу та криві згинальних моментів для цих моментів часу практично співпадають. Встановлено, що найбільші за модулем згинальні моменти трубопроводу під час послідовного перекачування двох різних нафтопродуктів є суттєво більшими, ніж згинальні моменти цих же нафтопродуктів при їх окремому перекачуванні. Одержані результати дослідження будуть корисні на практиці проектувальникам трубопроводів, по яких послідовно перекачуватимуть нафтопродукти з різною густиною

Ключові слова: однопрогінний балковий перехід; вісь труби; власні функції задачі вільних коливань; прогини осі трубопроводу; роздільне середовище; згинальний момент

Vol. 24, No. 1
2024

PROSPECTING AND DEVELOPMENT OF OIL AND GAS FIELDS

https://pdogf.com.ua/en

Received: 14.12.2023. Revised: 08.04.2024. Accepted: 31.05.2024

UDC 622.276.66

DOI: 10.69628/pdogf/1.2024.44

Improving the formulation of hydraulic fracturing fluid

Bohdan Mykhailyshyn*

Postgraduate Student
Ivano-Frankivsk National Technical University of Oil and Gas
76019, 15 Karpatska Str., Ivano-Frankivsk, Ukraine
https://orcid.org/0009-0007-6383-2735

Ivan Kuper

PhD in Technical Sciences, Associate Professor
Ivano-Frankivsk National Technical University of Oil and Gas
76019, 15 Karpatska Str., Ivano-Frankivsk, Ukraine
https://orcid.org/0000-0003-1058-1382

Abstract. The growing need to increase production of natural hydrocarbons makes hydraulic fracturing technology one of the key methods of production stimulation, so the need to improve the efficiency and cost-effectiveness of hydraulic fracturing, which can be achieved by optimising the fluid composition, is becoming an urgent issue. The aim of the study was to find effective formulations of hydraulic fracturing fluid that would have the structural and rheological properties necessary for successful hydraulic fracturing in wells with temperatures above 80°C. An empirical method of conducting laboratory studies of hydraulic fracturing fluid formulations is used. To substantiate the rheological properties of hydraulic fracturing fluids, they were tested. This method involved systematic testing of various combinations of fluid components to select the optimal composition that would meet the requirements of efficient and economical fracturing at elevated well temperatures. The main types of fracturing fluids and their formulations are analysed, and the results of laboratory studies on the selection of optimal parameters of fracturing fluid in a well with a formation temperature of 85°C are presented. The relationship between the chemical composition (formulation) of the fracturing fluid and its rheological properties at a temperature of 85°C is experimentally established. Using the method of formulation selection, the composition of the fracturing fluid was found that can withstand landslide pressures, is stable and does not collapse prematurely. The article proposes a formulation of a fluid that can be used during hydraulic fracturing in gas and oil fields. Practical implementation of the research results will improve the efficiency of hydraulic fracturing technology and increase the productivity of oil and gas wells

Keywords: bottomhole formation zone; well; fracking; linear gel; laboratory fluid tests; polymers

Introduction

Hydraulic fracturing is a widely used technique to stimulate hydrocarbon production by creating a network of highly conductive fractures in the area around the wellbore and in the remote reservoir zone. The created network of fractures not only improves the conductivity of the reservoir rock, but also increases the filtration surface area, which helps to intensify hydrocarbon production. This method can be used in both vertical and horizontal wells. Oil and gas companies are working to develop the most effective fluid composition to achieve the best possible reservoir conductivity after the operation. Linear or cross-linked guars are the most commonly used fluids in traditional fracturing operations (Zhao *et al.*, 2020). The main functions of these fluids are to form or open a crack (a fracture) and transport propane through the crack (Almubarak *et al.*, 2020). To maintain gel stability at the end of the fracturing process, various chemicals are used. During fracturing in high temperature wells, conventional guar-based polymer systems degrade faster than at low temperatures and require more guar to maintain stability, as indicated by

Suggested Citation: Mykhailyshyn, B., & Kuper, I. (2022). Improving the formulation of hydraulic fracturing fluid. *Prospecting and Development of Oil and Gas Fields*, 24(1), 44-54. doi: 10.69628/pdogf/1.2024.44.

*Corresponding author

Y. Huang *et al*. (2024). However, increased concentrations of guar in the fluid lead to an increase in residual decay products after destruction and, as a result, to contamination of the bottomhole formation zone and the formation as a whole, as reported by S. Liu *et al*. (2020). To solve these problems, various high-temperature stabilisers are added to improve the thermal stability of these fracturing fluids at temperatures above 85°C.

The chemical composition of hydraulic fracturing fluids mainly includes polymer systems, cross-linking agents, bactericides (biocides), breakers, buffers, clay stabilisers, deflectors, friction reducers, gel stabilisers, surfactants and demulsifiers, and temperature stabilisers (Wang *et al*., 2022a; 2022b). To obtain a high viscosity of the linear gel, polymers are used. L. Moroz *et al*. (2023) emphasised the importance of each chemical in the gel structure. Cross-linkers are used to bind polymer molecules together. Destructors (breakers) are added to break the bonds between the polymer molecules in the formation and cause its dehydration. Clay stabilisers are used to prevent clay swelling. Demulsifiers are used to prevent emulsion formation and reduce surface tension. Buffer solutions are used to control the pH, acidity or alkalinity of the solution, which affect the hydration of the polymer, the quality and the cross-linking time. For high temperatures, temperature stabilisers are used. Defoamers prevent foam formation. Friction reducers are used to reduce pressure losses during pumping. Insulating agents are also used to isolate the processing interval at the top and bottom.

To select fracturing fluid compositions for specific well conditions, it is important to experimentally determine the stability of their rheological characteristics, as indicated by H. Xu *et al*. (2023) over the expected period of hydraulic fracturing operations and their post-operational decomposition time, simulating reservoir conditions. This process involves taking into account the geological and operational characteristics of the well, including reservoir filtration properties, reservoir temperature, pressure and sensitivity of the reservoir rocks to fracturing fluid. In fact, according to A.K. Quainoo *et al*. (2022), this process highlights the need for a comprehensive understanding and tailored approach to hydraulic fracturing operations, emphasising the critical role of adapting fluid formulations to the unique conditions of each well. By carefully evaluating the rheological properties of fracturing fluids under conditions that mimic the surrounding formation properties, engineers can improve the efficiency and effectiveness of the fracturing process. This approach not only improves hydrocarbon production, but also minimises potential negative effects on reservoir performance and environmental impact. Experimental determination of fluid stability and rheological properties requires sophisticated laboratory equipment and methodologies that can accurately reproduce the high pressure and high temperature conditions in deep underground reservoirs. In addition, understanding the sensitivity of the reservoir rock to fracturing fluids is paramount to avoiding a reduction in permeability that could impede hydrocarbon flow to the wellbore, as discussed in paper by S. Al-Hajri *et al*. (2022).

Overall, optimising the fracturing fluid based on detailed reservoir characteristics and precisely executing fracturing operations is fundamental to maximising oil and gas production. An analysis of various studies indicates that although considerable work has been done to develop and optimise hydraulic fracturing fluids, the aspect of creating effective fluids without the addition of temperature stabilisers with minimal polymer loads and studying their rheological effects remains insufficiently researched. This indicates the potential for further research in this area, especially given the growing demands for environmental safety and efficiency of hydrocarbon production processes. This work is aimed at finding a combination of chemical elements to create fracturing fluids without the addition of temperature stabilisers at minimal polymer loads and studying their rheological effects.

Materials and Methods

Laboratory tests were carried out, with a combination of different formulations of chemicals and their quantities. The following equipment was used in the laboratory: an aerometer designed to determine the density of the liquid; a blender used to mix chemicals; electronic scales for accurate measurement of the amount of chemicals; an acidity meter with a temperature sensor for determining pH and temperature; an Ofite viscometer (800S model, Ofite Company, USA) for determining viscosity; a Brookfield rheometer (PVS model, Brookfield Company, USA) for determining viscosity under specified reservoir conditions. All instruments in the laboratory are certified and periodically calibrated. Laboratory tests were carried out to find the optimal formulation parameters aimed at reducing and avoiding formation contamination with additional polymer degradation products. The aim was to achieve the required rheological properties of hydraulic fracturing fluids, in which the system would be stable, restore its rheological properties after phase loads and not be prematurely destroyed. This article describes the step-by-step formulation tests for fracturing fluids. The article considers the most common chemical composition of water-based fracturing fluid in Ukraine (Table 1). A test was carried out in the laboratory to select the optimal parameters of the fracturing fluid at a temperature of 85°C.

Table 1. Names of chemicals used in the study

S	Salt stabiliser	Sodium D-gluconate (80%), crystallised silicon dioxide (20%)
W	Accelerated cross-linker	Ethylene glycol (30%), sodium tetraborate (30%), water (40%)
D	Slow cross-linker	Ulexite (55%), diesel fuel (45%)

Table 1. Continued

B	Bactericide	2, 2-dibromo-2-cyano acetamide (80%), sodium glucate (10%)
N	Gelling agent	Guar gum/resin, guar
G	Clay stabiliser	Ethylene glycol (30%), choline bicarbonate (50%), water (20%)
X	Demulsifier of surfactants	Mixture of surfactants (75%), water (20%), ethylene glycol (5%)
C	Liquid destructor	Ammonium persulfate
Z	Encapsulated destructor	Encapsulated ammonium persulfate

Source: created by the authors

The water tests were conducted, which were used to prepare the fracturing fluid. The next step was a test to increase the viscosity of the linear gel and a cross-linking test. After that, the fluid was tested on a rheometer, which performed stability, shear and fracture tests. The water was tested for compatibility with the chemicals used in the process according to API RP 45: Recommended practice for analysis of oilfield waters (1998), according to which water was tested for chemical and mechanical impurities, which included the following items, and API RP 39: Recommended practices on measuring the viscous properties of a cross-linked water-based fracturing fluid (1998). Determination of water purity, colour and transparency. Determination of the salt content: the percentage of salt in water should not exceed 1.5%, otherwise the gel will quickly dehydrate. Determination of iron content (Fe): the amount of iron in the water should not exceed 10 mg/l, if this amount is exceeded, partial cross-linking of the polymer is recorded, and the overall quality of the cross-linked gel deteriorates. Determination of sodium (Na^+), potassium (K) and chloride (Cl^-) content: if the water content is high, the gel is cross-linked; the value should be less than 500 mg/l. Determination of alkalinity, bicarbonate content (HCO_3^-): it affects the hydration of the polymer and increases the cross-linking time of the gel at high rates. Determination of rigidity: determined by the content of calcium (Ca^{2+}) and magnesium (Mg^{2+}) in the water, with a large amount affects the gel cross-linking time, increasing it. Determination of the content of sulfates (SO_4^{2-}): the high content of sulfates contributes to the formation of dense insoluble mineral deposits. Determining the pH level, which should be between 6.0 and 8.0: if the pH is below 6.0, this leads to a lack of cross-linking, if it is above 8.0, then the linear gel cross-links too quickly. The test is carried out by dipping a strip of litmus paper, a universal indicator, into water. After one or two minutes, the changed colour of the indicator paper is compared with the colour of the scale provided in the kit.

In order to thicken the water to form a linear gel (linear gel viscosity test), 4 tests were performed, including 3 tests with a gelling agent loading of 2.8 kg/m³ and one test with a loading of 3.0 kg/m³. The research (test) methodology is as follows: pre-selected water for hydraulic fracturing was heated to a temperature of 50 degrees. Then it was transferred to a blender cup in a volume of 0.5 m³. The gelling agent was added and hydration was carried out for 6.5 min with the blades in the blender rotating at 300 rpm. The gel was then transferred in a volume of 400 ml to an Ofite viscometer. During the test, the temperature, pH of the water and gel, hydration time, and viscosity before and after the addition of guar were recorded. The methodology for the linear gel cross-linking test was as follows: the linear gel was transferred to a 0.5-litre blender cup. A cross-linker was added and hydration was carried out with the blades in the blender rotating at 2,000 rpm. After adding the cross-linker and chemical reagents to the linear gel, the temperature, dome formation time, funnel closure time, and cross-linking time were recorded. A combination of a slow and fast borate cross-linker was used for cross-linking. The shear rate (cross-linked gel shear test) has units of rpm. A Brookfield rheometer was used to measure the shear rate. The rheometer uses a rotating cup and a fixed rod with a gap between them to simulate a flow transition. The speed of rotation of the cup provides the shear rate, and the rod measures the shear load or resistance force acting on the walls of the cup and rod (Montgomery, 2013). This is determined by measuring the torque on the rod. The shear rate is the relative velocity between the stationary rod and the rotating cup divided by the separation gap. In the test, after the cross-linking test, the sample was transferred to the cup and sheared at a constant speed of 100 rpm until the temperature was brought to equilibrium. After heating the liquid, the speed increased to 500 rpm. This was repeated at least 4 times in the range of 100-500-100-500 rpm. The chemical composition given in Table 1 was used for the study and Tests 1, 2, 3, 4 were performed with the chemical reagent loads given in Table 2.

Table 2. The chemical reagent loads, Tests 1-4

Value	Test 1	Test 2	Test 3	Test 4
N, kg/m³	2.8	2.8	2.8	3.0
G, l/m³	2.0	2.0	2.0	2.0
X, l/m³	1.0	1.0	1.0	1.0
S, kg/m³	-	0.6	0.5	0.5
D, l/m³	2.5	2.5	2.2	2.2
W, l/m³	1.0	1.0	1.0	1.0

Source: created by the authors

The main stages of testing the stability of the cross-linked gel were as follows. A sample of the cross-linked gel was taken and transferred to a Brookfield rheometer. The sample chamber recreates reservoir conditions, pressure and temperature that are as close as possible to those that occur during hydraulic fracturing. During the exposure, it is necessary to monitor changes in the structure and properties of the gel, whether the system behaves consistently for 1 hour. At the end of the exposure, the test results should be analysed. If the gel remains stable and retains its properties, it can be used in the hydraulic fracturing process. If signs of destruction are found, it is necessary to change the gel formulation and retest. Since this fluid was selected for high-temperature wells, 3 stability tests (5, 6, 7) were performed at 85°C with the parameters given in Table 3. The cross-linked gel destruction test is carried out in the same way as the stability test, but with the addition of a destructor. Liquid (Z) and encapsulated (C) breakers were used for destruction (Table 4).

Table 3. The chemical reagent loads, Tests 5-7

Value	Test 5	Test 6	Test 7
N, kg/m^3	2.8	3.0	2.8
G, l/m^3	2.0	2.0	2.0
X, l/m^3	1.0	1.0	1.0
S, kg/m^3	0.5	0.5	0.6
D, l/m^3	2.2	2.2	2.5
W, l/m^3	1.0	1.0	1.0

Source: created by the authors

Table 4. The chemical reagent loads, Tests 8-10

Value	Test 8	Test 9	Test 10
N, kg/m^3	2.8	3.0	2.8
G, l/m^3	2.0	2.0	2.0
X, l/m^3	1.0	1.0	1.0
S, kg/m^3	0.5	0.5	0.6
D, l/m^3	2.2	2.2	2.5
W, l/m^3	1.0	1.0	1.0
Z, kg/m^3	0.2	0.2	0.2
C, kg/m^3	0.035	0.015	0.07

Source: created by the authors

Results

Water testing for compatibility with the chemicals used. Hydraulic fracturing requires a large amount of water. It is necessary that the water from a particular source meets certain acceptable parameters. For this purpose, before each hydraulic fracturing operation, water from each source is delivered to the laboratory and a number of tests are carried out. Figure 1 shows the colour of the indicator (arrow on the left) after reacting with water and comparing it to the colour of the scale (arrow on the right). The results of the content of calcium and magnesium bicarbonates, sulphates, chlorides, phosphates and iron ions in the liquid used in the following tests are shown in Table 5. It can be concluded that this water is suitable for the preparation of hydraulic fracturing fluid after conducting the following tests according to API RP 39: Recommended practices on measuring the viscous properties of a cross-linked water-based fracturing fluid (1998).

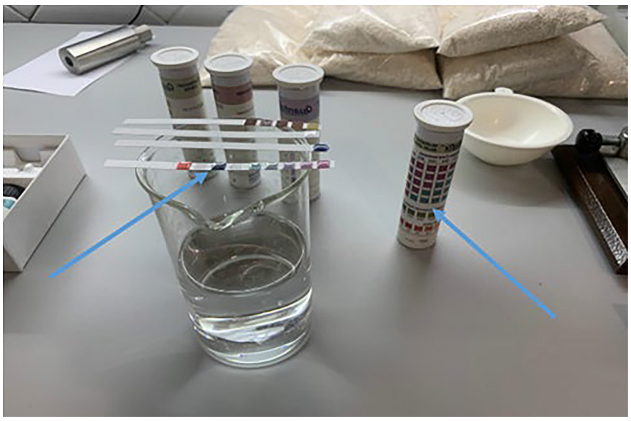

Figure 1. Testing water for substances

Source: created by the authors

Table 5. Testing water for impurity content

Value	Unit of measurement	Result	Norm
Density (25°C)	g/cm^3	0.998	1.005
pH	-	7.7	5-8.6
Na^+, K^+	mg/l	378.8	< 500
Ca^{2+}	mg/l	12	< 500
Mg^{2+}	mg/l	1	< 500

Table 5. Continued

Value	Unit of measurement	Result	Norm
Fe	mg/l	0	< 8
SO_4^{2-}	mg/l	80.3	< 100
Cl^-	mg/l	310.5	< 1,000
HCO_3^-	mg/l	410.7	< 600

Source: created by the authors

Test for increasing the viscosity of a linear gel. Traditionally, polymer systems based on guar are used to give fracturing fluids the necessary rheological properties. Despite their widespread use, such systems have disadvantages associated with changes in viscosity during pumping. An urgent problem is the insufficient viscosity recovery rate after changing the flow regime (from tubing to production string, from the string to perforations) and premature gel destruction. There is a problem of formation contamination with polymer degradation products. This is especially true at high reservoir temperatures in the well. Linear gel is a water-based liquid that is artificially thickened with guar-based chemicals. Guar is a long polymeric chain made up of mannose sucrose and galactose, called polysaccharides. After adding it to water, the viscosity of the liquid increases. Increasing the viscosity is necessary to ensure the effective ability of the linear gel to carry proppant. Table 6 shows the results of the study of four samples to increase the viscosity of a linear gel after adding guar to it.

Table 6. Linear gel test on a blender, Tests 1-4

Value	Test 1	Test 2	Test 3	Test 4
Water temperature, °C	50	49.7	52	53
Water pH level	7.70	7.9	7.9	7.8
Linear gel pH level	8.10	8.1	8.1	8.2
Viscosity, cP	13	13	13	14.5
Hydration time, min	6.5	6.5	6.5	6.5
Viscosity after 2 hours, cP	16.5	16.7	16.5	18

Source: created by the authors

The results of these studies show that this guar gains the required viscosity at these loads and this concentration can be used for subsequent tests. Due to the high temperature and well conditions for which this gel was prepared, it was necessary to increase the viscosity and add a cross-linker to avoid premature propane settling on the bottom hole and producing a stopper.

Linear gel cross-linking test. A cross-linked gel consists of the same materials as a linear gel, but a cross-linking agent is added to increase the viscosity of the linear gel from less than 10 cP to the range of 100 or 1,000 cP. Higher viscosity increases the fracture width so it can accept higher propane concentrations, reduces fluid loss to improve fluid efficiency, improves the fluid's ability to transport propane, and reduces friction pressure. Based on the experience of preparing liquids, if premature formation/disappearance of the funnel occurs or this time does not last longer than 40 seconds, the experiment should be carried out with other concentrations, as the gel will not be stable. The test was conducted according to the methodology described in the relevant section (Table 7). The cross-linking time of the fracturing fluid is an important element in the pumping process, as the cross-linking time must be shorter than the time it takes for the fluid to travel from the surface to the formation.

Table 7. Linear gel test on a blender, Tests 1-4

Value	Test 1	Test 2	Test 3	Test 4
Formation/disappearance of the funnel/cross-linking time, s	12/15/1.15	25/30/3.30	20/25/3.15	15/20/1.50
Cross-linked gel temperature, °C	40	40.5	42	40
Cross-linked gel pH level	8.41	8.49	8.42	8.45

Source: created by the authors

Cross-linked gel shear test. This test is carried out to determine the stability of the system under shear loads during the pumping process. Namely, the gel flows out of the tubing into the production string and passes through the perforations into the formation. The fluid shear stress is equal to the force of resistance on the plates divided by the area of the plates and has units of voltage or pressure (e.g. psi). The shear rate (or velocity gradient) is the relative velocity of the two plates divided by the distance between the plates.

The Brookfield rheometer used in the study is designed for measurements under elevated pressure and temperature conditions and is used for quality control and management in rheological testing. The rheometer is designed to measure the viscosity of liquid Newtonian media, as well as to construct and record rheological curves of

non-Newtonian media at high pressures and temperatures. After the shear test, the fluid should have a low shear sensitivity. The time to restore the gel viscosity to 400 cP, after reducing the shear rate, should not be: the beginning of viscosity recovery is 5 seconds and the full viscosity recovery is 1 minute. Figure 2 shows the gel flowing from the tubing into the production string (Section 1) and the gel entering the fracture through the perforations (Section 2).

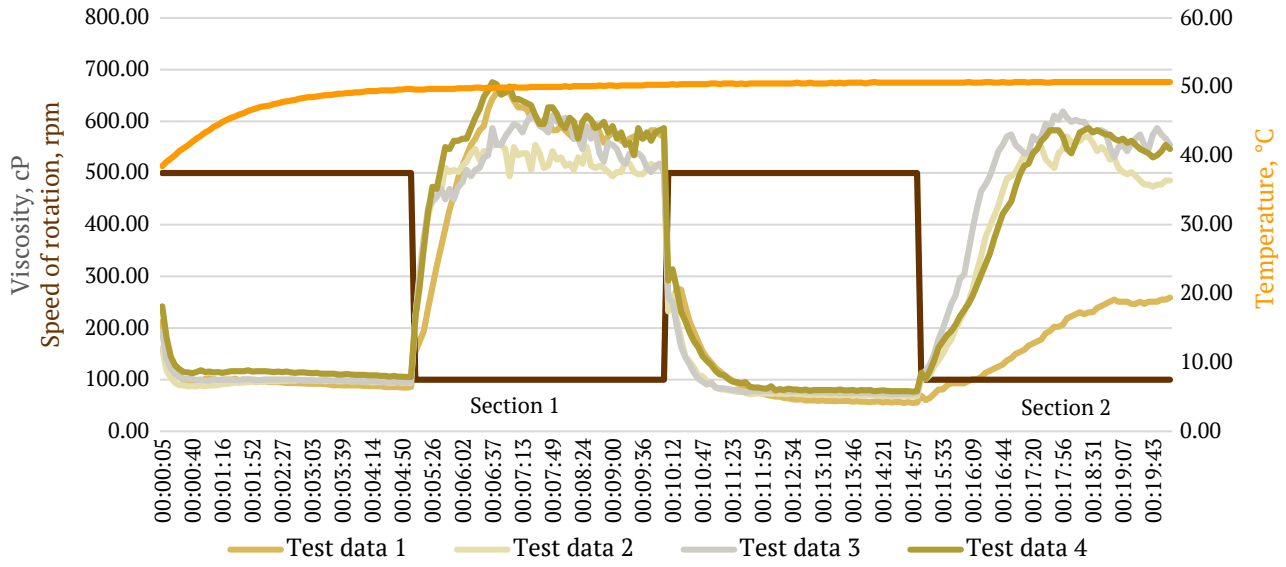

Figure 2. Cross-linked gel shear tests

Source: created by the authors

The first experiment showed a negative result, as the gel did not regain its rheological properties after changing the speed at section 2 (Test 1).

After the addition of the salt stabiliser, the system began to restore its characteristics and gained the required viscosity (Test 2, 3, 4). Since Test 3 is the best at restoring its characteristics, a gel stability study was conducted with this formulation.

Cross-linked gel stability test. The cross-linked gel stability test is performed to ensure that the system will behave consistently and not lose viscosity during the pumping process. During hydraulic fracturing, the viscosity of the fluid should not drop below 400 cP, as this is the minimum viscosity of the fracturing fluid that can hold the proppant in suspension. The results of the test are shown in Figure 3. The values obtained before installation on the rheometer are shown in Table 8.

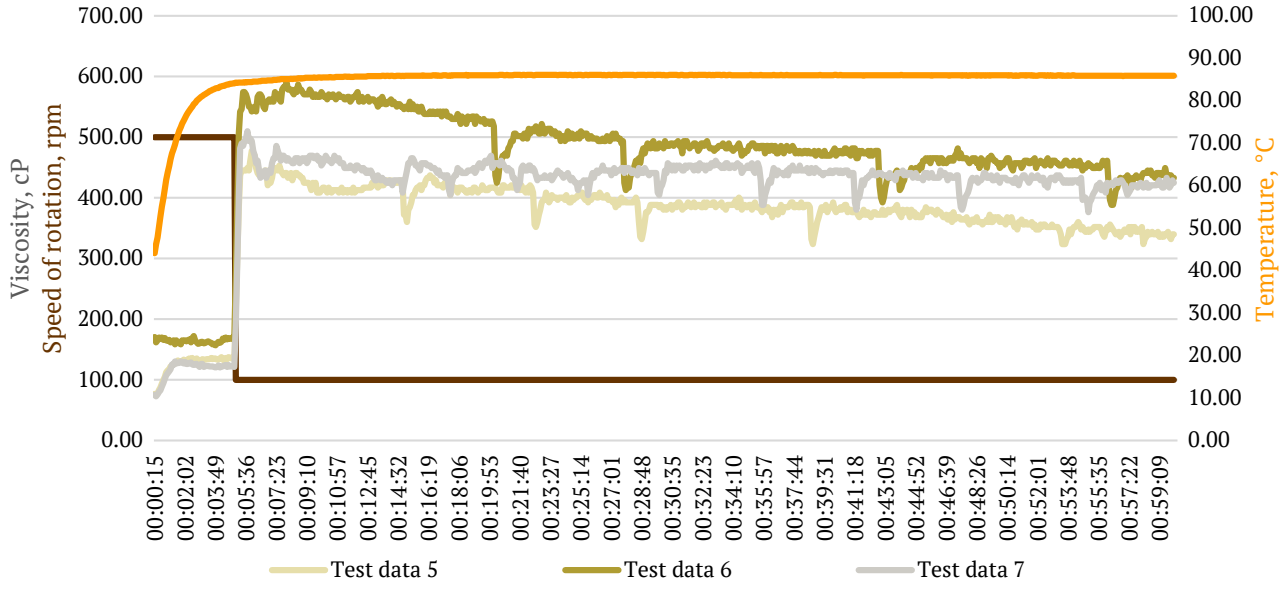

Figure 3. Cross-linked gel stability tests

Source: created by the authors

Table 8. Blender test, Tests 5-7

Value	Test 5	Test 6	Test 7
Water temperature, °C	53.4	52.2	54
Water pH level	7.70	7.8	7.78
Linear gel pH level	8.08	8.1	8.2
Viscosity, cP	13	15	13
Hydration time, min	6.5	6.5	6.5
Time of cross-linking/formation/disappearance of the funnel, s	17/19/2	17/22/1.40	17/20/2
Cross-linked gel temperature, °C	43	42	43
Cross-linked gel pH level	8.40	8.4	8.4

Source: created by the authors

From this graph, it can be concluded that these systems behave stably over time in the range of 350-600 cP, while Test 5 showed that a low concentration of guar leads to a drop in viscosity of 100 cP. Increasing the guar content in Test 6 results in an increase in viscosity at the beginning, but a decrease in viscosity over time of 150 cP. In Test 7, a smaller drop in viscosity (only 50 cP) was achieved with a lower concentration of guar, by increasing the salt stabiliser from 0.5 to 0.6 kg/m^3 and the concentration of slow crosslinker from 2.2 l/m^3 to 2.5 l/m^3. These systems are stable, so the following destruction tests are carried out.

Destruction test of cross-linked gel. This test is an important stage in the process of preparing for hydraulic fracturing, making sure that the gel will break down after the work is completed and will not remain in a viscous form in the formation.

There are slow-acting (encapsulated) and fast-acting (live) destructors. The active ingredient is ammonium persulfate. Often it is necessary to carry out a combination of fast and slow action to achieve the desired result. Table 9 shows the parameters of Tests 8-10 on the blender.

Table 9. Blender test, Tests 8-10

Value	Test 8	Test 9	Test 10
Water temperature, °C	42	45	46
Water pH level	7.90	7.96	7.92
Linear gel pH level	8.04	8.16	8.11
Viscosity, cP	13.5	13	13
Hydration time, min	6.5	6.5	6.5
Time of cross-linking/formation/disappearance of the funnel, s	16/18/1.40	12/15/1.30	17/20/2
Cross-linked gel temperature, °C	37	40	43
Cross-linked gel pH level	8.30	8.32	8.3

Source: created by the authors

Figure 4 shows that the time for complete gel degradation is 20 min, 30 min and 1 hour and 20 min (Tests 8-10). Depending on the amount of proppant per 1 m^3 and the pumping volume, the time required to ensure that the gel does not prematurely break down during the pumping process is set to a value that is sufficient. Also, after the gel is pumped into the formation, it is necessary for it to immediately begin to degrade.

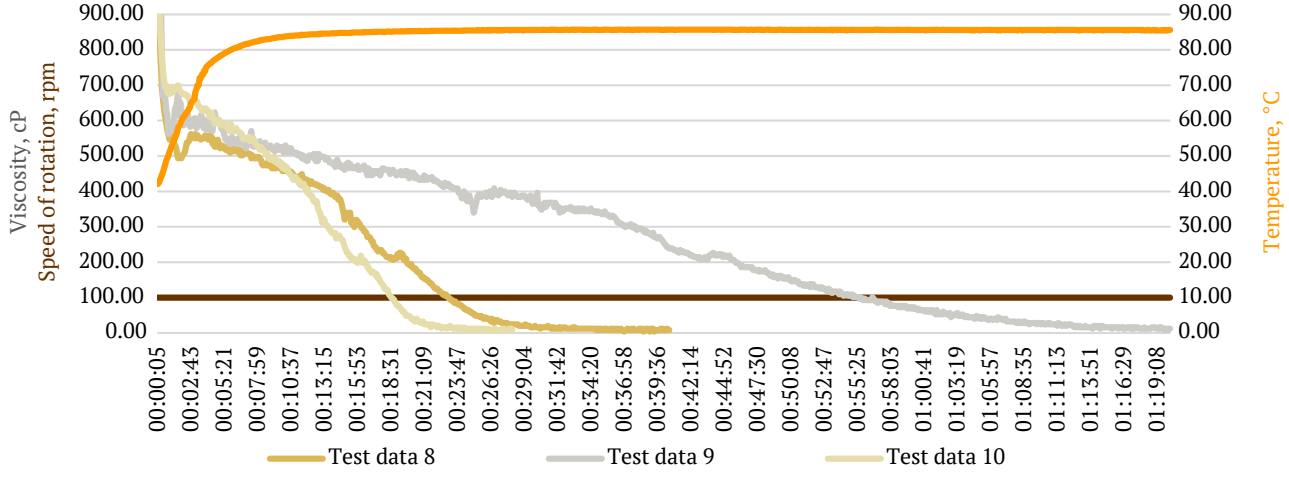

Figure 4. Performing a destruction test on a rheometer

Source: created by the authors

In Table 9, with a guar loading of 2.8 kg/m^3 and the addition of a live breaker of 0.035 kg/m^3 in Test 8, a small amount of pumping can be performed. For larger pumping volumes, it will be necessary to increase the guar concentration to 3.0 kg/m^3 according to Test 9 and reduce the live breaker concentration. A high content of live breaker (Test 10) reduces the pumping time and the risk of premature degradation. Fluid control is the most critical aspect of hydraulic fracturing and must be carried out continuously. For these reasons, fluid tests are carried out not only in the stationary laboratories of contractors, but also directly at the well, in the field laboratory. If the water has passed all the criteria, a polymer and other chemicals are added to it, reagents are used to produce a linear gel, and a bacteria test is carried out, as there are cases when water in wells becomes unsuitable for gel formation. The linear gel sample should not lose viscosity by more than 2 cP/hour. If this drop is recorded, it is necessary to determine from which container the water for this sample was taken and replace it with a new one. Fluid quality control continues during operation. A sample of the linear and cross-linked gel is taken from each stage, the viscosity and cross-linking time must be without deviations, in case of deviations during fluid pumping, it is necessary to re-inject the fluid into the formation, stop, find the cause and repeat the stimulation work. The fluid was required to have a viscosity above 450 cP, not to drop during the pumping period, and to restore its viscosity to this value after shear stress. A well-chosen formulation of chemicals ensured a stable viscosity. Thus, formulations using chemicals from Tests 8-10 can be successfully used for hydraulic fracturing planning.

Discussion

The fracturing fluid must meet the following requirements: compatibility with the formation and formation fluid; minimum friction values; gain of the required viscosity and maintenance of the viscosity index during all stages of hydraulic fracturing; low percentage of filtration into the formation; maximum decomposition of reagents after hydraulic fracturing with minimal formation colmatation; sufficient economic efficiency; ability to transport the unclogging agent into the depth of the fracture; ability to create the required fracture width; possibility of rapid fluid extraction after fracturing and destruction (destruction) of the gel; in the case of clays, preventing their swelling; possibility of preventing re-crosslinking after destruction (Moroz *et al*., 2021). The study was aimed at analysing the chemical composition and effectiveness of hydraulic fracturing fluids, in particular, the impact of polymer systems, cross-linking agents, biocides, and other components. The obtained results indicate the importance of optimising the fluid composition to increase the efficiency of hydraulic fracturing, which correlates with the data of current research in this area.

By analysing the effect of guar concentration on the viscosity of the linear gel, it was found that an increase in guar concentration increases the viscosity of the gel, which in turn provides more efficient transportation of proppant. These results are confirmed by the research of J. Song *et al*. (2020), which also highlights the importance of accurate polymer dosing to achieve optimal rheological properties of the liquid. The author's observations on the rate of recovery of gel viscosity after changing the flow regime partially contrast with the conclusions of the study by A.N. El-hoshoudy *et al*. (2020), which indicates a less significant effect of guar concentration on the rate of viscosity reduction. This may be due to differences in testing methodologies and the characteristics of the water samples used.

The addition of a salt stabiliser was found to be effective in improving the stability of the gel at high temperatures, consistent with the work of H. Khan *et al*. (2021). This underscores the importance of an integrated approach to formulating the chemical composition of fracturing fluid. Also interesting is the opinion of researchers X. Cao *et al*. (2021), who conducted a comparative study of hydraulic fracturing fluids for high-temperature formations with a high salt content, synthetic polymer-based fluids with liquids derived from guar gum. They found that guar gum-based fluids exhibited better shear and temperature resistance, as well as the ability to carry proppant in such challenging conditions. However, the presence of solid residues after the destruction of the gel of guar gum liquids prevents their use in the oil industry. The study shows the prospects of polymer-based synthetic fluids with improved rheological characteristics as an alternative to guar gum systems.

Another aspect of the study involved the analysis of cross-linked gel destruction. It has been established that the use of a combination of fast-acting and slow destructors allows achieving controlled gel disintegration that meets the requirements of efficient hydraulic fracturing. These results are consistent with data from the study by Z. Qu *et al*. (2021), which also demonstrates the importance of choosing the type and concentration of destructors to optimise the gel degradation process. In this study and in the study by W. Kang *et al*. (2020) it is shown that in addition to the main reagents that are present in the hydraulic fracturing fluid contains stabilisers, friction reducers and surfactants, which makes it resistant to high temperatures, improves penetration into the pores of the reservoir, prevents the formation of stable emulsions, minimises capillary effects, protects against corrosion and deposits. These properties make the gel a more efficient and versatile tool for working with oil and gas reservoirs.

An important contribution of this study is the emphasis on the need for an individual approach to each well, taking into account its unique conditions, which is also noted in the paper by T. Jatykov & K. Bimuratkyzy (2022), which considers the problem of optimising the composition of hydraulic fracturing fluids in high-temperature oil and gas fields on the example of the Jurassic oil and gas fields located in the west of Kazakhstan. The study conducted a series of laboratory tests to select appropriate chemicals based on scientific and practical approaches. Tests included checking the thermal stability of the fluid, shear and stability tests. Additionally, emulsion breakdown tests, water analysis, cross-linking time, pH measurements and gel

tests were performed. Based on these tests, gelling agents, cross-linkers, breakers and various additives such as demulsifiers, pH buffers, clay inhibitors and biocides were selected. Each component had its own chemical equivalent with the desired concentration. The developed fracturing fluid was successfully used in a 20-tonne fracturing operation in Jurassic sandstones with bottomhole temperatures of up to 105°C and permeability of about 3 mD. The operation was successful and resulted in increased production and encouraging long-term effects. Comparing the results with the presented study, the authors agree with the conclusions of T. Jatykov & K. Bimuratkyzy (2022) who said that the choice of hydraulic fracturing fluid composition at high temperatures requires a careful approach and the use of specialised laboratory tests. Adapting the composition of chemicals to the specific conditions of the field can significantly improve fracturing results and increase well productivity. This confirms that, despite the general trends and recommendations, each fracking case requires a detailed analysis and may differ in terms of the optimal fluid composition.

P. Sharma & V.K. Kudapa (2021) found a decrease in cross-linking time with an increase in the concentration of cross-linking agents. These studies were conducted with a different purpose of creating a fluid to block water in the oil wellbore, but the methodology for creating the gel correlates with the findings of this study. Research by G.G. Vargas *et al*. (2020) focused on the rheological characteristics of a cross-linked water-based guar gum gel. It was found that the gel behaves like a viscoelastic liquid and is slippery even on rough surfaces. This characteristic is important for the fracturing process because it facilitates the movement of the gel along the wall. Particular attention was paid to the maximum stress above which the gel slips, indicating its practical significance for estimating the total pressure drop during hydraulic fracturing. These studies are relevant and it is necessary to conduct additional tests of the rheological properties of the resulting formulation in future studies.

Some studies, like the one by X. Cao *et al*. (2021), focused on optimising water-based gel formulations for hydraulic fracturing to ensure efficient crack formation while minimising environmental impact and reservoir damage. For example, the development of high-temperature resistant, clean and environmentally friendly fracturing fluid systems aims to address reservoirs with conditions that rapidly degrade conventional fracturing fluids. Systems have been developed to maintain efficient rheological properties and stability at extreme temperatures, providing better fracture formation and proppant transport in tight sandstone formations. In the same study, similar results were obtained, but the method of achieving the result was different.

The study proved that with a lower guar content, the required viscosity can be maintained, which in turn will lead to a reduction in formation contamination after gel breakdown. Therefore, the found formulations, namely the number of chemicals in Tests 8-10, can be used to create a hydraulic fracturing design. The next step is to perform hydraulic fracturing and analyse the impact of this formulation on the formation and production after hydraulic fracturing. The discussion not only analysed the results in detail in the context of current research, but also emphasised the importance of an individual approach to each case of hydraulic fracturing, identifying ways to further improve the technology. Based on the comparative analysis, it can be concluded that the authors' research makes a significant contribution to understanding the interaction of chemical components in hydraulic fracturing fluids and their impact on process efficiency. However, the identified differences indicate the need for further detailed research to develop optimal liquid formulations, taking into account a variety of reagents.

Conclusions

A comprehensive study was carried out to analyse the main requirements for fracturing fluids and optimise their formulations for use at a formation temperature of 85°C. This work contributes to a deeper understanding of the importance of selecting appropriate chemical components and their concentrations to improve the efficiency of the fracturing process. The aim set at the beginning of the study was achieved. Particular attention was paid to optimising the fracturing fluid formulation, which would not only achieve the required viscosity and rheological properties but also ensure their stability during the operation. The results of the study showed that the selection of water compatible with chemicals is critical to the preparation of an effective fracturing fluid. Testing of different types of guars has shown that choosing a higher quality guar allows you to achieve the desired viscosity at lower concentrations, which has a lower impact in terms of degradation products. Experiments aimed at analysing the rheological characteristics of cross-linked gels under shear loads confirmed the ability of three specific concentrations to restore the required viscosity above 450 cP.

Further study of the stability of these gels showed that the two selected formulations effectively retained their properties for one hour without reducing their viscosity to below 450 cP. The study and destruction of the cross-linked gel highlighted the importance of choosing the right concentration of destructors to ensure rapid gel disintegration after the fracturing procedure and faster cleaning of the wellbore, including deeper destruction of the gel without the formation of lumpy clots during its disintegration. These findings highlight the need for detailed monitoring of fracturing fluid parameters not only at the laboratory stage but also during well operations. Further research should focus on the development of new gel and fracturing agent formulations with improved environmental performance and higher stability at extreme temperatures, paving the way for optimisation and increased hydrocarbon recovery after hydraulic fracturing.

Acknowledgements

None.

Conflict of Interest

None.

References

[1] Al-Hajri, S., Negash, B.M., Rahman, M.M., Haroun, M., & Al-Shami, T.M. (2022). Perspective review of polymers as additives in water-based fracturing fluids. *ACS Omega*, 7(9), 7431-7443. doi: 10.1021/acsomega.1c06739.

[2] Almubarak, T., Ng, J.H.C., AlKhaldi, M., Panda, S., & Nasr-El-Din, H.A. (2020). Insights on potential formation damage mechanisms associated with the use of gel breakers in hydraulic fracturing. *Polymers*, 12(11), article number 2722. doi: 10.3390/polym12112722.

[3] API RP 39: Recommended practices on measuring the viscous properties of a cross-linked water-based fracturing fluid. (1998). Retrieved from https://standards.globalspec.com/std/997097/api-rp-39.

[4] API RP 45: Recommended practice for analysis of oilfield waters. (1998). Retrieved from https://standards.globalspec.com/std/1647351/api-rp-45.

[5] Cao, X., Shi, Y., Li, W., Zeng, P., Zheng, Z., Feng, Y., & Yin, H. (2021). Comparative studies on hydraulic fracturing fluids for high-temperature and high-salt oil reservoirs: Synthetic polymer versus guar gum. *ACS Omega*, 6(39), 25421-25429. doi: 10.1021/acsomega.1c03394.

[6] El-hoshoudy, A.N., Zaki, E.G., & El-Saeed, S.M. (2020). Experimental and Monte Carlo simulation of palmitate-guar gum derivative as a novel flooding agent in the underground reservoir. *Journal of Molecular Liquids*, 302, article number 112502. doi: 10.1016/j.molliq.2020.112502.

[7] Huang, Y., Yao, X., Dai, C., Wu, Y., Li, L., & Yuan, B. (2024). A supramolecular reinforced gel fracturing fluid with low permeability damage applied in deep reservoir hydraulic fracturing. *Gels*, 10(1), article number 2. doi: 10.3390/gels10010002.

[8] Jatykov, T., & Bimuratkyzy, K. (2022). A chemical design example of hydraulic fracturing fluids in high-temperature hydrocarbon reservoirs: Case study. *Trends in Sciences*, 19(12), article number 4610. doi: 10.48048/tis.2022.4610.

[9] Kang, W., Mushi, S.J., Yang, H., Wang, P., & Hou, X. (2020). Development of smart viscoelastic surfactants and its applications in fracturing fluid: A review. *Journal of Petroleum Science and Engineering*, 190, article number 107107. doi: 10.1016/j.petrol.2020.107107.

[10] Khan, H., Spielman-Sun, E., Jew, A., Bargar, J., Kovscek, A., & Druhan, J. (2021). A critical review of the physicochemical impacts of water chemistry on shale in hydraulic fracturing systems. *Environmental Science & Technology*, 55(3), 1377-1394. doi: 10.1021/acs.est.0c04901.

[11] Liu, S., Huang, J., Tang, S., Shi, S., Wu, X., & Liu, X. (2020). Experimental study on the damage of artificial fracture permeability in coal during the flow back of guar-based fracturing fluid. *Geofluids*, 2020, article number 8302310. doi: 10.1155/2020/8302310.

[12] Montgomery, C. (2013). Fracturing fluids. In A.P. Bunger, J. McLennan & R. Jeffrey (Eds.), *Effective and sustainable hydraulic fracturing* (ch. 1). London: IntechOpen. doi: 10.5772/56192.

[13] Moroz, L., Uhrynovskyi, A., & Kogut, G. (2023). Investigation of the effect of polymer concentration in fracturing fluid on crack size and permeability during hydraulic fracturing. *Archives of Materials Science and Engineering*, 122(2), 70-77. doi: 10.5604/01.3001.0053.9594.

[14] Moroz, L., Uhrynovskyi, A., & Popovych, N. (2021). Study of hydraulic fracturing at oil wells to intensify production. *InterConf*, 87, 332-337. doi: 10.51582/interconf.21-22.11.2021.040.

[15] Qu, Z., Wang, J., Guo, T., Shen, L., Liao, H., Liu, X., Fan, J., & Hao, T. (2021). Optimization on fracturing fluid flowback model after hydraulic fracturing in oil well. *Journal of Petroleum Science and Engineering*, 204, article number 108703. doi: 10.1016/j.petrol.2021.108703.

[16] Quainoo, A.K., Bavoh, C.B., & Negash, B.M. (2022). Rheological and viscoelastic property characterizations of amino acid-based hydraulic fracturing fluids. *Energy & Fuels*, 36(7), 3539-3548. doi: 10.1021/acs.energyfuels.1c04396.

[17] Sharma, P., & Kudapa, V.K. (2021). Study on the effect of cross-linked gel polymer on water shutoff in oil wellbores. *Materials Today: Proceedings*, 48(5), 1103-1106. doi: 10.1016/j.matpr.2021.07.506.

[18] Song, J., Navarrete, R., Asadi, M., & Jin, B. (2020). New high viscosity friction reducers for proppant transport in hydraulic fracturing. In *SPE international conference and exhibition on formation damage control* (article number SPE-199330-MS). Lafayette: Society of Petroleum Engineers. doi: 10.2118/199330-ms.

[19] Vargas, G.G., Andrade, R.M., Loureiro, B.V., & Soares, E.J. (2020). Rheological properties of a cross-linked gel based on guar gum for hydraulic fracture of oil wells. *Journal of the Brazilian Society of Mechanical Sciences and Engineering*, 42, article number 498. doi: 10.1007/s40430-020-02579-w.

[20] Wang, J., Guo, P., Jiang, H., & Zhou, F. (2022a). A novel multifunction fracturing fluid compounding of nano-emulsion and viscous slickwater for unconventional gas and oil. *Arabian Journal of Chemistry*, 15(5), article number 103749. doi: 10.1016/J.ARABJC.2022.103749.

[21] Wang, M., Cheng, H., Wei, J., Zhang, K., Cadasse, D., & Qin, Q. (2022b). High-temperature-resistant, clean, and environmental-friendly fracturing fluid system and performance evaluation of tight sandstone. *Journal of Environmental and Public Health*, 2022, article number 5833491. doi: 10.1155/2022/5833491.

[22] Xu, H., Zhou, F., Li, Y., Su, H., Yang, S., Yao, E., & Zhu, Y. (2023). Preparation and properties evaluation of novel silica gel-based fracturing fluid with temperature tolerance and salt resistance for geoenergy development. *Arabian Journal of Chemistry*, 16(12), article number 105324. doi: 10.1016/j.arabjc.2023.105324.

[23] Zhao, M., Li, Y., Xu, Z., Wang, K., Gao, M., Lv, W., & Dai, C. (2020). Dynamic cross-linking mechanism of acid gel fracturing fluid. *Colloids and Surfaces A: Physicochemical and Engineering Aspects*, 607, article number 125471. doi: 10.1016/j.colsurfa.2020.125471.

Удосконалення рецептури рідини гідророзриву

Богдан Михайлишин

Аспірант
Івано-Франківський національний технічний університет нафти і газу
76019, вул. Карпатська, 15, м. Івано-Франківськ, Україна
https://orcid.org/0009-0007-6383-2735

Іван Купер

Кандидат технічних наук, доцент
Івано-Франківський національний технічний університет нафти і газу
76019, вул. Карпатська, 15, м. Івано-Франківськ, Україна
https://orcid.org/0000-0003-1058-1382

Анотація. Зростаюча потреба в нарощуванні видобутку природніх вуглеводнів робить технологію гідравлічного розриву пласта одним із ключових методів інтенсифікації видобутку, тому актуальним питанням стає необхідність підвищення ефективності та економічності гідророзриву, що може бути досягнуто за рахунок оптимізації складу рідини. Мета дослідження полягала в пошуку ефективних рецептур технологічної рідини для гідравлічного розриву пласта, які б мали структурно-реологічні властивості необхідні для успішного проведення гідророзриву у свердловинах із температурою більше 80 °С. Використано емпіричну методику проведення лабораторних досліджень рецептур рідин гідророзриву. Для обґрунтування реологічних властивостей рідин для гідравлічного розриву пласта було проведено їх тестування. Цей метод передбачав систематичне тестування різних комбінацій компонентів рідини з метою підбору оптимального складу, який би відповідав вимогам ефективного та економічного гідророзриву за підвищеної температури свердловин. Проаналізовано основні види рідин гідророзриву і їх рецептури, наведено результати лабораторних досліджень із підбору оптимальних параметрів рідини гідророзриву у свердловині з пластовою температурою 85 °С. Експериментально встановлено взаємозв'язок між хімічним складом (рецептурою) рідини для гідророзриву і її реологічними властивостями за температури 85 °С. Методом підбору рецептур знайдено склад рідини гідророзриву, яка витримує зсувові навантаження, стабільна та не руйнується передчасно. Запропоновано рецептуру рідини, яку можна використати під час проведення гідравлічного розриву пласта на газових і нафтових родовищах. Практична реалізація результатів дослідження дозволить підвищити ефективність технології гідророзриву пласта й збільшити продуктивність нафтових і газових свердловин

Ключові слова: привибійна зона пласта; свердловина; гідравлічний розрив пласта; лінійний гель; лабораторні тести рідини; полімери

Vol. 24, No. 1
2024

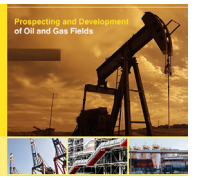

PROSPECTING AND DEVELOPMENT OF OIL AND GAS FIELDS

https://pdogf.com.ua/en

Received: 20.11.2023. Revised: 21.03.2024. Accepted: 31.05.2024

UDC 553.98.061.4

DOI: 10.69628/pdogf/1.2024.55

Evaluation of the influence of lithological and stratigraphic sections structure and capacitance-filtration parameters on the results of geophysical surveys of wells

Dmytro Fedoryshyn

Doctor of Geological Sciences, Professor
Ivano-Frankivsk National Technical University of Oil and Gas
76019, 15 Karpatska Str., Ivano-Frankivsk, Ukraine
https://orcid.org/0009-0004-5348-9564

Oleksandr Trubenko*

PhD in Geological Sciences, Dean
Ivano-Frankivsk National Technical University of Oil and Gas
76019, 15 Karpatska Str., Ivano-Frankivsk, Ukraine
https://orcid.org/0000-0003-3418-439X

Serhii Fedoryshyn

PhD in Geological Sciences, Associate Professor
Ivano-Frankivsk National Technical University of Oil and Gas
76019, 15 Karpatska Str., Ivano-Frankivsk, Ukraine
https://orcid.org/0009-0005-9274-7244

Ihor Mykhailovskyi

Postgraduate Student
Ivano-Frankivsk National Technical University of Oil and Gas
76019, 15 Karpatska Str., Ivano-Frankivsk, Ukraine
https://orcid.org/0009-0007-7948-4026

Abstract. Increasing hydrocarbon production from reservoir rocks of complex structure within the Neogene system of the Bilche-Volytske zone of the Precarpathian trough is a rather multifaceted problem that needs to be substantiated by conducting comprehensive geophysical, petrophysical and petrographic studies. The aim was to substantiate the physical-mechanical, electrical acoustic and petrophysical parameters based on the results of geophysical studies in a thin-layered Neogene section of gas and gas condensate fields within the Bilche-Volytske zone of the Precarpathian trough. The methodology for studying the complex Neogene sediments within the Bilche-Volytske zone of the Precarpathian trough was based on the quality of geophysical and petrophysical data obtained directly during drilling of exploration and development wells. In addition, the dominant role was played by the results of laboratory experimental studies of core samples, reflecting reservoir thermobaric conditions. Based on the results of such comprehensive geological and geophysical studies, it was established that the readings of geophysical methods are significantly affected by the thin-layered structure of the geological section, which is lithologically represented by the interlayering of sandstones, siltstones and mudstones. It has been found that the downhole instruments used in geophysical expeditions have a significant impact on the readings of geophysical methods. Accordingly, the research results are aimed at improving the efficiency of hydrocarbon exploration and control of their extraction. Therefore, the availability of highly informative integrated geophysical surveys, in particular, multi-probe acoustic logging, high-frequency induction logging isoparametric probing and repeated neutron logging, allows optimising conclusions regarding the prospects

Suggested Citation: Fedoryshyn, D., Trubenko, O., Fedoryshyn, S., & Mykhailovskyi, I. (2022). Evaluation of the influence of lithological and stratigraphic sections structure and capacitance-filtration parameters on the results of geophysical surveys of wells. *Prospecting and Development of Oil and Gas Fields*, 24(1), 55-66. doi: 10.69628/pdogf/1.2024.55.

*Corresponding author

for hydrocarbon discovery in complex thin-layer sections. The introduction of new approaches to the identification of such layers and strata will improve the information content of geological and geophysical methods and increase the hydrocarbon yield within the Bilche-Volytske area of the Precarpathian trough

Keywords: lithotypes; reservoir; porosity and permeability coefficients; electrical resistance; pores; acoustic impedance; electrical and acoustic probes

Introduction

The issue of increasing hydrocarbon production in the western region of Ukraine is linked to the known oil and gas bearing zones where commercial oil and gas reserves have already been proven. These zones include the Krukenytsia sub-zone of the Bilche-Volytske zone of the Precarpathian trough, where a number of gas fields have been discovered. These deposits are confined to anticlinal structures of the Upper and Lower Dashava sediments of the Neogene system, inherited and covering the uplifted areas of the Miocene basement, the erosion relief of which is controlled by the gypsum anhydrite horizon. The study of such complex reservoir rocks by geophysical methods of well logging is sometimes difficult. This applies to the interpretation of electrical and acoustic readings, which do not fully correspond to the actual geophysical parameters of the formations that fill the Neogene section. Establishing the influence of rock matrix skeleton composition, type of fluid saturating them, presence of bound water and the other characteristics on physical and petrophysical values of reservoir rocks allows to increase the efficiency of geophysical surveys. Increasing the information content of the results of comprehensive geophysical surveys of complex reservoir rocks will help identify additional promising hydrocarbon accumulation sites, which will allow increasing their reserves.

Many scientists have been studying the deep structure of the sedimentary layer and determining the prospects for oil and gas in the Krukenytsia Basin. In particular, Y. Krupskyi (2020) pointed out the peculiarities of the geodynamic development of the Bilche-Volytske zone and outlined the prospects for oil and gas content of the stratigraphic section. He also highlighted a new interpretation of the main regularities in the location and formation of hydrocarbon deposits from the perspective of the geodynamic development of the Carpathian Region. S. Anikeyev & S. Rozlovska (2021) analysed in more detail the features of the deep geological structure of the subsoil of the western region of Ukraine based on seismic surveys and proposed further directions for oil and gas exploration based on seismic data. In addition, the geological informativeness of the morphology of anisotropic transformations of potential fields in the study of fault tectonics of the Ukrainian Carpathians and adjacent depressions was clarified. The work of M. Pavlyuk *et al*. (2021) substantiates the formation of tectonic faults and the creation of structural objects with prospects for hydrocarbons. The main attention is paid to hydrogeological criteria for assessing oil and gas prospects on the example of substantiation of new prospecting objects in the platform autochthon under the Pokuttia-Bukovyna Carpathians thrust.

In the works of S.S. Kurovets *et al*. (2018) and O.M. Karpenko *et al*. (2021), low-porosity productive rocks of the Sarmatian sediment reservoirs of the Precarpathian trough were identified, their petrophysical parameters were substantiated, and the patterns of deviation of fluid filtration parameters through low-porosity rocks from Darcy's law were established. Based on the data from the well logging and using statistical methods of studying the lithological and facies dissection of the oil and gas reservoir, statistical relationships between natural radioactivity and organic carbon content were established. Y.M. Koval & I.O. Fedak (2022) identified promising areas with favourable structural, tectonic and paleohydrodynamic conditions for the formation of hydrocarbon deposits in the sediments of the Lower Dashava and Upper Dashava sub-suites. Also, M. Yershov *et al*. (2022) conducted research on the study of temporal patterns of time series trends of data from hydrogeological monitoring stations located in the Carpathian Region, which is a cross-border territory of Ukraine. Based on the results of the studies, the researchers found that the low resistivity of the reservoir layers of Neogene sediments is caused by the electrical conductivity of the grains of rock-forming minerals, namely pyrite and chlorite.

In the process of saturation of complexly constructed thin-layered sediments of the Sarmatian, Badenian and Helvetian stages of the Neogene system, the results of well studies using traditional methods are affected by an ambiguous assessment of the nature of saturation with potentially oil and gas-saturated reservoir rocks. Accordingly, the purpose of the study was to identify the factors that cause ambiguity in the thin-layer section and to unambiguously identify productive horizons in the course of well logging, which leads to the omission of productive gas-saturated reservoir rocks. Accordingly, the task was to evaluate the quality of the results of the geophysical survey used to dissect a thinly layered geological section, taking into account the mineralogical structure of the rock matrix, the nature of their saturation and their impact on the readings of geophysical methods. In addition, it was necessary to substantiate and adapt filtration and capacitance parameters to similarly complex reservoir rocks in neighbouring exploration and production fields.

Materials and Methods

In the course of prospecting and exploration of reservoir rocks formed under different conditions of sedimentation in lithological and stratigraphic sections and hydrocarbon-saturated traps within the Krukenytsia depression, a number of tasks arise that are solved by means of

geological logging. Given the complexity of the geological structure of the prospecting and exploration areas of the Bilche-Volytske zone, it became necessary to substantiate the geological structure of the gas and gas condensate fields that are promising for hydrocarbons (Kurovets *et al*., 2021). In the course of the study, it was necessary to take into account and detail the project for drilling exploration wells, including reference wells with maximum core sampling. On the basis of the selected core, an experimental collection of samples was formed that meets the requirements of mathematical statistics (GSTU 41-00032626-00-025-2000, 2001). Rock studies included determination of the chemical composition of rock-forming minerals, their structure, establishment of conditions of their formation, quantification of the content of basic minerals, structural features and presence of micro-impurities. To identify the main radioactive elements (U(Ra), Th, and K), nuclear-physical studies were used to determine the distribution of radioactive isotopes in a thin-layered section with sand layers from 0.15 m to 0.45 m thick in Neogene deposits of gas condensate fields in the Bilche-Volytske zone of the Precarpathian trough (Fedoryshyn *et al*., 2015).

Taking into account the geological heterogeneity of the Neogene sediments of the Bilche-Volytske zone of the Precarpathian trough, the core material was studied by comprehensive petrophysical research. First of all, a granulometric analysis was carried out to separate sand (> 0J mm), siltstone (0.1-0.01 mm) and clay (< 0.01 mm) fractions. The granulometric analysis is based on the distribution of clay and sandy-siltstone fractions in the core, which is carried out by washing and settling in water and sieving the fraction > 0.01 mm on sieves. A particular feature of particle size analysis is the need to destroy the rock structure to separate it into mineral grains, fragments and cementing particles. Core testing for carbonation (C_c) was carried out using hydrochloric acid. The volumetric method was used for the study. It is based on determining the volume of carbon dioxide (CO_2), which was released after the reaction of the carbonate component with hydrochloric acid (HCI). Absolute permeability (K_{ap}) is measured on cylindrical samples by the method of stationary filtration at different differential pressures. Open porosity measurements were also carried out (K_p) by the weight method by saturating cylindrical core samples with kerosene. The residual gas saturation was modelled on the core samples using the centrifugation method by obtaining a capillary pressure curve for the sample with residual water saturated with kerosene. The specific electrical resistivity of fully and partially water-saturated rocks and the specific electrical resistivity of formation water (model) were also measured to calculate the porosity parameter P_p and the saturation parameter P_s. These parameters are the main characteristics for constructing petrophysical dependencies of the type $P_p = f(K_p)$, $P_s = f(K_s)$, which were used for operational interpretation of the geophysical methods of well logging.

The results of the research are the basis for the future identification and evaluation of specific productive gas and gas condensate-saturated reservoirs within the lithological and stratigraphic exploration sections (Ivaniuta, 1998). It should also be noted that the effectiveness and reliability of the established geophysical and petrophysical parameters will be affected by the value of reservoir pressure, temperature and physical and mechanical parameters of the stratified rocks. In addition, the structure of lithotypes is influenced by the presence of a rift structure that stretches along the Krakovets Fault, from the Polish-Ukrainian border, in a strip of several to 10 km. Thus, to solve the tasks set, the results of well logging in the wells of the Vizhomlia gas field were analysed, namely the section of Neogene sediments, where intervals of gas and condensate saturated formations, which are mainly represented by sandstones and siltstones, were identified. The completed geophysical survey consisted of a mandatory set of well logging data, which allows to successfully solve both general geological tasks of lithological dissection and correlation of geological sections and to establish industrial and geophysical characteristics (identification of reservoir rocks, determination of their porosity, effective thickness, oil and gas saturation, and contact mapping).

Processing and interpretation of the source materials of the well logging data begins with the division of the geological section into layers and strata, which starts with the identification of the boundaries of the layers and determination of their reservoir characteristics. The task is solved with the help of computerised Geoposhuk technology (Krasnozhon *et al*., 2003). The processing process consists of several successive processing stages: section splitting into layers and interlayers, determination of the resistivity of these layers and the flushing fluid, quality assessment of well logs, evaluation of the filtration capacity of rocks, identification of reservoir and cover rocks and determination of their saturation. The construction of a correlation geological section begins with the formation of an integrated working database, which is loaded into a window for operational interpretation. The next stage is the construction of geophysical data sheets, where the section was divided into layers and interlayers and the quality of logging materials was assessed. Comprehensive interpretation begins with an assessment of the filtration and reservoir properties of rocks and reservoirs using a universal formula interpreter, and a geophysical conclusion is generated based on the results of logging interpretation. As a result of the consolidated interpretation of the logging data, a correlation geological profile was built along a given well line. The porosity coefficient, physical and mechanical parameters, and rock matrix compression ratio are calculated using the following formulas:

$$\beta_{rm} - \frac{1}{V}\left(\frac{dV_p}{dP}\right)P_{rp}^{t};$$
$$\beta_{por} = -\frac{1}{V_{por}}\left(\frac{dV_p}{dP}\right)P_{por}^{t}, \quad (1)$$

where β_{rm} and β_{por} are, respectively, the compression ratio of the rock matrix and its void space. Taking into account that rock-forming minerals are characterised by a low value of the compression coefficient in the rock matrix, the most informative is the void compression coefficient. This

coefficient changes with depth according to the hyperbolic law (Dentith *et al*., 2020). The porosity parameter of reservoir rocks decreases at a reservoir pressure of 150 MPa to 17-18%. With the increase of saturation of gas-saturated reservoir rocks with water under conditions of increasing effective pressure and temperature, the specific electrical resistivity increases. In this case, the calculation of the resistivity of the rock is performed by the following differential equation:

$$\frac{d\rho_p}{\rho_p} = \frac{1}{\rho_p}\left[\frac{d\rho_p}{dP_{ef}}\right] P_{rp}^{t^0} \times dP_{ef} + \frac{1}{\rho_p}\left[\frac{d\rho_p}{dP_{rp}}\right] P_{ef}^{t^0} dP_{rp} + \\ + \frac{1}{\rho_p} \times \frac{d\rho_p}{dt} dt = K_{rm} dP_{ef} - K_{elw} dP_{rp} - (\alpha t)\rho dt, \quad (2)$$

where K_{rm} – coefficient of relative change in specific electrical resistance per unit of effective stress determined by isothermal pressure; ρ_p – electrical resistivity; $P_{rp}^{t^0}$ – reservoir pressure with temperature at a given depth; P_{ef} – effective pressure within the reservoir; K_{elw} – coefficient of change in electrical resistivity of water per unit change in reservoir pressure; αt, ρ – coefficients determined by isobaric heating or cooling of water-saturated rock with temperature change. In an approximate form, the equation for the relationship between the resistivity of reservoir rocks in Neogene deposits, taking into account reservoir pressures, will be as follows:

$$\frac{\rho_p(P_{rp}t^0)}{\rho} \approx \frac{\rho_{r_{ef}} - \rho_{r_{rp}}}{\rho_{ac}} \times \frac{\rho_{r_{rp}}}{\rho_{ac} P_{rp}} \times \frac{\rho_{ef}^{t^0}}{\rho_{ac}}, \quad (3)$$

where $\rho_p(P_{rp}t^0)$ – the resistivity of the rock in reservoir conditions; ρ_{ac} – the resistivity of the rock under atmospheric conditions; $\frac{\rho_{r_{ef}} - \rho_{r_{rp}}}{\rho_{ac}}$, $\frac{\rho_{r_{rp}}}{\rho_{rt}}$ and $\frac{\rho r_{ef}}{\rho(P_{rp})}$ – relative changes in the resistivity of the rock under effective and reservoir pressures $P_{ef} - P_{rp} = const$; $\rho_{r_{pt}}$, ρ_{r_p} – resistivity at the initial and current pore pressures. In order to exclude the influence of the resistivity of the free fluid on the porosity parameters, the following formula can be used:

$$\frac{P_r^{ef}}{\rho_p} \approx \frac{P_p^{p^{ef}}}{P_p} \times \frac{P_p^{Pin}}{P_p^{rp}} \frac{P_{rp}^t}{P_{ef}}, \quad (4)$$

where $P_p^{P_{rp}t}$ – the parameter of rock porosity with specified thermodynamic conditions; P_p – similar parameter at initial atmospheric conditions; $\frac{P_{pt}}{P_p}$ – a ratio that characterises a partial change in the porosity parameter due to the influence of temperature.

Results and Discussion

The effectiveness of productive reservoir identification and tapping and interpretation of the logging results largely depends on the study of lithological and petrophysical characteristics of reservoir rocks, physical and chemical properties of fluids, technological conditions of drilling, reservoir pressures and temperatures, and the reliability of stratigraphic sectioning of the studied sections. The geological structure of gas fields in the Bilche-Volytske zone is based on Miocene terrigenous sediments that are inconsistently located on terrigenous carbonate platform Mesozoic complexes. These sediments differ in terms of sedimentation conditions and physical and petrophysical characteristics of reservoirs and bedrock. The main difficulties that arise in the process of studying Miocene sediments by geophysical methods are their thin-layered structure, high clay content of sandstones and polymictic-ity. Such structure and physical and petrophysical features of rocks are inherent mainly in the deposits of the Neogene system, which is represented by overburdened rocks of the Stebnytsia and Balytska formations, as well as autochthonous deposits of the Carpathian, Badenian and Sarmatian. A characteristic feature of the sediments that make up the Carpathian stage is the low resistivity of sandstones and the diversity of their mineralogical composition. In order to study the rocks and their characteristic features, comprehensive studies allowed to develop a classification of these sediments and determine their geophysical and petrophysical characteristics.

According to the mineralogical description of polished sections made from the core samples of the Carpathian sediments and the analysis of the results of nuclear-physical studies, the following classification types can be distinguished. Sandstones are represented by the following types: gravelly sandstones with chlorite-calcite and chlorite-clay cement, sandstones of different grains with chlorite-clay cement, medium-grained sandstones with calcite cement containing single grains of glauconite, fine-grained sandstones with chlorite-clay, chlorite-calcite, calcite-clay and calcite cement containing single glauconite grains, and siltstone with clay-calcite cement. Siltstones are gravelly-sandy with clay-calcite and chlorite-clay quartz cement. The mudstones are calcareous. In most of the exploration areas, oil, gas and condensate deposits are confined to quartz, feldspar sandstones, siltstones, clay shales, limestones and dolomites cemented with clay-carbonate, halite and mixed cements (Bulakh *et al*., 2022). The void space of this type of terrigenous, thinly laminated rocks of complex structure is represented by intergranular pores and cracks, which were obtained from the created collection.

The identified rock types mostly differ in the ratio of clastic components and cement composition, which is due to ancient changes in the supply of clasts, which now determine the reservoir properties of the rocks. Fine-grained sandstones with hydromica-clay cement formed during this period (well 5-Letnia 1,607.3 m deep) consist mainly of wedge-shaped and semi-rounded quartz fragments (70-80%) with a size of 0.3-0.1 mm. Most of the quartz particles have wave attenuation and traces of compression, which indicates that they were removed from ancient metamorphosed rocks. Among quartz, there are single fragments of zircon and muscovite. The fragments are cemented by an unevenly hydro-mica-clay aggregate, which has a filmy structure, and the pore space structure is clotting. Hydromica in the form of clumps up to 0.1 mm in size (5-8%) covers quartz fragments with films or sticks to them, rarely forming a mixture with a fine clay substance containing, in some cases, small pieces of illite. In the authors' opinion, such layers were formed in a coastal environment with good sorting of debris against the background of rapid

bottom sinking and sedimentation, which kept the debris from rounding. Although the porosity of the rock is low, there may be good collector rocks alongside these rocks, which were formed on ancient bars, beaches, and shoals.

Fine-grained sandstones with chlorite-glauconite-clay cement contain fewer fragments deposited during the formation period. Compared to the sandstone described above, the bulk of the rock is composed of angular and semicircular quartz fragments with 65-75% quartz, often closed to each other. Particles with a size of 0.3-0.5 mm make up approximately 10-5%, 0.3-0.1 mm, 40-50%, and 0.1-0.05 mm, approximately 3-8%. The distribution of fragments is chaotic (Fig. 1). The cement of the rock is mainly clayey, finely dispersed, and striped. In the bulk of the clay substance, fragments of hydrochloride (2-3%) are sometimes found near quartz fragments. In addition, there are dark green chlorite-glauconite inclusions of irregular shape, rarely in the form of round peas, the size of which is close to the size of the fragments, between the fragments. There is an indentation of the fragments into green clots of glauconite inclusions, which indicates their consedimentary nature.

Figure 1. Fine-grained sandstone with chlorite-glauconite clay cement

Source: created by the authors

Sandstones with chlorite-calcite cement are similar in composition to siltstone types. They are composed mainly of quartz fragments (55-70%), with less wedge-shaped fragments than clayey varieties. The sorting of fragments in such rocks is better; in cement, chlorite and glauconite are closely fused together to create irregularly shaped clots. Pyrite inclusions are observed alongside and within these clots. The distribution of chlorite and glauconite is uneven, with their content reaching 1-5% in different areas. The calcite in the cement is granular and well crystallised. The grain size is 0.1-0.3 mm. In some areas, the grain size reaches 1 mm and a poikilite structure appears; in some places, quartz grains are intensively destroyed by calcite on the periphery and along individual cracks. Such sandstone is a poor reservoir, as calcite is additionally subject to partial recrystallisation and compaction. Increased porosity of such rocks can be expected in places where various fragments of siltstone are found among quartz fragments. The latter may indicate consedimentary erosion of the shoal, hydrodynamic activity of water, and better sediment washing.

According to the description of the grinds, a silty, multigrained sandstone with clay-calcite cement formed under the same conditions consists of quartz fragments that differ significantly in size and grain sorting. Individual grains do not touch each other and are often unevenly scattered. The amount of fragments and cement is 45-55%; the cement is fine-crystalline and crystallised and unevenly distributed. In some places, calcite grains are 5-7 mm in size, round or amoebic in shape, and usually fill the intergranular space of large pores (about 5%) and cement a number of quartz fragments to form poikilite structures. In some cases, single inclusions of pyrite are found in such sandstones, and there are areas where its content reaches 1-5%. The rock has uneven porosity. The pores are mostly intergranular and distributed along microcracks; their size reaches thousandths of a mm. There are also large pores of 0.1-0.2 mm in size, rarely larger. The rocks were formed mainly in shallow lagoonal conditions, which resulted in their good reservoir properties.

At the same time, silty sandstone with chlorite-calcite cement is mostly composed of 50-70% quartz fragments, the particles of which are mostly angular, poorly sorted and have a size of 0.6-0.1 mm. A small part of this type of rock consists of semi-angular, semi-rolled fragments, which usually do not touch each other. Some of them have a wave-like extinguishment and are intersected by quartz veins. The rock contains single fragments of zircon, albite

and staurolite. The cement is mainly calcite of the basal type; the pore space is filled with grains of crystallised calcite. In addition, single pyrite clots are present in the cement. The rock was formed in lagoonal conditions in a low-reducing environment with rapid sedimentation. As a rule, it has poor reservoir properties, but in the horizons closer to the shore, rocks with high filtration properties can be expected. In the core samples taken from the Sarmatian deposits, there is a hidden, uncoordinated overlay of siltstone with calcite cement (light areas) on sandy siltstone with calcite-clay cement (dark areas) (Fig. 2). Clumps of clay (dark) are observed at the boundary of these rocks, with quartz fragments more massive than the bulk of the overlying sandstone.

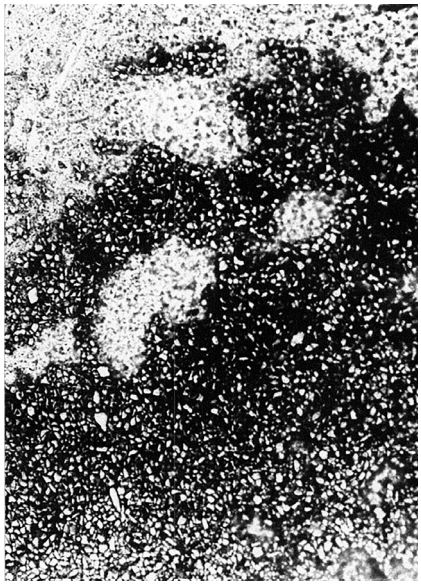

Figure 2. Sandy siltstone with calcite-clay cement

Source: created by the authors

The facies transition at the interbeddedness of silty sandstone with hydromica clay cement into silty mudstone (Fig. 3) clearly shows a gradual decrease in the amount of small fragments at the sandstone-silty mudstone interface. Quartz fragments are well sorted, fine-grained, and up to 0.5 mm in size, accounting for 1-2%. The sandstone cement, like the bulk of the mudstone, consists of a finely dispersed, poorly crystallised hydromica-clay aggregate. The hydromica clay mass is enriched with pyrite by 5-15%.

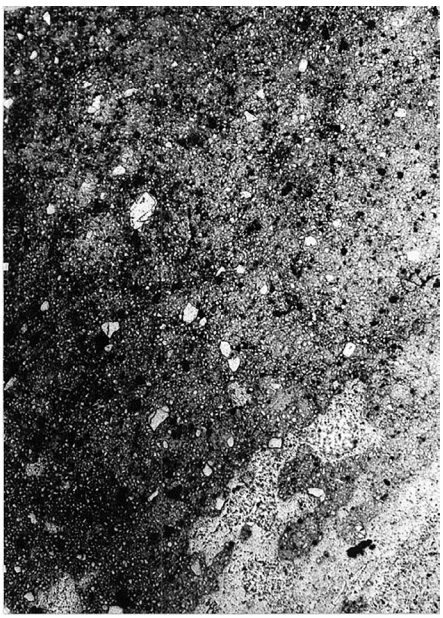

Figure 3. Silty sandstone with hydromica clay cement

Source: created by the authors

Along with small pyrite cubes, there are more massive rounded clots 0.001-0.005-0.03 mm in size. In some places, there are brownish clots, fragments of montmorillonite with a weakly pronounced concentric and compression-deformed structure. Judging by the slight difference in the size of the fragments, it can be assumed that the coastline moved a short distance, and changes in rock formation were determined by the submergence of the basin floor and an increase in its depth in this area. With regard to the mineralogical composition and structure of the siltstone, it was found that the sandy siltstone with glauconite-clay-calcite cement consists mainly of fragments of well-sorted siltstone material. This feature of the structure indicates sedimentary consedimentation and the demolition of more massive fragments to the place of rock formation by currents. The sand fraction in the rock is insignificant and amounts to 1-5%. Comprehensive geophysical surveys performed both in the open hole and in the cased hole allowed to highlight a number of physical and petrophysical factors that significantly affect the readings of radioactive, acoustic and induction methods (Ganat, 2020). As can be seen from the correlation profile (Fig. 4), a number of reservoir rocks with characteristic petrophysical and geophysical parameters are observed within the complexly constructed Neogene sediments.

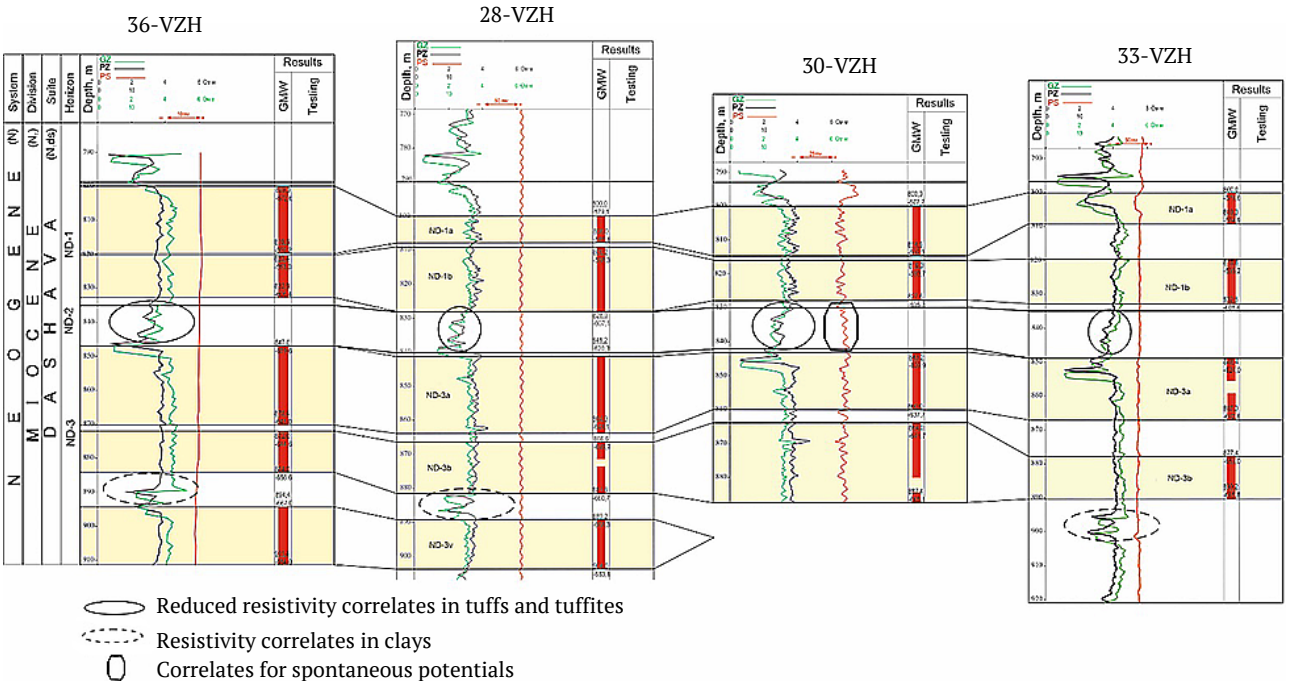

Figure 4. Correlation profile along the line of wells 36-Vzh-28-Vzh-30-Vzh-33-Vzh

Source: created by the authors

When constructing the correlation profile, the results of the well logging were taken into account, as were the established petrophysical capacitive and filtration parameters, which allowed to assess the prospects for oil and gas condensate reservoirs. Given that the presence of physically bound water, including crystalline bound water and residual oil, was found in reservoir rocks, it can be argued that their content will also affect the readings of electrical, acoustic and radioactive methods (Kuzmenko *et al.*, 2019). This is especially true for sandstones and siltstones in the geological sections of the Svydnytsia, Vizhomlia and Lypovets fields (Ftemov *et al.*, 2021). The rock types that were identified are mostly distinguished by their characteristic structure, the ratio of fragmentary components and cement composition, which determine reservoir properties (Dubei *et al.*, 2022).

It should also be noted that fine-grained sandstones are mainly characterised by the presence of chlorite-glauconite cement, which will also affect, along with the coefficient of bound water and residual oil, the electrical and radioactive parameters of geophysical methods. Sandstones with chlorite-calcite cement, which are similar in composition to siltstone varieties, are also gas and condensate reservoirs (Cannon, 2015). Their structure is similar to sandstones and consists of 55-70% quartz fragments, mostly semicircular and angular. This is mostly typical for the Letnia field (well 5 Letnia, depth 1,988.5 m; 1,579.0 m; 1,592.5 m), where wedge-shaped quartz fragments are less abundant than clay minerals of various types. The sorting of this type of fragment is better, but the cement material consists of chlorite and glauconite, which are closely fused together to create irregular shapes. Pyrite inclusions also appear in the middle of these clusters. The distribution of chlorite and glauconite is uneven, but their content reaches 1-5% within the Neogene sediments. Thus, in addition to the above, the readings of complex geophysical surveys, in particular electrical and radioactive, will be affected by the above minerals and the coefficients of physically bound water and residual gas and oil saturation. In addition, depending on the structural structure of the reservoir rock

and the value of the porosity coefficient, the physical and mechanical parameters will be deformed under the influence of the pressure gradient and the matrix compression ratio (Dubei & Dubei, 2023).

The value of the coefficient K_{rm} is determined provided that P_{rp} and t^0 – *const*. Taking into account the shallow depths of Neogene sediments, as well as insignificant compression of the solid phase of reservoir formation in the processes of hydrocarbon accumulation, it can be stated that in the zones of reservoir pressure depression, it does not significantly change the coefficient K_{rm}. In this case, the value of the coefficient K_{rm} for sandstones and siltstones is determined by the established value of the effective stress that causes a change in the tortuosity of pore channels and, accordingly, their moisture content (Fig. 5). It should be noted that the coefficient (αt) will depend on changes in the electrical conductivity of free and physically bound water in reservoir rocks, pore geometry and volume, temperature changes, and the presence of thermally conductive inclusions. Based on the results of laboratory petrophysical studies of the selected core samples, graphs of the relative electrical resistivity were constructed (Cannon, 2015) versus pressure change for polymict and monomict pressure rocks.

As can be seen from the plots for individual resistivity ratios, changes in pressure will not affect changes in

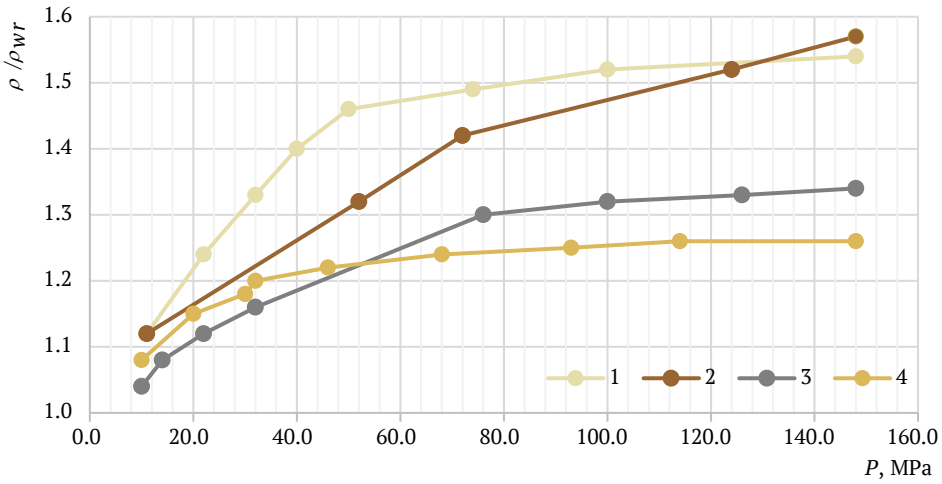

Figure 5. Relative change of relative electrical resistivity with pressure for polymict-type reservoir rocks

Note: 1 – fine-grained quartz-feldspar sandstone with carbonate-clay cement; 2 – fine-grained quartz-feldspar sandstone with clay cement; 3 – medium-grained quartz sandstone with clay cement; 4 – medium-grained quartz sandstone with clay-carbonate cement

Source: created by the authors based on O. Trubenko & S. Fedoryshyn (2011)

relative electrical resistivity. However, in the range of reservoir pressure changes from 20 MPa to 60 MPa, which is typical for the structure of Neogene deposits, the relative resistivity will increase with increasing reservoir pressure as well as with changes in temperature at a given depth. Thus, it was found that a pressure change of up to 50 MPa has virtually no effect on the porosity parameter P_p (Dubei & Dubei, 2023). Considering the above, the following can be written:

$$\frac{P_p^{ef}}{P_p} = \frac{P_r^{ef}}{\rho_p}. \quad (5)$$

By substituting expression (4) into formula (5), an expression was obtained that allows to estimate the relationship between the porosity parameter and the value of the rock resistivity depending on the nature of its saturation. Summarising the results of the core material studies, the following expression can be stated:

$$\frac{P_p{}^{P_{rp}t}}{P_p} \approx \frac{P_p{}^{P_{ef}}}{P_p} \times \frac{P_p{}^{P_{in}}}{P_p{}^{P_{rp}}} \times \frac{P_{rp}^t}{P_{ef}}, \quad (6)$$

where $\frac{P_p{}^{P_{ef}}}{P_p}, \frac{P_p{}^{P_{in}}}{P_p{}^{P_{rp}}}$ are, respectively, the ratios that highlight the partial changes in the rock porosity parameter under the action of the effective stress under the conditions $P_{in} = const$, $P_{ef} = 0$, $t = const$. The obtained equations describe the relationship between the rock porosity parameter and its resistivity within the Neogene deposits of the Bilche-Volytske zone of the Precarpathian trough and can be used to evaluate the results of electrical studies, as well as to increase the informativeness of petrophysical parameters of mathematical and statistical correlations in the process of calculating hydrocarbon reserves. In the process of searching for hydrocarbons in thin-layered Neogene formations using integrated geological and geophysical methods, there is often a problem of identifying reservoir rocks, assessing their saturation, determining porosity, and permeability. As a result, a significant proportion of hydrocarbons is lost, which leads to a decrease in actual gas and condensate production within the exploration areas at the stage of exploration drilling. Experimental studies of

the core collection of rocks that fill the Neogene section allowed to determine their structural structure, petrophysical parameters, cement type and mineral composition of clay cement. In most cases, within the exploration geological areas filled with the Sarmatian formation, significant fracturing, bulk and interlayer clay, polymicticity are observed in some places, and in some intervals, significant residual water saturation is noted in the rocks.

Based on this, the existing search complex of well logging data is not informative in some cases. In particular, this applies to acoustic and electric well logging, which are basic in the process of identifying reservoir rocks and assessing their hydrocarbon saturation. Acoustic surveys of thinly layered Sarmatian sediments are mainly carried out with single-probe and dual-probe probes (DALT-4, 6, 8, 9). Taking into account that the dependence of the interval time of acoustic oscillations does not allow obtaining accurate information about the type of porosity (granular, cavity, fracture), as well as the nature of saturation, the morphology of the results obtained loses its informative value. In this case, the Willy-Gregory formula, as well as the constructed two-dimensional petrophysical dependence of the $\Delta T = f(K_p)$ type, does not give reliable results, and the recorded acoustic logging curve is not informative; therefore, the indicated constructions based on theoretical calculations showed significant differences in the porosity curves, despite the same initial data.

Such a discrepancy is explained by the fact that the time of the ultrasonic longitudinal wave travel through the rock, depending on the change in the porosity value, obeys the minimum law at a conditional value of 40-45%; the wave propagation speed in the rock is equal to the wave speed in water. Therefore, the relationship ($Vp = Vw$) has a rather complex shape and is usually not linear. Thus, when the rock porosity is higher (30-35%), the longitudinal wave velocity will be close to its propagation in water. In real conditions, the propagation speed of an ultrasonic wave obeys a different law, i.e. it depends on the density of rock grains, mineralogical composition and type of porosity. Based on the above, it is recommended to use acoustic borehole devices in the process of complex acoustic surveys DAT-1, BAL-4,6. In some cases, it is not possible to determine the gas or oil saturation of reservoir rocks using standard electrical methods. Physically, this occurs when different concentrations of drilling mud come into contact with a constant rock solution, which changes the diffusion potential (U_d) and increases the resistivity according to the formula:

$$U_d = K_d \times lg \frac{\rho_1}{\rho_2}, \quad (7)$$

where ρ_1 – a resistivity of the NaCl solution; ρ_2 – resistivity of the solution formed in the rock; K_d – diffusion coefficient. Therefore, an increase in the concentration of chemical reagents in the drilling mud causes sharp changes in the diffusion-adsorption potential, such as an increase in the concentration of NaCl. Therefore, chemicals are used in the drilling process (CSC, CMC and hypan), which are weakly alkaline or alkaline in nature and have a much lower oxidation capacity, and, accordingly, the potential of clays, which leads to changes in the potentials of sandstones and siltstones. In this case, the informative value of direct methods, in particular, spontaneous potentials (PS).

A widespread set of electrical geophysical survey methods that solve the problem of hydrocarbon exploration are the standard methods (BKZ, BC, IR, PS), which are called isoresistive interpretation methods. The most effective is the method of high-frequency induction logging isoparametric sounding (HFILS). Unlike the above-mentioned set of electrical methods, the principle of operation of the HFILS method is based on high frequencies and provides high-resolution recording of electrical properties of the borehole zone and rocks of the geological section in the radial and vertical directions of the well. Therefore, the use of high frequencies makes it possible to obtain clear signals even in a low-conductivity environment (up to 120 ohms). This method of determination is not affected by the concentration and composition of chemicals used in the well completion process.

G. Sun *et al.* (2023) described the results of a detailed study of a thin section core, thin section analysis, mineral analysis and geochemical analysis to investigate thin layers and nodules of dolostone in the Qingshankou Shale in Gulong Sag. The geological structure and development of thin layers and nodules of dolomite is associated with the dry and hot climate of the sediments and was formed under the influence of hydrothermal fluids. These studies were carried out on the example of thin layers and nodules for dolomite deposits. Neogene deposits of gas fields in the Bilche-Volytske zone also have a thin-layered structure but are represented by a terrigenous section and, accordingly, the research methodology is somewhat different from that for a carbonate section. Considering the work of X. Qiu & Y. Wang (2024), attention should be paid to the study of sedimentary rocks, the characteristics of the reservoir of which are described and studied in detail using conventional grinds, cast grinds, graphical representations of particle size and scanning electron microscopy experiments. These studies were conducted using sedimentology and sedimentary geology, which are used to analyse the sedimentary environment of the basin. These studies have made little or no use of the logging data, and therefore such sedimentary models should be supplemented with geophysical characterisation.

F. Olita *et al*. (2023) carried out a geological analysis based on the results of new lithological and structural data obtained during a detailed geological survey and supplemented by logging data obtained during hydrocarbon exploration. The geophysical surveys were carried out at a depth of up to 1 km (deep electroresistive tomography), which revealed the buried structural and geological characteristics of the study area. By combining surface and subsurface data, a forecast of the structural situation and the presence of geofluids at a depth of up to 1 km was made. Geological and structural cross-sections were also constructed to clarify the geometry of structures in the

subsurface, facilitating early hydrocarbon recovery and circulation of hypothermal fluids and associated gases rising from deeper reservoirs. These studies have been carried out to a depth of 1 km, while hydrocarbon deposits in the Bilche-Volytske zone of the Precarpathian trough lie at somewhat deeper depths and require a different approach to their study.

The core material from 28 wells in the central part of the Dnipro-Donetsk Basin was studied by L. Stryzhak *et al.* (2020) using lithological and petrographic methods. The results of the study confirmed the processes of lithogenetic transformations of the rock matrix that occurred in deeply submerged sandstones (more than 5,000 m). Based on the nature of structural and mineralogical transformations, the secondary (post-sedimentation) processes of lithogenesis of terrigenous rocks-collectors of hydrocarbons were established, and their influence on the reservoir properties and, accordingly, on the reflection in geophysical parameters was revealed. Such studies need to be linked to the geological logging data to fully understand the processes of secondary transformation of the reservoir rock matrix.

Similar studies were conducted for the lithological and facies dissection of ore deposits based on geological and well data to clarify the genesis of the formation of deposits and hydrocarbon sources within the Yablunivska structure of the Dnipro-Donetsk Basin by O.M. Karpenko *et al*. (2021). The authors used cluster and factor analyses, as well as the method of interpreting K. Passy's well log data, to quantify the organic carbon (OC) content in the rock. The results of the studies made it possible to establish certain regularities in the geological structure and identify lithological heterogeneities in the spatial distribution of sedimentary and facies rock lithotypes, as well as facies rock types, thickness of their radioactive layers and organic carbon content. Such studies should be complemented by laboratory core studies, which will allow for a deeper and more comprehensive assessment of the reservoir structure.

Such studies are informative for the needs of rapid analysis of poorly studied geological sections where the parameters are determined directly from the logging diagrams. The inclusion of information on petrophysical properties of reservoir rocks from selected core samples can provide reliable information on the potential productivity and characteristics of the reservoir rock, which will lead to an increase in the accuracy of their assessment. However, to assess the impact of the structure of lithological and stratigraphic sections and capacitance-filtration parameters on the readings of the logging results, new methods and techniques should be introduced to create reliable petrophysical models of complex thin-layer geological sections to improve the efficiency of their interpretation.

Conclusions

According to the results of the description of the polished sections, the porous rock is enriched with foraminifera remains and turns into a silty marl. The amount of foraminifera shells reaches 30-50%. Pyrites and brown organic matter are located around the foraminifera. The cementing substrate is sharply enriched with clay substance, in which glauconite is closely fused with pyrite. The fragments contain single particles of amber, staurolite, and zircon with black and brown borders, which indicates that the fragments were removed from the weathering crust of the neighbouring land of the platform, which was being eroded. Clay clots contain almost no foraminifera, but pyrite inclusions are present. Such features of the rock structure suggest that Neogene sediments were formed in the underwater part of the delta of the ancient river flow. They may be associated with rocks with good reservoir properties.

It has also been established that siltstones with quartz-clay cement consist of well-sorted quartz fragments 0.1-0.5 mm in size, which are in contact with each other. There are single inclusions of zircon and garnet, washed glauconite. Clay cement is localised in some pores and does not always completely fill them. About 5% of intergranular large pores are filled with rounded or amoebic calcite clots. The rock was formed in a coastal shallow water environment, which determines its good reservoir properties. Changes in the rock cement led to changes in its structure and deterioration of reservoir properties. Accordingly, the productive intervals in Miocene sediments are filled with highly porous, medium-porous and low-porous reservoirs, which are characterised by significant facies, lithological and petrophysical changes that significantly affect the results of the well logging.

As a result of laboratory experimental studies of core material taken from Neogene sediments, a complex structure of reservoir rocks was established, taking into account the influence of tectonic structure on the formation of sandstones, clays and siltstones. Based on the obtained parameters of porosity and permeability of productive reservoir rocks, the graphs of interrelationships and relative electrical resistivity with changes in reservoir pressure were constructed, in particular for polymict and monomict reservoir rocks. From the graphs established by the results of experimental studies, it is clear that for certain relative electrical resistivity ratios, pressure does not affect the change in the electrical conductivity of reservoir rocks. However, with an increase in reservoir pressure in the range from 20 to 60 MPa, the relative resistivity will increase as the dynamics of rock compaction increase. To exclude the influence of the resistivity of the free fluid on the porosity parameters, the derived formula (4) can be used. The task of further research is to test the results in neighbouring fields, the geological section of which is represented by similar rocks. Also, in the future, it is necessary to develop consolidated petrophysical models for this type of reservoir rocks and improve them.

Acknowledgements

None.

Conflict of Interest

None.

References

[1] Anikeyev, S., & Rozlovska, S. (2021). Anisotropic transformations of regional gravi-magnetic fields of the Ukrainian Southeast Carpathian. *Geodynamics*, 2(31), 66-83. doi: 10.23939/jgd2021.02.066.

[2] Bulakh, O., Bezrodna, I., & Yemets, V. (2022). Mathematical modelling of the Bashkir's and Serpukhiv's sandstones of the Yablunivske field based on petrophysical data. In *16th international conference monitoring of geological processes and ecological condition of the environment* (pp. 1-5). Kyiv: Taras Shevchenko National University of Kyiv. doi: 10.3997/2214-4609.2022580234.

[3] Cannon, S. (2015). *Petrophysics: A practical guide*. Hoboken: John Wiley & Sons Inc. doi: 10.1002/9781119117636.

[4] Dentith, M., Enkin, R.J., Morris, W., Adams, C., & Bourne, B. (2020). Petrophysics and mineral exploration: A workflow for data analysis and a new interpretation framework. *Geophysical Prospecting*, 68(1), 178-199. doi: 10.1111/1365-2478.12882.

[5] Dubei, N., & Dubei, M. (2023). Methodological developments for taking into account of layer heterogeneity at the design stage of underground gas storage. In *International conference of young professionals "GeoTerrace-2023"* (pp. 1-5). Lviv: Lviv Polytechnic National University. doi: 10.3997/2214-4609.2023510044.

[6] Dubei, N., Dubei, M., Boiko, A., & Mykhailiv, I. (2022). Study of the influence of geological features of layers – collectors on gas deposit development processes using 3D modeling. In *International conference of young professionals "GeoTerrace-2022"* (pp. 1-5). Lviv: Lviv Polytechnic National University.

[7] Fedoryshyn, D., Fedoryshyn, S., & Lyzun, S. (2015). *Nuclear and physical methods of wells research*. Ivano-Frankivsk: Ivano-Frankivsk National Technical University of Oil and Gas.

[8] Ftemov, Y., Fedoriv, V., & Maniuk, V. (2021). Petrophysical models for estimating filtration-capacity parameters of complex reservoir rocks at Kachalivske oil and gas condensate field. In *Geoinformatics* (pp. 1-6). Kyiv: European Association of Geoscientists & Engineers. doi: 10.3997/2214-4609.20215521017.

[9] Ganat, T.A. (2020). Hydrocarbon exploration. In *Technical guidance for petroleum exploration and production plans* (pp. 1-11). Cham: Springer. doi: 10.1007/978-3-030-45250-6_1.

[10] GSTU 41-00032626-00-025-2000. (2001). *Coefficient of water saturation of rocks. Method of measurement by centrifugation of samples*. Kyiv: Ministry of Ecology and Natural Resources of Ukraine.

[11] Ivaniuta, M.M. (Ed.). (1998). *Atlas of oil and gas fields of Ukraine*. (Vol. 4). Lviv: Tsentr Yevropy.

[12] Karpenko, O.M., Ohar, V.V., Karpenko, I.O., & Bezrodna, I.M. (2021). Differentiation of Rudov Beds based on the statistical methods on geological and geophysical data. *Naukovyi Visnyk Natsionalnoho Hirnychoho Universytetu*, 1, 5-10. doi: 10.33271/nvngu/2021-1/005.

[13] Koval, Y.M., & Fedak, I.O. (2022). Allocation of polymictic sandstones in a complex geological section of oil and gas wells of the Dnipro-Donetsk depression. *Oil and Gas Power Engineering*, 1(37), 7-14. doi: 10.31471/1993-9868-2022-1(37)-7-14.

[14] Krasnozhon, M.D., Kosachenko, V.D., Tulchynsky, V.G., Karpenko, O.M., & Fedoryshyn, D.D. (2003). *Methodical guide to the study of computerized technology "Geoprospecting"*. Ivano-Frankivsk: Ivano-Frankivsk National Technical University of Oil and Gas.

[15] Krupskyi, Yu. (2020). *Geology and oil and gas content of the western region of Ukraine*. Lviv: SPOLOM.

[16] Kurovets, I., Hrytsyk, I., Prykhodko, O., Chepusenko, P., Kucher, Z., Mykhalchuk, S., Melnychuk, S., Lysak, Yu., & Petelko, L. (2021). Petrophysical models of deposits of the menilite suite of the oligocene flysh of the Carpathians and the Precarpathian deep. *Geology & Geochemistry of Combustible Minerals*, 3-4(185-186), 33-43. doi: 10.15407/ggcm2021.03-04.033.

[17] Kurovets, S.S., Artym, I.V., & Kurovets, I.M. (2018). Researching the fracturing of the reservoir rocks. *Journal of Hydrocarbon Power Engineering*, 5(1), 1-6.

[18] Kuzmenko, E., Bahrii, S., & Dzoba, U. (2019). The depth range of the Earth's natural pulse electromagnetic field (or ENPEMF). *Journal of Geology, Geography and Geoecology*, 27(3), 466-477. doi: 10.15421/111870.

[19] Olita, F., Giampaolo, V., Rizzo, E., Palladino, G., Capozzoli, L., De Martino, G., & Prosser, G. (2023). Investigation of the geological structure of the Tramutola area (Agri Valley): Inferences for the presence of geofluids at shallow crustal levels. *Geosciences*, 13(3), article number 83. doi: 10.3390/geosciences13030083.

[20] Pavlyuk, M., Lazaruk, Y., Shlapinsky, V., Savchak, O., Kolodiy, I., Ternavsky, L., & Kovalchuk, N. (2021). The formation and criteria of oil- and gas-bearing potential of hydrocarbon accumulations of the western oil-gas region of Ukraine. *Geology & Geochemistry of Combustible Minerals*, 1-2(183-184), 14-44. doi: 10.15407/ggcm2021.01-02.

[21] Qiu, X., & Wang, Y. (2024). Evaluation of sedimentary characteristics of the Chang 9 oil layer formation in the Yanchang Formation, Ordos Basin. *Applied Sciences*, 14(10), article number 4035. doi: 10.3390/app14104035.

[22] Stryzhak, L.I., Aleksieienkova, M.V., & Stryzhak, V.P. (2020). Lithogenesis of terrigenous rocks and its influence on filtration-capacity properties of lower carbon reservoirs in the central part of the Dnieper-Donets Basin. *Collection of Scientific Works of the Institute of Geological Sciences of the National Academy of Sciences of Ukraine*, 13, 80-88. doi: 10.30836/igs.2522-9753.2020.220668.

[23] Sun, G., Dong, W., Zhang, X., Zhong, J., & Sun, N. (2023). Study on dolomite thin layers and nodules in the Qingshankou formation shale oil reservoir of Gulong Sag. *Energies*, 16(10), article number 3981. doi: 10.3390/en16103981.

[24] Trubenko, O., & Fedoryshyn, S. (2011). Geological and petrophysical parameters as criteria for assessing reservoir properties of reservoir rocks and quality of tires. *Scientific Bulletin of Ivano-Frankivsk National Technical University of Oil and Gas*, 3(29), 41-45.

[25] Yershov, M., Davybida, L., & Shtohryn, L. (2022). Temporal analysis of the long-term hydrogeological monitoring data of the Carpathian Region (Ukraine). In *16th international conference monitoring of geological processes and ecological condition of the environment* (pp. 1-5). Kyiv: Taras Shevchenko National University of Kyiv. doi: 10.3997/2214-4609.2022580106.

Оцінка впливу будови літолого-стратиграфічних розрізів та ємнісно-фільтраційних параметрів на покази результатів геофізичних досліджень свердловин

Дмитро Федоришин

Доктор геологічних наук, професор
Івано-Франківський національний технічний університет нафти і газу
76019, вул. Карпатська, 15, м. Івано-Франківськ, Україна
https://orcid.org/0009-0004-5348-9564

Олександр Трубенко

Кандидат геологічних наук, декан
Івано-Франківський національний технічний університет нафти і газу
76019, вул. Карпатська, 15, м. Івано-Франківськ, Україна
https://orcid.org/0000-0003-3418-439X

Сергій Федоришин

Кандидат геологічних наук, доцент
Івано-Франківський національний технічний університет нафти і газу
76019, вул. Карпатська, 15, м. Івано-Франківськ, Україна
https://orcid.org/0009-0005-9274-7244

Ігор Михайловський

Аспірант
Івано-Франківський національний технічний університет нафти і газу
76019, вул. Карпатська, 15, м. Івано-Франківськ, Україна
https://orcid.org/0009-0007-7948-4026

Анотація. Підвищення видобутку вуглеводнів із порід-колекторів складної будови, в межах неогенової системи Більче-Волицької зони Передкарпатського прогину, є доволі багатогранною проблемою, яку необхідно обґрунтувати шляхом проведення комплексних геофізичних, петрофізичних та петрографічних досліджень. Метою було обґрунтувати фізико-механічні, електричні, акустичні та петрофізичні параметри за результатами геофізичних досліджень у тонкошаруватому неогеновому розрізі газових та газоконденсатних родовищ у межах Більче-Волицької зони Передкарпатського прогину. Методика вивчення складнопобудованих неогенових відкладів у межах Більче-Волицької зони Передкарпатського прогину базувалася на якості результатів геофізичних та петрофізичних досліджень, отриманих безпосередньо в процесі буріння пошукових і розвідувальних свердловин. Окрім цього домінуючу роль відігравали результати лабораторних експериментальних досліджень взірців керну з відображенням пластових термобаричних умов. За результати таких комплексних геолого-геофізичних досліджень встановлено, що на покази геофізичних методів суттєво впливає тонкошарувата будова геологічного розрізу, що літологічно представлена перешаруванням пісковиків, алевролітів та аргілітів. З'ясовано, що значний вплив на покази геофізичних методів мають свердловинні прилади, які використовуються у геофізичних експедиціях. Результати досліджень спрямовані на підвищення ефективності пошуків вуглеводнів та контролю їхнього вилучення, тому наявність високо інформаційних комплексних геофізичних досліджень, зокрема багатозондового акустичного каротажу, високочастотного індукційного каротажного ізопараметричного зондування та повторного нейтронного каротажу дозволяє оптимізувати висновки на предмет перспективності виявлення вуглеводнів у складнопобудованих тонкошаруватих розрізах. Впровадження нових підходів до виділення таких пластів та прошарків дозволить підвищити інформативність геолого-геофізичних методів та приріст вуглеводнів у межах пошукових площ Більче-Волицької зони Передкарпатського прогину

Ключові слова: літотипи; колектора; коефіцієнти пористості та проникності; електричний опір; пори; акустичний імпеданс; електричні та акустичні зонди

Розвідка та розробка нафтових і газових родовищ

Науково-технічний журнал

Том 24, № 1, 2024

Відповідальний редактор:
О. Поліщук

Комп'ютерна верстка:
О. Глінченко

Підписано до друку 31.05.2024 р. Формат 60*84/8
Умовн. друк. арк. 8
Тираж: 300 прим.

Адреса видавництва:
Івано-Франківський національний технічний університет нафти і газу
76019, вул. Карпатська, 15, м. Івано-Франківськ, Україна
Тел.: +380 (342) 54-72-66
Факс: +380 (342) 54-71-39
E-mail: info@pdogf.com.ua
https://pdogf.com.ua/uk

Prospecting and Development of Oil and Gas Fields

Scientific and Technical Journal

Vol. 24, No. 1, 2024

Managing Editor:
O. Polishchuk

Desktop Publishing:
O. Glinchenko

Signed for print 31.05.2024. Format 60*84/8
Conventional printed pages 8
Circulation 300 copies

Publishing Address:
Ivano-Frankivsk National Technical University of Oil and Gas
76019, 15 Karpatska Str., Ivano-Frankivsk, Ukraine
Tel.: +380 (342) 54-72-66
Fax: +380 (342) 54-71-39
E-mail: info@pdogf.com.ua
https://pdogf.com.ua/en